

# Probabilistic Earthquake Damage Prediction for Reinforced Concrete Building Components

Peter C. Brown

A thesis  
submitted in partial fulfillment of the  
requirements for the degree of

Master of Science in Civil Engineering

University of Washington

2008

Program Authorized to Offer Degree:  
Department of Civil and Environmental Engineering

University of Washington  
Graduate School

This is to certify that I have examined this copy of a master's thesis by

Peter C. Brown

and have found that it is complete and satisfactory in all respects,  
and that any and all revisions required by the final  
examining committee have been made.

Committee Members:

---

Laura Lowes

---

Dawn Lehman

---

John Stanton

Date: \_\_\_\_\_

# TABLE OF CONTENTS

	Page
List of Figures .....	iv
List of Tables .....	v
1 Introduction .....	1
1.1 Research Objective and Method .....	2
1.2 Organization .....	5
2 Engineering Demand Parameters, Damage States and Methods of Repair ...	6
2.1 Introduction .....	6
2.2 Engineering Demand Parameters .....	7
2.3 Damage .....	8
2.3.1 Concrete Cracking .....	9
2.3.2 Concrete Spalling and Crushing .....	10
2.3.3 Failure .....	11
2.3.4 Characterization of Damage Using Laboratory Measurements .....	12
2.4 Method of Repair .....	12
2.4.1 Method of Repair 0: Cosmetic Repair .....	14
2.4.2 Method of Repair 1: Epoxy Injection of Cracked Concrete ...	14
2.4.3 Method of Repair 2: Patching of Spalled Concrete .....	16
2.4.4 Method of Repair 3: Removal and Replacement of Damaged Concrete .....	18
2.4.5 Method of Repair 4: Removal and Replacement of Damaged Rebar .....	18
2.5 Grouping Damage Data to Enable Prediction of Required Repair ....	19
2.6 Summary and Conclusion .....	20
3 Statistical Analysis of Data .....	22
3.1 Introduction .....	22
3.2 Standard Probability Distributions .....	22
3.2.1 Normal Distribution .....	23
3.2.2 Lognormal Distribution .....	24
3.2.3 Weibull Distribution .....	25
3.2.4 Beta Distribution .....	26
3.2.5 Stepwise CDF .....	27
3.3 Method of Maximum Likelihood .....	27
3.4 Testing of Goodness-of-Fit .....	28
3.4.1 Kolmogorov-Smirnov Test (K-S) .....	28
3.4.2 Chi-Square Test ( $\chi^2$ ) .....	30
3.4.3 The Lilliefors Test .....	31
3.5 Summary and Conclusion .....	32
4 RC Beam-Column Joints .....	33
4.1 Introduction .....	33
4.2 Experimental Data Characterizing Performance of Building Joints....	34
4.2.1 Introduction .....	34

4.2.2	Criteria Used to Identify Specimens for the Study – Interior Joints .....	34
4.2.3	Experimental Data Used in the Study – Interior Joints .....	38
4.2.4	Factors that Determine Earthquake Performance - Interior Joints .....	44
4.2.5	Criteria Used to Identify Specimens for the Study – Exterior Joints .....	45
4.2.6	Experimental Data Used in the Study – Exterior Joints .....	49
4.2.7	Factors that Determine Earthquake Performance - Exterior Joints .....	50
4.3	Engineering Demand Parameters, Damage States and Methods of Repair for Joints .....	51
4.3.1	Engineering Demand Parameter (EDP) .....	51
4.3.2	Damage Measure (DM) .....	53
4.3.3	Method of Repair (MOR) .....	55
4.4	Damage versus Engineering Demand Parameter .....	56
4.4.1	Introduction .....	56
4.4.2	Interior Joints .....	56
	4.4.2.1 Impact of Design Parameters on Damage Progression on Interior Joints .....	59
4.4.3	Exterior Joints .....	70
	4.4.3.1 Impact of Design Parameters on Damage Progression on Exterior Joints .....	72
4.5	EDP versus MOR .....	74
4.6	Evaluation of the Fragility Functions .....	76
4.7	Comparison of Damage of Older and Modern Interior Joints .....	83
4.8	Comparison of Damage of Exterior and Modern Interior Joints .....	84
4.9	Summary and Conclusion .....	85
4.9.1	Summary .....	85
4.9.2	Conclusions .....	86
4.9.3	Recommendations for Future Research .....	88
5	Structural Walls .....	90
5.1	Introduction .....	90
5.2	Previous Experimental Research .....	92
5.2.1	Introduction .....	92
5.2.2	Experimental Data .....	92
5.2.3	Characteristics of Wall Specimens .....	93
5.2.4	Wall Specimen Properties and Damage Data .....	97
5.3	Engineering Demand Parameters Specific to Walls .....	101
5.4	Damage States for Walls .....	102
5.5	Predicting Damage as a Function of Demand .....	104
5.5.1	Introduction .....	104
5.5.2	Identification of Preferred EDP .....	104

5.5.3	Identification of Design Characteristics that Determine	
	Damage Progression .....	107
5.5.3.1	Damage State versus Drift – Wall Shape .....	107
5.5.3.2	Damage State versus Drift – Impact of Aspect Ratio...	108
5.5.3.3	Damage State versus Drift – Shear Demand –	
	Capacity Ratio .....	109
5.6	Methods of Repair for Walls.....	113
5.7	Fragility Functions for Walls .....	114
5.7.1	Use of Empirical Data to Calibrate Fragility Functions .....	116
5.8	Evaluation of the Fragility Functions .....	119
5.9	Effective Stiffness versus Drift .....	119
5.9.1	Earthquake Demand and Effective Stiffness Data .....	120
5.9.2	Investigation of the Impact of Design Parameters on	
	Effective Stiffness .....	121
5.9.3	Development of an Effective Stiffness versus Drift Model.....	123
5.10	Summary and Conclusions .....	126
5.10.1	Summary.....	126
5.10.2	Conclusions .....	127
5.10.3	Recommendations for Future Work .....	128
6	Summary and Conclusions .....	129
6.1	Summary.....	129
6.2	Conclusions .....	133
6.3	Future Work .....	134
7	References .....	136
A.	Appendix – Joints .....	142
B.	Appendix – Shear Walls.....	151
C.	Appendix – Modern Joint Distributions and Goodness-of-Fit Parameters .....	170
D.	Appendix – Shear Wall Distributions and Goodness-of-Fit Parameters .....	173

## LIST OF FIGURES

	Page
Figure 4.1 Pictures and Descriptions of DMs associated with MORs .....	56
Figure 4.2 Damage State versus EDP – Interior Joints .....	58
Figure 4.3 DS versus EDP, Grouped by Shear Demand .....	60
Figure 4.4 DS versus EDP, Grouped by Transverse Steel Ratio .....	61
Figure 4.5 DS versus EDP, Grouped by % of Steel Provided.....	62
Figure 4.6 DS versus EDP, Grouped by Col. Depth/Bar Diameter.....	63
Figure 4.7 DS versus EDP, Grouped by Bond Index .....	64
Figure 4.8 DS versus EDP, Grouped by Beam to Col. Strength Ratio .....	65
Figure 4.9 DS versus EDP, Grouped by Column Axial Load .....	66
Figure 4.10 DS versus EDP, Grouped by Beam to Col. Width Ratio.....	67
Figure 4.11 DS versus EDP .....	73
Figure 4.12 Fragility Functions – Drift .....	79
Figure 4.13 Fragility Functions – $F(D,N)$ .....	80
Figure 4.14 Fragility Functions – $F(\gamma,N)$ .....	81
Figure 5.1 DS versus EDP – Walls .....	106
Figure 5.2 DS versus Drift – Walls .....	111
Figure 5.3 DMs with MOR for Walls with Pictures .....	114
Figure 5.4 Fragility Functions – Walls .....	118
Figure 5.5 Effective Stiffness versus Drift .....	122
Figure 5.6 Effective Stiffness versus Drift – Equation .....	125

## LIST OF TABLES

	Page
Table 4.1      Design Details Reduced Data Set – Interior Joints.....	42
Table 4.2      Design Details Joints Not in the Reduced Data Set.....	43
Table 4.3      Design Details and Load Data for Exterior Joints .....	48
Table 4.4      Empirical Parameters for Eq. 4.4 .....	52
Table 4.5      Empirical Parameters for Eq. 4.5 .....	53
Table 4.6      Description of DSs for Joints .....	54
Table 4.7      MORs for Joints .....	55
Table 4.8      Statistical Characteristics of EDP-MOR Data – Joints .....	75
Table 4.9      Lilliefors Test results for Lognormal Distributions – Joints .....	77
Table 4.10      Lambda and Zeta for Modern Joints .....	82
Table 5.1      Experimental Details for Structural Walls .....	100
Table 5.2      Mean and Coefficient of Variation for Drift .....	112
Table 5.3      MORs for Structural Walls .....	114
Table 5.4      Statistical Characteristics of EDP-MOR Data – Walls .....	116
Table 5.5      Lognormal Distributions Parameters – Walls .....	117
Table 5.6      Goodness-of-Fit test for Walls – Lognormal Distribution .....	119

# 1 Introduction

The state-of-the-art in performance-based earthquake engineering (PBEE) includes the use of a probabilistic framework to assess performance and the use of measures that are meaningful to building owners to define performance. Researchers at the Pacific Earthquake Engineering Research Center (PEER) have developed a probabilistic approach to PBEE design in which the result of a building evaluation is a continuous function describing the mean annual probability that loss, due to earthquake loading, will exceed a specific dollar value (Cornell and Krawinkler 2000). To quantify annualized loss and propagate uncertainty through the evaluation process, it is necessary to develop a series of probabilistic relationships that include: the probability of earthquake intensity exceeding a specific level at the building site, the probability of engineering demands exceeding specific levels conditioned on the earthquake intensity level, the probability of structural and non-structural damage exceeding specific levels conditioned on the earthquake demand and the probability of loss exceeding a specific dollar value conditioned on the damage level. The research presented here focuses on the last two of these relationships, those linking earthquake demands with structural damage and structural damage with economic impact.



Multiple approaches are appropriate for using information about building performance to develop relationships linking earthquake demand with structural damage and economic loss. It is generally understood that considering damage and loss at the component level introduces the most information into the process. The models developed here support this approach. Specifically, probabilistic relationships, referred to as fragility functions, are developed that link component-specific engineering demands with damage states and the methods of repair required to restore damaged components. Given a required method of repair standard estimating procedures may be used to assess economic impact.

Two types of reinforced concrete (RC) components are considered in this study: modern beam-column joints and walls. In collecting experimental data to develop these models, modern joints were considered to have design details approaching the ACI 318-05 Building Code (ACI 318 2002) requirements for special moment frames, as discussed in Section 4.2. Concrete walls were limited to rectangular and barbell-shaped walls with transverse reinforcement in the boundary elements as discussed in Section 5.2.4.

## **1.1 RESEARCH OBJECTIVE AND METHOD**

The objective of this study is to develop fragility functions that, given a measure of earthquake demand, define the probability that a specific method of repair will be required to restore a damaged beam-column joint or wall to pre-earthquake condition.

To accomplish this objective, the process employed by Pagni and Lowes (2006) was used. Pagni and Lowes developed fragility functions for RC joints with detailing typical of pre-1970 construction. Essentially this process comprises:

- 1) Establish criteria for use in determining which experimental tests will be included in the study. These criteria include design parameters and test-method characteristics.
- 2) Identify potential measures of earthquake demand: For the current study, engineering demand parameters (EDP) are used to define the earthquake demand on structural components. This follows the nomenclature established by the Pacific Earthquake Engineering Research Center (PEER). To enable accurate prediction of damage and required repair, an EDP should be highly correlated with damage. For the EDP to be practical for use, it must be computed as part of a typical structural analysis. Potential EDPs are drift, number of displacement cycles, displacement ductility and joint strain as well as functions of these scalar EDPs.
- 3) Identify measures of damage: For the current study, the damage sustained by a structural component is a damage measure (DM). This follows the nomenclature established by PEER. DMs are quantified by damage states (DS). DSs describe the extent of concrete cracking, concrete spalling, yielding of reinforcing steel, crushing of concrete, and buckling and fracture of reinforcing steel. The ideal DS

is correlated with an EDP and may be used to determine the method of repair required to restore a damaged component to pre-earthquake conditions.

- 4) Determine methods of repair (MOR) that can be used to restore damaged components. Pagni and Lowes (2006, 2004) consulted construction professionals and repair manuals to determine appropriate MORs for older beam-column joints and bridge columns. These MORs are considered to be appropriate also for modern joints and walls.
- 5) Link DSs and MORs: Specifically, it is necessary to identify the DSs that are repaired using specific MORs and the specific DS that triggers the use of a specific MOR.
- 6) Develop, using the results of previous experimental research, a data set comprised of EDP-DS data points for all specimens that meet the criteria for inclusion in the study.
- 7) Calibrate standard probability functions: Experimental data and established linkages between DS and MOR are employed to generate EDP-MOR data sets. These data sets may be used to develop empirical functions defining the probability that a specific MOR will be required given a specific value of an EDP. Standard probability distributions are used to model these empirical functions. Standard goodness-of-fit tests are used to evaluate how well standard probability distributions fit the experimental data.

## **1.2 ORGANIZATION**

The research effort is presented in this report as follows: Chapter 2 provides a general discussion of engineering demand parameters, damage states and methods of repairs. Chapter 3 presents the statistical methods employed to generate and evaluate analytical fragility functions. Chapter 4 presents the development of fragility functions for modern beam column joints. Chapter 5 presents the development of fragility functions for planar structural walls. Chapter 6 summarizes the work and presents conclusions and recommendations for future work.

## **2 Engineering Demand Parameters, Damage States and Methods of Repair**

### **2.1 INTRODUCTION**

Data from previous experimental studies provide a basis for developing component-specific fragility functions. To use these data it is necessary to identify 1) engineering demand parameters (EDPs) that efficiently predict observed damage, 2) a series of damage states (DSs) that characterize the progression of damage under earthquake loading and are appropriate for use in determining the specific repair method that will be employed, and 3) methods of repair that can be used to restore a damaged joint to pre-earthquake condition.

The results of a previous study by Pagni and Lowes (2006), which developed fragility functions for older joints, were used to identify demand parameters, damage states and methods of repair for modern joints in the current study. In part, this was done to enable comparison of fragility functions for older and modern joints. However, evaluation of the process used to identify appropriate demand parameters and methods of repair for older joints indicated that it was appropriate also for modern joints. Additionally, evaluation of the experimental data compiled for the current study

indicated that many of the damage states identified for older joints were appropriate also for modern joints. Some modifications to the previously proposed list of damage states were made to better represent damage progression in modern joints.

Pagni and Lowes (2006) was used as a basis also for identifying EDPs, DS and MORs for structural walls. It was found that a subset of the engineering demand parameters used in Pagni and Lowes (2006) was appropriate for use on the structural walls. A larger set of engineering demand parameters was investigated to ensure that the chosen parameter was the most appropriate; this is discussed in greater detail in Section 5.3. The results presented in Pagni and Lowes (2006) and an assessment of the available damage data was used to produce a comprehensive list of damage states for structural walls. The methods of repair used in Pagni and Lowes (2006) were also used for structural walls since the damage sustained by the components was similar and the methods of repair required were the analogous.

## **2.2 ENGINEERING DEMAND PARAMETERS**

An engineering demand parameter (EDP) is a scalar or functional quantity that defines the earthquake demand on a component at any point in the load history. In developing fragility functions, the objective is to identify an EDP that most accurately and precisely predicts damage. The domain of potential EDPs is limited by the range of experimental data published by researchers and the range of demand measures that can be computed using available software for analysis.

For the current study, multiple demand measures were considered for both joints and walls. The results of Pagni and Lowes (2006) were used to identify potential EDPs for modern joints. These included: maximum inter-story drift, number of displacement cycles, maximum joint shear strain, a function of maximum inter-story drift and number of displacement cycles, and a function of maximum joint shear strain and number of displacement cycles. The results of experimental tests of planar walls were used to identify potential EDPs for walls. These included: maximum inter-story drift, number of displacement cycles, and a function of maximum drift and number of displacement cycles. Additionally, for both joints and walls, the correlation between damage and other measures of demand, such as maximum shear stress demand or maximum shear stress demand-capacity ratios, was investigated to determine if more accurate damage-prediction models could be developed by grouping data.

### **2.3 DAMAGE**

Damage measures (DMs) describe the damage sustained by a component during an earthquake. DSs quantify damage, defining specific values or ranges of the DMs. In this study DSs define maximum concrete crack widths, the extent of concrete spalling, the extent of concrete crushing, and the initiation of buckling and fracture of reinforcing steel, which can result in failure of the component. The ideal DS is highly correlated with demand and determines the MOR required to restore a damaged

component to per-earthquake condition. DSs are limited to the domain of damage data reported by experimental researchers.

To determine DSs for the current study, the results of previous experimental research were reviewed to determine the type and extent of available damage data and to determine DSs that could be linked with repair. Pagni and Lowes (2006) identified a series of damage states for older beam-column joints that 1) best characterize the progression of damage in joints and 2) best determine the appropriate method of repair for the component. Review of experimental research indicated that many of these DSs were appropriate also for characterizing damage progression in modern joints. The DSs employed for modern joints, which represent a modification of those used for older joints, are presented in Section 4.3. Review of previous experimental research indicated that many fewer damage data were available for walls and, thus, many fewer DSs should be used to characterize the progression of damage in walls. The DSs employed for walls are presented in Section 5.4. The following sections discuss the basic DMs employed in the current study and the identification of specific DSs that can trigger specific MORs.

### **2.3.1 Concrete Cracking**

The first indication of damage in RC components subjected to earthquake loading is typically the initiation, propagation and opening of concrete cracks. Ideally concrete cracking would be defined on the basis of residual crack width, the maximum crack



width observed once earthquake loading has ceased and cracks have closed under gravity loading. Residual crack width is used currently by engineers to determine the type of repair required for an earthquake damaged component. However, experimental researchers rarely report residual crack width. Only maximum concrete crack widths are reported consistently. Thus; for the current study, maximum concrete crack width under earthquake loading was used as a conservative estimate of residual crack width.

In defining damage states associated with concrete cracking, two critical DS are the concrete crack width at which surface finishes, such as paint or plaster, have to be repaired and the crack width at which epoxy injection of cracks is required to restore the component to its pre-earthquake strength and stiffness. Pagni and Lowes (2006) recommend that the development of visible, hairline cracking be used as an indicator of the need to replace surface finishes. Pagni and Lowes (2006) recommend also that a crack width of 0.02 in. be used as the maximum crack width beyond which epoxy injection is required for repair.

### **2.3.2 Concrete Spalling and Crushing**

Spalling of the concrete covering reinforcing steel and crushing of the core concrete are typically the next phases of damage development for RC components. Spalling describes concrete that has become detached from the outer most layer of reinforcement in the component. Crushing of core concrete describes concrete within

the layers of longitudinal steel that has become fragmented. Pictures of test specimens and researchers' statements were used to quantify the extent of spalling and crushing.

In defining damage states associated with concrete spalling and crushing, the critical point is the development of extensive spalling that requires replacement, rather than just patching, of the concrete. Typically concrete must be replaced, rather than patched, if spalling exposes a sufficient length of longitudinal reinforcement that concrete-steel bond may be deteriorated. For joints, Pagni and Lowes (2006) recommend that replacement is required if 80% or more the joint surface area spalls.

### **2.3.3 Failure**

If damage is severe, an RC component may be considered to fail. This requires that the component be replaced. This may be characterized by a loss in lateral or gravity load carrying capacity. Typically, RC components fail as a result of buckling and/or fracture of reinforcing steel. Pagni and Lowes (2006) reviewed experimental data for older joints and identified three potential mechanisms for significant strength loss: loss of gravity load-carrying capacity due to buckling of column longitudinal reinforcement, complete anchorage failure for beam longitudinal reinforcement passing through the joint, which could be expected to result in loss of beam moment capacity, and pull-out of discontinuous beam reinforcement resulting in loss of beam moment capacity. However, modern design codes (ACI 318 2002) require beam bars be continuous

through the joint; thus, only bar buckling and fracture are potential failure mechanisms for modern joints. Following review of experimental data, failure for walls was defined as buckling or fracture of longitudinal reinforcement in the boundary element.

#### **2.3.4 Characterization of Damage Using Laboratory Measurements**

Concrete cracking, spalling and crushing may be observed in the field and have traditionally been used to determine the required method of repair. However, additional data are available from laboratory and numerical simulation. Two such damage measures are used in this study. The first is yielding of the reinforcing steel. For both walls and joints, yielding of reinforcing steel could be expected to result in widening of residual crack widths. Additionally, yielding of transverse reinforcement could be expected to accompany buckling of longitudinal reinforcement in either the boundary element of a wall or in the joint core. Yielding of reinforcing steel is defined by strain gage data. The second damage measure defined by numerical data was failure defined as a loss in lateral load capacity of more than 20%.

### **2.4 METHOD OF REPAIR**

The economic impact of structural damage due to earthquake loading is defined by the cost of the repair method required to restore the structure to pre-earthquake conditions and, since accomplishing the repair typically impacts the functionality of the structure,

the time required to accomplish the repair. Thus, the method of repair required to restore the damage component may be used to assess the economic impact of the earthquake damage.

Pagni and Lowes (2006) reviewed the results of previous experimental research, reviewed manuals of standard practice, and interviewed practicing engineers to identify 1) the MOR that may be used to restore the strength and stiffness of earthquake damaged RC components and 2) damage measures that trigger the use of a particular MOR. Specifically, FEMA 308 Repair of Earthquake Damaged Concrete and Masonry Wall Buildings (ATC 1998) and ACI 546-96 Concrete Repair Guide (1996) were used as a basis for defining and validating MOR. Additionally, for beam-column joints, the results of studies by Jara et al. (1989), Tasai (1992), Karayannis (1998) and Filiatrault (1996) provided further validation that the proposed repair methods may be used to restore strength and stiffness. For walls, studies by Wang et al. (1975) and Vallenat et al. (1979), and Lefas and Kotsovos (1990) validate the proposed repair methods.

The proposed repair methods include: MOR 0) repair cosmetic finishes, MOR 1) epoxy inject concrete cracks, MOR 2) patch spalled concrete, MOR 3) remove and replace crushed concrete, and MOR 4) replace reinforcing steel. These repair methods and the damage measures that trigger the use of specific MOR are discussed below.

#### **2.4.1 Method of Repair 0: Cosmetic Repair**

When earthquake damage is limited to minor cracking, the strength and stiffness degradation of the component will not be significant and repair will not be required to restore the component to pre-earthquake conditions. However, even narrow cracks may reduce fire resistance and allow for water infiltration into damaged surfaces. Additionally, damaged surfaces may reduce the functionality of the structure for occupants. Thus, even minor cracking may require repair to restore surface finishes.

Pagni (2003) defines MOR 0 to include removing, repairing and/or replacing finishes including but not limited to plastering, taping, painting, replacing wallpaper, and recoating and resealing to increase water resistance and/or fire protection. These repairs have no structural impact and do not contribute to strength or stiffness of the component.

Interviews with practicing engineers (Pagni 2003) suggested that the damage level at which MOR 0 was typically determined by the building owner and varied substantially. Pagni and Lowes (2006) recommended employing MOR 0 for hairline cracking up through maximum crack widths of 0.02 in. These recommendations were employed for the current study as well.

#### **2.4.2 Method of Repair 1: Epoxy Resin Injection of Cracked Concrete**

If concrete cracking is significant, repair may be necessary to restore the components stiffness and strength, as well as to ensure that it is not susceptible to water infiltration,

corrosion and fire damage. Typically, epoxy resin or cementitious grout is injected into cracks to restore cracked RC components. Pagni and Lowes (2006) define MOR 1 Epoxy Injection of Cracked Concrete to include all activities associated with epoxy injection of cracks as well as repair of surface finishes. This MOR is comparable to Structural Repair 1 defined in FEMA 308.

Epoxy injection is typically accomplished either by drilling holes along the concrete crack and using pressure injection to push epoxy through these holes to fill the cracks, or by injecting into one area of cracking in the specimen and applying a vacuum to another area of cracking in the specimen to pull the epoxy through (ACI 2003). Epoxy injection may be used on cracks with widths from 0.002 in. to 0.75 in.

The results of previous research verify that that epoxy injection can restore component strength and stiffness to very near approximate pre-earthquake conditions. Tsonos (2001) subjected two half scale exterior beam-column joints to reverse cyclic loading with maximum drift levels of 4.3% and proceeded to repair the joints with pressure epoxy injection; he found that the repaired joints exhibited strength and stiffness characteristics similar to the original findings. Also, French et al. (1990) subjected interior beam-column joints with high bond-stress demands to cyclic lateral loading with a maximum inter-story drift of 3%, used both pressure injection and vacuum impregnation techniques to repair the joints, and observed that the repaired joints had stiffness' that exceeded 85% of the original stiffness, and strengths

approximately equal to the original strength. Similar results could be expected for concrete walls.

For the current study, specimens with maximum crack width in excess of 0.02 in. were considered to require epoxy injection of cracks to restore strength and stiffness.

#### **2.4.3 Method of Repair 2: Patching of Spalled Concrete**

Surface concrete may spall when subjected to moderate to severe earthquake loading. To ensure that the stiffness and strength of the component is restored and to protect the reinforcing steel from corrosion, fire damage, etc. the spalled concrete must be removed and replaced.

MOR 2 involves the patching of surface concrete damage and epoxy injection of cracks; it does not deal with the extensive removal damaged concrete. Method of Repair 2 includes some of the activities specified in FEMA 308 Structural Repair 3. A mortar mix that consists of sand, pea gravel and either a latex modified concrete or an organic base material, such as Portland cement, must be applied to the damaged area after all the spalled and loosened concrete has been removed and the area has been cleaned (FEMA 308).

Previous research shows that patching spalled concrete with a cementitious material restores strength and stiffness to earthquake damaged components. For example, Karayannis et al. (1995) used a paste with low shrinkage, high compressive

and tensile strength, rapid hardening properties, and adhesion properties that were enhanced by the addition of an adhesive to the paste repaired to repair an exterior joint that exhibited spalling of the concrete cover. The strength and stiffness of the repaired joint were comparable to the original, simulated pre-earthquake loading conditions.

The critical issue in linking MOR 2 with DSs is determining the extent of concrete spalling that can adequately be repaired by patching and the extent of spalling that requires replacement of member concrete to ensure restoration of strength and stiffness. Pagni and Lowes (2006) state

*Discussions with engineers and contractors as well as consideration of bond-zone conditions resulted in the decision that, if a substantial area of joint core concrete has spalled, resulting in exposure of most or all of the column longitudinal reinforcement in the joint region, then patching of the spalled concrete is not sufficient.*

Thus, spalling of sufficient concrete to expose a significant area of reinforcing steel that potentially may buckle was considered the limit beyond which replacement rather than patching is required to repair the component. For beam-column joints, spalling of more than 80% of the joint surface area was considered to require concrete replacement rather than just repair. For walls, the initial spalling of the concrete cover as specified within the research document was the limit considered to require replacement rather than just repair of the concrete.



#### **2.4.4 Method of Repair 3: Removal and Replacement of Damaged Concrete**

The removal and recasting of the damaged concrete in a component may be required if spalling of cover concrete is extensive or concrete damage extends to crushing of the core concrete. MOR 3 expands on the activities of MOR 2 to include the removal and replacement of damaged and potentially damaged concrete. To ensure that full bond capacity is recovered, all of the damaged and potentially damaged concrete must be removed and enough new material must be placed around the exposed reinforcement. Standard concrete mix including sand and coarse aggregate is a common replacement material. If more than 6 in. of concrete thickness is removed, mechanical anchorage devices, such as epoxy-embedded dowel bars, are recommended to ensure bond between new and existing concrete (FEMA 308, ACI 546R). MOR 3 employs chipping or jack-hammering to ensure that all the potentially damaged concrete is removed and it also uses typical concrete mixes where MOR 2 does not use either. When the repair requires considerable concrete to be removed shoring may be required to redistribute the gravity load, which will vastly increase the time and cost requirements of the repair.

#### **2.4.5 Method of Repair 4: Removal and Replacement of Damaged Rebar**

Longitudinal reinforcement in a column or boundary element may buckle or fracture under earthquake loading, if exposed as a result of spalling and/or crushing of the concrete. Mechanical connections must be used to replace the reinforcement if this

occurs. Rebar in a beam or web that has been damaged due to deformation may be replaced using MOR 4 as well.

All the actions required to replace the reinforcing steel are included in MOR 4, which include shoring the structure, removing concrete using chipping or jack-hammering, removing the damage sections of reinforcing steel, replacing the reinforcing steel, placing epoxy-embedded dowel bars as necessary and replacing the concrete. Mechanical connections such as a sleeve, splice, or threaded coupler are generally used to connect new and existing reinforcing steel (FEMA 308). Method of Repair 4 is comparable to Structural Repair 4 as defined by FEMA 308.

## **2.5 GROUPING DAMAGE DATA TO ENABLE PREDICTION OF REQUIRED REPAIR**

Pagni and Lowes (2006) developed models defining the probability of earthquake damage requiring, at least, the use of a specific MOR. This requires combining data so that individual data points defined a specific EDP value and the MOR required to restore the component, given that damage level. Pagni and Lowes (2006) identified three plausible approaches to combining the data:

- **Method One:** For each individual specimen, the EDP-damage state pairs for all of the damages states associated with a specific method of repair are used. This method results in the most data points for each method of repair, but also

results in more dispersion and skews the method of repair towards higher EDP levels.

- **Method Two:** For each individual specimen, the EDP-damage state pair for the lowest damage state associated with a specific method of repair is used. This method also introduces some bias towards higher EDP levels, though less than for Method One.
- **Method Three:** Only data for the lowest damage state are used for each method of repair. This method results in the fewest data for each method of repair.

Method Two was chosen for use because this method balances the need to reduce the bias towards higher EDP levels with the need for a large and representative data set. Additionally, this method was used by Pagni and Lowes (2006), enabling comparison of the fragility functions developed here and in the previous study.

## 2.6 SUMMARY AND CONCLUSION

The development of fragility functions requires the identification of EDPs that efficiently predict observed damage, DSs that characterize the progression of damage under earthquake loading and enable determination of the required MOR, and MORs that may be used to restore components to their pre-earthquake condition. The results of the study by Pagni and Lowes (2006) were used as a guideline for identification of

appropriate EDPs, DSs and MORs for joints and walls as well as for determining the DS that triggers the need for a specific MOR.

### **3 Statistical Analysis of Data**

#### **3.1 INTRODUCTION**

For both beam-column joints and walls, the same analytical process was used to develop fragility functions characterizing the potential that a particular building component will require a specific MOR to restore it to pre-earthquake conditions. Once data were collected linking EDPs with MORs, these data were modeled using standard probability distributions. The method of maximum likelihood was used to fit these distributions to the data. Then, standard goodness-of-fit testing was performed to evaluate the distributions. Finally, a preferred distribution was identified for use. Matlab (Mathworks 2005) was used to determine distribution parameters and complete the goodness-of-fit testing. The probability distributions considered and the analysis process used are presented in the following sections.

#### **3.2 STANDARD PROBABILITY DISTRIBUTIONS**

Within the context of this study, a fragility function defines the probability that at a minimum, a specific MOR will be required given a specific value of an earthquake demand measure. Thus, each repair-specific fragility function is a cumulative

probability distribution with an EDP as the random variable. Pagni and Lowes (2006) considered four standard probability distributions in developing fragility functions for older joints: normal, lognormal, Weibull and beta. The same four distributions were considered as part of this study. In addition to the standard probability distributions, the Stepwise probability distribution function (CDF), which may be considered the empirical CDF, is defined for each data set.

The following sections present each distribution in equation form and provide a discussion of the advantages and disadvantages of the distribution. In all of the equations, the variable  $x$  is used to represent the EDP while  $\mu$  and  $\sigma$  represent the mean and standard deviation of the population. For each standard probability distribution, the probability density function (PDF), rather than the cumulative distribution function (CDF) is provided.

### 3.2.1 Normal Distribution

The normal distribution is the most commonly used probability distribution and is appropriate for describing many data sets. The normal distribution is defined for data ranging in valued from negative to positive infinity:

$$f_x(x) = \frac{1}{\sigma_x \sqrt{2\pi}} \exp \left[ -\frac{1}{2} \left( \frac{x - \mu_x}{\sigma_x} \right)^2 \right] \text{ for } -\infty \leq x \leq \infty \quad 3.1$$

where  $\mu_x$  and  $\sigma_x$  are, respectively, the mean and standard deviation of the population, which may be estimated from a sample of the population as follows:

$$\mu_x = \frac{\sum_{i=1}^n x_i}{n} \quad 3.2$$

$$\sigma_x = \sqrt{\frac{\sum_{i=1}^n (x_i - \mu_i)^2}{n}} \quad 3.3$$

where  $x_i$  is a single observation of the variable and  $n$  is the size of the sample

The potential EDPs considered in the current study are always positive. Since the normal distribution is defined for  $-\infty \leq x \leq \infty$ , use of the normal distribution results in a finite probability that a negative EDP will require a specific MOR. Thus, the normal distribution is not desirable for use in the current study.

### 3.2.2 Lognormal Distribution

The lognormal distribution is similar to the normal distribution, but is defined only for positively valued data. Since, the potential EDPs are always positively valued, the lognormal distribution is appropriate for use in the current study. The lognormal distribution is defined:

$$f_x(x) = \frac{1}{\sqrt{2\pi}\zeta_x x} \exp\left[-\frac{1}{2}\left(\frac{\ln x - \lambda_x}{\zeta_x}\right)^2\right] \quad 0 \leq x \leq \infty \quad 3.4$$

where delta is the coefficient of variation,  $\lambda_x$  and  $\zeta_x$  are the mean and variance of the natural log of the data defined by:

$$\lambda_x = \ln \mu_x - \frac{1}{2} \zeta_x^2 \quad 3.5$$

$$\zeta_x^2 = \ln \left[ 1 + \left( \frac{\sigma_x}{\mu_x} \right)^2 \right] = \ln(1 + \delta^2) \quad 3.6$$

### 3.2.3 Weibull Distribution

The Weibull distribution is an asymptotic extreme value distribution, which arises from an underlying distribution that is limited in a tail of interest. Use of the Weibull distributions implies that the current study is defining the PDF of the minimum EDP beyond which a specific MOR is required. The Weibull distribution is defined by

$$f_x(x) = \frac{k}{w} \left( \frac{x}{w} \right)^{k-1} \exp \left[ - \left( \frac{x}{w} \right)^k \right] x \geq 0 \quad 3.7$$

where  $\mu$  and  $\sigma$  for the population are used to solve for  $w$  and  $k$ , such that

$$\mu = w \Gamma \left( 1 + \frac{1}{k} \right) \quad 3.8$$

where  $\Gamma$  is the gamma function. The gamma function may be defined using the polynomial approximation when

$$0 \leq \Gamma(1+x) \leq 1 \quad 3.9$$

This criterion is met for the data considered in this study. Thus,  $\Gamma(1+x)$  may be approximated as

$$a_1 = -0.575, \quad a_2 = 0.951, \quad a_3 = -0.0699, \quad a_4 = 0.425, \quad a_5 = -0.101 \quad 3.10a$$

and

$$|\varepsilon(x)| \leq 5 \times 10^{-5} \quad 3.10b$$

where  $\varepsilon$  is the lower limit of the initial distribution.



The Weibull distribution is appropriate for use in the current study because it  
 1) provides moderately accurate results with small data sets and 2) represent a broad range of distribution shapes so that the distribution with the best fit can be selected.

### 3.2.4 Beta Distribution

The Beta distribution is defined:

$$f_x(x) = \frac{1}{B(q,r)} \frac{(x-a)^{q-1}(b-x)^{r-1}}{(b-a)^{q+r-1}} \quad a \leq x \leq b \quad 3.11$$

where  $a$  and  $b$  are the upper and lower bounds of the data,  $q$  and  $r$  are distribution parameters and  $B(q,r)$  is the beta function, defined:

$$B(q,r) = \frac{\Gamma(q)\Gamma(r)}{\Gamma(q+r)} \quad 3.12$$

where  $\Gamma$  is the gamma function. If the upper and lower limits of the mean,  $\mu$ , and variance,  $\sigma^2$ , of  $x$  are known, then the distribution parameters  $q$  and  $r$  can be estimated using

$$\mu_x = a + \frac{q}{q+r}(b-a) \quad 3.13$$

$$\sigma_x^2 = \frac{qr}{(q+r)^2(q+r+1)}(b-a)^2 \quad 3.14$$

The beta distribution is appropriate for use when the variable is known to be bounded by an upper and lower limit, which is the case in the current study.

### 3.2.5 Stepwise CDF

The Stepwise distribution is an empirical CDF so the PDF is not provided for this distribution. The Stepwise CDF,  $S_n(x)$  is defined by

$$S_n(x) = \begin{cases} 0, & x < x_1 \\ \frac{m_i}{n+1}, & x_m \leq x \leq x_{m+1} \\ 1, & x > x_n \end{cases} \quad 3.15$$

where  $x_i$  is the value of the  $i^{\text{th}}$  data point in the data set,  $m_i$  is the rank (from lowest to highest) of data point  $x_i$  and the total number of data points in the set is  $n$ . The range of the data set defines the extreme values,  $x_1$  and  $x_m$ . If the data set is considered small, as in this study, the rank is normalized by the number of data points plus one,  $n+1$ . The Stepwise CDF,  $S_n(x_i)$ , may be considered the empirical distribution, as such it does not have a functional form but is defined by all of the data points. Since it requires the use of all the data points it is not ideal for modeling purposes, but it is valuable for use in evaluating the functional CDF.

## 3.3 METHOD OF MAXIMUM LIKELIHOOD

The CDFs and PDFs discussed above are defined by the mean and variance of the data population. These parameters may be estimated given a sample of the data, which is what the EDP data set represents. This approach is considered the “Method of Moments” for calibration of the distribution. However, if the mean and standard deviation of the population are estimated using the sample data, additional error is

introduced. This error may be large for a small sample, which is often the case for this study.

To eliminate this error, the “Method of Maximum Likelihood” may be used to estimate the PDF parameters and thus “fit” the PDFs to the data. The Method of Maximum Likelihood finds the distribution parameters,  $p$ , that maximizes the likelihood function:

$$L(x_1, x_2, \dots, x_n; p) = f_x(x_1, p) f_x(x_2, p), \dots, f_x(x_n, p) \quad 3.16$$

where  $f_x$  is the selected probability density function. This approach was used for the current study. The Matlab function **mle** was used to compute distribution parameters using the Method of Maximum Likelihood.

### 3.4 TESTING GOODNESS-OF-FIT

Once the standard probability functions had been fit to the data, standard goodness-of-fit tests were used to evaluate how well the probability functions model the data and to identify the best possible PDF. For the current study, three tests were used: the Kolmogorov-Smirnov (K-S), the Chi-Square ( $\chi^2$ ), and the Lilliefors tests.

#### 3.4.1 Kolmogorov-Smirnov Test (K-S)

The K-S test provides a numerical confirmation of the visual analysis for the best fit of the curve when comparing distribution functions to the Stepwise CDF. The test is accomplished by first finding

$$D_n = \max |F_x(x_i) - S_n(x_i)| \quad 3.17$$

where  $D_n$  is the K-S test parameter,  $F_x$  is the CDF of the selected distribution function, and  $S_n$  is the rank of the Stepwise function. Next, the K-S test value,  $D_n^\alpha$ , is determined.  $D_n^\alpha$  is defined by the significance level,  $\alpha$ , and the size of the sample data set,  $n$ . The significance level,  $\alpha$ , defines the percent of unacceptable distributions that could be expected to pass the test. If  $\alpha$  increases then  $D_n^\alpha$  increases as well;  $D_n^\alpha$  values for different  $\alpha$  values can be found from standard mathematical tables (Haldar and Mahadevan 2000). The significance level is related to the probability of the K-S test parameter being less than or equal to the critical value by Eq.3.18.

$$P(D_n \leq D_n^\alpha) = 1 - \alpha = P^\alpha \quad 3.18$$

where  $P^\alpha$  is the CDF of the K-S parameter at the confidence level of  $1-\alpha$ . If  $D_n < D_n^\alpha$  then the K-S test indicates that the distribution is acceptable with a  $\alpha$ . The Matlab function **kstest** was used to accomplish the K-S test with  $\alpha = 5\%$ .

The K-S test has the advantage that it is appropriate for use with any sample size. However, the K-S test has the limitations: 1) it only applies to continuous distributions, 2) it is more sensitive to the goodness of fit of the center of the distribution than the tails of the distribution, 3) the distribution must be fully specified, so that if some parameters are estimated the test is no longer valid. This third point is particularly critical for the current study, in which the distribution parameters are fit on

the basis of the data sample. Thus, the K-S test is not strictly valid for the current study.

### 3.4.2 Chi-Square test ( $\chi^2$ )

The  $\chi^2$  test compares the observed and theoretical frequency with which the data are modeled by the chosen distribution, within given intervals. The proposed distribution is considered to be appropriate for modeling the data at a confidence level,  $\alpha$ , if

$$E^{x^2} < c_{1-\alpha, f} \quad 3.19$$

where  $c_{1-\alpha, f}$  is the  $\chi^2$  parameter and the error value,  $E^{x^2}$ , and the degrees of freedom,  $f$ , are defined by

$$E^{x^2} = \sum_{i=1}^m \frac{(n_i - e_i)^2}{e_i} \quad 3.20$$

$$f = m - 1 - k \quad 3.21$$

where the observed frequency,  $n_i$ , is the actual number of times the demand occurs in each interval, the theoretical frequency,  $e_i$ , is the expected number of times the demand occurs in each interval,  $m$  is the number of intervals, and  $k$  is the number of parameters in the distribution, which is two for all distributions. The  $\chi^2$  test also requires selecting a confidence level,  $1-\alpha$ ;  $\alpha$  was chosen as 5% for the current study. The Matlab function **icdf** was used to compute  $c_{1-\alpha, f}$ .

In applying the  $\chi^2$  test, it is desirable that  $m$  and  $e_i$  be at least five for satisfactory results (Haldar and Mahadevan 2000) and the total number of data points exceed 50 (Kottegoda and Rosso 1997). The main advantage of the  $\chi^2$  test is that it can be applied to a distribution for which parameters are estimated from a data sample. The main disadvantage of the  $\chi^2$  test is its sensitivity to the size of the data set and how the data are grouped into intervals. The Matlab function **icdf** uses the preferred approach for defining intervals, with approximately the same number of observations are contained in each interval.

### 3.4.3 The Lilliefors Test

Lilliefors test (1967) tests the goodness of fit of the normal distribution for a given data set. For the current study it was used, with the data and the log of the data, to evaluate the acceptability of the normal and lognormal distributions. The Lilliefors test was chosen because, unlike the K-S and  $\chi^2$  tests, it is appropriate for use when distribution parameters are unknown and is exact for small sample sizes, both of which were true for the current study. If the maximum deviation between the empirical CDF and the normal CDF exceeds the critical value of the Lilliefors test for a given significance level, then the hypothesis that the data may be modeled using the normal distribution may be rejected. Applying the Lilliefors test to the log of the data, the hypothesis that the log of the data may be modeled using the normal distribution was evaluated. This hypothesis is equivalent to the hypothesis that the raw data may be modeled using the

lognormal distribution. The Matlab function **lillietest** was used to accomplish the Lilliefors test with a significance level of 5%.

### **3.5 SUMMARY AND CONCLUSION**

The distributions selections considered in the development of the fragility functions included normal, lognormal, Weibull, and Beta distributions. Since the data sets used in the current study were relatively small, the method of maximum likelihood was used to “fit” distribution parameters to the data, rather than the more commonly employed method of moments. For each data set and probability distribution, standard goodness-of-fit tests were used to evaluate how well the function modeled the data. The standard goodness-of-fit tests considered were the K-S,  $\chi^2$  and Lilliefors tests.

## **4 RC Beam-Column Joints**

### **4.1 INTRODUCTION**

Building inventories in most regions include structures of varying ages. Structures built prior to 1967 typically have design details that could be expected to result in non-ductile response under earthquake loading and significant damage at low to moderate earthquake demand levels (Mosier 2000). Structures with modern detailing are expected to exhibit ductile response and develop significant damage only under severe earthquake demands. This chapter presents the development of fragility functions for interior and exterior beam-column building joints with detailing typical of modern construction and compares these with fragility functions developed for pre-1967 joints (Pagni and Lowes 2006). Research activities include the development of experimental data sets, review of experimental data to identify engineering demand parameters that efficiently predict damage, identification of damage states that may be linked with commonly used methods of repair, development of fragility functions that quantify the likelihood a method of repair will be required given a specific measure of earthquake demand, and comparison of fragility functions for different joint configurations and for joints with different design details.



## **4.2 EXPERIMENTAL DATA CHARACTERIZING PERFORMANCE OF BUILDING JOINTS**

### **4.2.1 Introduction**

The results of previous experimental investigations of the earthquake response of beam-column building joints were reviewed to develop a data set to support development of fragility functions. The following sections describe the criteria used to choose tests for the current study, present the test specimens, and discuss design characteristics that could be expected to affect damage progression. Interior beam-column joints are presented first followed by exterior beam-column joints.

### **4.2.2 Criteria Used to Identify Specimens for the Study – Interior Joints**

Tables 4.1 and 4.2 provide design details for interior building joints used in this study. Three criteria were used to identify specimens for use. First, only laboratory specimens with design details representative of modern construction in zones of high seismicity were included. Initially, “representative of modern construction in zones of high seismicity” was defined as joints that have 1) transverse reinforcement, 2) sufficient strength to enable development of the flexural yield strength of the beams framing into the joint, and 3) column-to-beam flexural strength ratios that ensure columns do not exhibit yielding in flexure. However, this initial data set included a number of joints with design parameters that deviated substantially from the 2002 American Concrete Institute (ACI) Building Code (ACI 318 2002) requirements for joints in special

moment frames (SMF), which are expected to sustain deformations into the inelastic range. Thus, a second, reduced, data set was assembled that included only joints with design details approaching the 2002 ACI Code requirements for joints in SMF. It should be noted that this reduced data set includes joints with a wide range of design parameters, but that none of these design parameters was found to be highly correlated with damage (Section 4.4). Code requirements for SMF pertaining to joint design and the range of design parameters defining the reduced data set are as follows:

1. Building columns are typically rectangular with hoop reinforcement. For these beam-column joints, the 2002 ACI Code requires that the total cross-sectional area of rectangular hoop reinforcement,  $A_{sh}$ , not be less than

$$A_{sh} = 0.3 \left( sh_c \frac{f'_c}{f_{yh}} \right) \left[ \left( \frac{A_g}{A_{ch}} \right) - 1 \right] \quad 4.1$$

or

$$A_{sh} = 0.09 sh_c \frac{f'_c}{f_{yh}} \quad 4.2$$

where  $s$  is the hoop spacing,  $h_c$  is the depth of the column,  $f'_c$  is the concrete compressive strength,  $f_{yh}$  is the nominal yield strength of the transverse steel,  $A_g$  is the gross area of the column, and  $A_{ch}$  is the area of the column measured out-to-out of transverse reinforcement, and units are inches and psi. Joints with transverse reinforcement ratios equal to the ACI Code required minimum, plus

or minus 50%, were included in the reduced data set. Actual, rather than nominal material strengths were used.

2. To ensure adequate anchorage of beam longitudinal reinforcement that is continuous through the joint, the 2002 ACI Code requires that the column dimension parallel to the axis of the beam reinforcement exceed  $20d_b$  where  $d_b$  is the maximum diameter of the beam longitudinal reinforcement. Joints with column depths ranging from  $10d_b$  to  $30d_b$  were included in the reduced data set.
3. The nominal shear strength of joints confined on two opposite faces, as is the case for interior beam-column building joints with no out-of-plane beams or slabs, is defined as  $15\sqrt{f'_c}A_j$  psi where  $f'_c$  is the concrete compressive strength in psi, and  $A_j$  is the cross-sectional area of the joint in square inches, which is defined equal to the cross-sectional area of the column. Following the ACI Code specified design procedure, it is required that the design joint shear strength exceed the joint shear stress demand, which is computed using the recommendations of ACI Committee 352 (2002). For the current study, interior beam-column joints with maximum shear stress demands ranging from  $7.5\sqrt{f'_c}A_j$  to  $22.5\sqrt{f'_c}A_j$  were included in the reduced data set.
4. The sum of the column flexural strengths above and below the column must not be less than 1.2 times the sum of the beam flexural strengths on either side of the joint. This is intended to produce flexural yielding in the beams and limit

the possibility that column yielding will result in a soft-story mechanism (ACI Com. 352 2002). Only joints with column-to-beam strength ratios not less than 1.2 were included in the reduced data set. However, because column yielding was considered to be representative of older rather than modern construction, no sub-assemblages that exhibited column yielding were included in the initial, full data set. Thus, this criterion resulted in only one specimen being excluded from the reduced data set.

The second criterion used to identify specimens for the study was laboratory test configuration. Only laboratory tests with the same basic sub-assemblage configuration and load pattern were used. Sub-assemblages from two-dimensional building frames, comprising the joint, the beams framing into the joint and extending to mid-span, and the columns framing into the joint and extending to mid-height were included in the study. Joints with out-of-plane framing members, and slab-beam-column joints were not included in the study. Lateral loading was applied as a shear load at the top of the column and reacted by shear loads at the base of the column and beam ends. If, under earthquake loading, beams and columns develop a point of contra-flexure at mid-span, then this laboratory load distribution is representative of earthquake loading in a real building. Simulated earthquake load was applied pseudo-statically by forcing the top of the column through a prescribed cyclic displacement history (relative to the beam ends and column base) consisting of one or more cycles at

increasing maximum displacement demands. In some cases, a constant axial load was applied at the top of the column to represent gravity load.

The third criterion used to identify test specimens for inclusion in the study was the availability of damage data. A specimen was included in this study only if the researchers provided sufficient data characterizing the progression of damage in the joint. In many cases, researchers did not publish data characterizing maximum concrete crack widths, the extent of cracking, or the extent of spalling, nor did they provide pictures from which these damage measures could be determined. In many cases the lack of sufficient damage data eliminated joint specimens from use in the study.

#### **4.2.3 Experimental Data Used in the Study – Interior Joints**

Eleven test programs and 45 test specimens were found that met the criteria employed initially to identify test specimens. Of these, 10 tests programs and 24 test specimens met the more stringent design criteria and were included in the reduced data set. Test specimens are listed in Table 4.1 and 4.2. Following is a brief discussion of the test programs and test specimens:

- *Beckingsale et al. (1980)* investigated the response of joints subjected to cyclic loading, proposed mechanisms of shear resistance and made recommendations for design. Data from all three of the specimens tested by Beckingsale et al. were used in the current study (B11, B12, B13).

- *Birss et al. (1978)* investigated the elastic and post-yield response of joints subjected to cyclic loading, using experimental data to validate a proposed design method. Data from both of the specimens tested by Birss et al. were used (B1, B2).
- *Durrani and Wight (1982)* tested six full-scale sub-assemblages, three with continuous slabs and three without, to investigate the effect of transverse reinforcement and the presence of slabs on joint response. Data from the three test specimens without slabs were used in the current study (X1, X2, X3).
- *Endoh et al. (1991)* tested four half-scale sub-assemblages, two with normal-weight and two with lightweight concrete, to investigate beam bar anchorage and joint shear strength. Data from the normal-weight test specimens that exhibited beam yielding prior to joint failure was used (HC).
- *Hayashi et al. (1993)* tested eleven half-scale sub-assemblages under cyclic loading to investigate beam-bar anchorage in the joint and evaluate a proposed model. Only data from one test (NO. 47) were used in the current study. Sufficient damage data were provided only for this specimen.
- *Joh et al. (1991a, 1991b)* investigated the impact of joint and beam transverse reinforcement as well as beam eccentricity on earthquake response. They concluded that increasing the volume of transverse reinforcement results in decreased bar slip, increased energy dissipation, and increased post-cracking stiffness. Only specimens with concentric connections were used in the current study (B1, B2, B8-HH, B8-HL, B8-LH and B8-MH).

- *Milburn and Park (1982)* investigated the effect of relocating the beam plastic hinge away from the column face and of joint transverse reinforcement volume on earthquake response. The results of the study verified the adequacy of NZS 3101:1982 (Standards Association of New Zealand) and showed that hinge relocation resulted in easier detailing of the joint. Data from two interior joint tests conducted by Milburn and Park were used (Unit 1-2).
- *Otani et al. (1984)* tested twelve joint sub-assemblages, six with spandrel walls built continuous with the beams and six without spandrel walls, to evaluate the effect of transverse reinforcement ratio and beam bar anchorage length on response. It was concluded that a minimum ratio of column depth to beam bar diameter must be maintained and that a method to estimate the yield and ultimate deflection was needed for design. Data from sub-assemblages without spandrel walls were used (J1-J6).
- *Park and Ruitong (1988)* investigated the effect of transverse reinforcement and beam bar diameter on earthquake response. Four joint sub-assemblages, one designed per NZS 3101:1982 (Standards Association of New Zealand) and three designed with reduced transverse reinforcement ratios and/or reduced beam-bar anchorage lengths, were tested. Data from all four test specimens were used in the current study (Unit 1-4).
- *Teraoka et al. (1990) and Teraoka et al. (1997)* investigated the earthquake response of joints constructed using high-strength materials and used experimental data to validate design and response models. Data for six sub-assemblages from the first test

series (HNO-1 to HNO-6) and five from the second test series (HJ-2, HJ4 to HJ-9, HJ-12 and HJ-14) were used for the current study. Sufficient damage data were provided only for these specimens.

- *Zaid et al. (2001)* tested four building joint sub-assemblages under cyclic loading to investigate joint shear strength, beam-bar average bond strength, and the impact of joint transverse reinforcement on these quantities. The researchers concluded that joint detailing could improve shear resistance, energy dissipation and joint deformation capacity. Data for two sub-assemblages, which had typical detailing and exhibited beam yielding, were used for the current study (S1, S2).



Table 4.1. Design Details and Load Data for Experimental Test Specimens in the Reduced Data Set

Specimen	f'c (psi)	Trans. Steel Ratio (%)	Ratio of Provided to Required Trans. Steel	Min. Column Depth / Beam Long. Steel Dia.	Max. Bond Index, $\mu$	Max. Shear Stress Demand/ $\sqrt{f'c}$ (psi)	Column to Beam Strength Ratio	Col. Axial Load / f'cAg	Beam to Column Width Ratio
Birss-B1	4047	0.92	1.27	22.9	14.4	9.3	1.2	0.05	0.78
Durrani-X1	4980	0.76	0.68	19.0	18.3	13.2	1.8	0.05	0.77
Durrani-X2	4880	1.15	1.05	19.0	18.5	13.5	1.9	0.06	0.77
Durrani-X3	4500	0.76	0.75	19.0	19.2	10.4	1.5	0.05	0.77
Endoh-HC	6016	0.63	0.47	30.1	11.6	15.8	1.6	0.00	0.67
Hayashi-NO47	7865	0.79	0.53	21.1	14.9	13.0	2.1	0.18	0.75
Joh-B8-MH	4076	0.42	0.63	23.1	19.9	8.7	0.0	0.14	0.67
Milburn-Unit 2	6802	2.54	1.44	20.3	13.3	15.3	1.2	0.10	0.75
Otani-J1	3727	0.28	0.45	23.1	20.6	13.7	1.9	0.00	0.67
Otani-J2	3485	0.57	0.97	23.1	21.4	14.6	0.0	0.00	0.67
Otani-J4	3727	0.28	0.45	23.1	20.6	13.3	0.0	0.00	0.67
Otani-J6	4167	0.43	0.61	23.1	16.9	9.0	1.6	0.00	0.67
Park-Unit 2	5221	1.58	1.04	20.3	14.8	8.5	2.8	0.00	0.75
Teraoka-HJ-2	7823	0.79	0.56	25.0	20.5	16.2	2.2	0.20	0.75
Teraoka-HJ-4	7823	0.79	0.56	21.1	14.9	20.4	2.1	0.20	0.75
Teraoka-HJ-5	7823	0.79	0.56	21.1	25.1	22.0	1.8	0.20	0.75
Teraoka-HJ-6	7823	0.79	0.56	21.1	33.4	21.4	1.9	0.20	0.75
Teraoka-HJ-9	12801	1.01	0.86	21.1	26.1	22.3	1.8	0.20	0.75
Teraoka-HNO1	12858	0.86	0.60	25.0	15.6	16.6	2.0	0.17	0.75
Teraoka-HNO3	12858	0.86	0.68	18.2	15.5	21.9	1.3	0.17	0.75
Teraoka-HNO4	12858	0.86	0.68	18.2	21.2	19.8	1.1	0.17	0.75
Teraoka-HNO5	16954	0.86	0.48	25.0	13.6	17.3	1.7	0.13	0.75
Zaid-S1	3481	0.36	0.46	30.0	16.0	8.1	4.5	0.05	0.67
Zaid-S2	3481	0.36	0.50	30.0	16.0	7.6	1.6	0.05	0.67
reduced set of test specimens	Min.	0.28	0.45	14.2	11.6	7.6	0.0	0.00	0.67
	Max.	2.54	1.44	30.1	44.2	22.3	4.5	0.36	0.88
	Ave.	0.79	0.70	22.3	19.5	14.5	1.6	0.11	0.73
	C.O.V.	0.59	0.38	0.17	0.36	0.33	0.6	0.87	0.07

Table 4.2. Design Details and Load Data for Experimental Test Specimens Not Included in the Reduced Data Set

Specimen	f <sub>c</sub> (psi)	Trans. Steel Ratio (%)	Ratio of Provided to Required Trans. Steel	Min. Column Depth / Beam Long. Steel Dia.	Max. Bond Index, $\mu$	Max. Shear Stress Demand/ sqrt(f <sub>c</sub> ) (psi)	Column to Beam Strength Ratio	Col. Axial Load / f <sub>c</sub> Ag	Beam to Column Width Ratio
Beckingsale-B11	5207	1.82	1.87	24.1	12.4	9.3	2.0	0.05	0.78
Beckingsale-B12	5018	1.82	1.94	24.1	12.7	9.6	1.4	0.05	0.78
Beckingsale-B13	4554	1.46	1.71	24.1	13.3	10.3	2.1	0.26	0.78
Birss-B2	4569	0.23	0.32	22.9	13.5	8.5	1.2	0.44	0.78
Joh-B1	3901	0.22	0.34	23.6	19.9	7.5	0.0	0.15	0.50
Joh-B2	3269	0.22	0.33	23.6	19.9	13.8	0.0	0.17	0.93
Joh-B8-HH	3713	0.61	3.08	23.1	20.8	8.9	0.0	0.15	0.67
Joh-B8-HL	3974	0.61	2.88	23.1	20.1	8.8	0.0	0.14	0.67
Joh-B8-LH	3429	0.22	0.31	23.1	19.9	11.1	0.0	0.17	0.67
Milburn-Unit 1	5990	2.54	1.64	25.4	11.6	15.1	1.3	0.10	0.75
Otani-J3	3485	1.71	2.90	23.1	21.4	16.0	0.0	0.00	0.67
Otani-J5	4167	0.28	0.40	23.1	19.5	12.7	0.0	0.00	0.67
Park-Unit 1	6657	1.30	0.69	25.4	10.3	5.1	2.9	0.00	0.75
Park-Unit 3	5250	0.56	0.31	25.4	11.6	4.8	2.7	0.00	0.75
Park-Unit 4	5816	0.81	0.46	20.3	14.1	6.6	2.6	0.00	0.75
Teraoka-HJ-12	12801	1.01	0.86	18.2	21.1	37.8	1.2	0.20	0.75
Teraoka-HJ-14	17068	1.01	0.65	18.2	18.3	34.2	1.3	0.20	0.75
Teraoka-HJ-7	12801	1.01	0.86	18.2	14.9	23.6	1.8	0.20	0.75
Teraoka-HJ-8	12801	1.01	0.86	18.2	21.1	23.0	1.9	0.20	0.75
Teraoka-HNO2	12858	0.86	0.60	25.0	15.6	24.1	2.0	0.17	0.75
Teraoka-HNO6	16954	0.86	0.52	18.2	18.5	25.7	1.2	0.13	0.75
all test specimens (includes Reduce Set)	Min.	0.22	0.31	14.2	10.3	4.8	0.0	0.00	0.50
	Max.	2.54	3.08	30.1	44.2	37.8	2.9	0.44	0.93
	Ave.	0.90	0.94	22.2	18.4	14.5	1.3	0.12	0.73
	C.O.V.	0.64	0.77	0.13	0.34	0.50	0.7	0.88	0.09

#### 4.2.4 Factors that Determine Earthquake Performance - Interior Joints

The specimens listed in Tables 4.1 and 4.2 have design details representative of modern construction and were subjected to similar simulated earthquake loads in the laboratory. However, there are differences in specimen design and load characteristics that might be expected to result in variability in the observed damage patterns. For example, the results of several studies suggest that increasing the volume of joint transverse reinforcement reduces damage and delays failure (Durrani and Wight 1982, Pessiki et al. 1990, Joh et al. 1991a,b). The results of previous research indicate also that joint performance, as defined by the extent of damage and/or the drift level at which strength loss initiates, deteriorates with joint shear stress demand (Meinheit and Jirsa 1981, Durrani and Wight 1982). The results of several studies indicate that increased bond stress demand results in increased damage and reduced drift capacity (Park and Ruitong 1988, Leon 1990). In this study the bond index,  $\mu$ , which is equal to the average beam-bar bond stress in the joint, normalized by the square root of the concrete compressive strength, assuming the reinforcing bar yields on opposite sides of the joint was used to assess bond demand. The bond index is defined as

$$\mu = \frac{d_b f_y}{2l_d \sqrt{f_c}} \quad 4.3$$

where  $d_b$  is the diameter of the beam reinforcement bar,  $f_y$  is the steel yield strength,  $l_d$  is the beam-bar anchorage length within the joint (assumed equal to the column in-plane cross-section height), and  $f_c$  is the concrete compressive strength. A

few researchers have considered the impact of column axial load on joint performance, but the results of these studies are not conclusive (Bonnaci and Pantazopoulou 1993, Kitayama et al. 1991).

The impact of these parameters on damage progression is presented in Section 4.4.2.1.

#### **4.2.5 Criteria Used to Identify Specimens for the Study – Exterior Joints**

Table 4.3 list design details for the exterior beam-column joint specimens used in this study. The same three criteria that were used to identify interior joints for use in this study were used for exterior joints. First, only exterior joints with design details representative of modern construction were included in this study. Evaluation of experimental data indicated that relatively few exterior joint test specimens had design details that met current code requirements (ACI 318-02) for SMF. Thus, for the current study, “representative of modern construction” was defined as having sufficient strength to develop beam yield strength and joint design parameters that fell within 50% of the ACI Code requirements for SMF.

1. Eq. 4.1 and 4.2 define the area of transverse reinforcement required by the Code for building joints, including exterior joints. Joints with transverse reinforcement that had transverse reinforcement ratios equal to the code requirement plus or minus 50% were included in the data set. Karayannis et al

(1995) did not report  $f_{yh}$  in their report so the transverse reinforcement was assumed to have a nominal strength of 40 ksi and an actual strength of 50 ksi.

2. The ACI Code requires that beam longitudinal reinforcement be anchored with 90° hooks in the exterior joint and have an anchorage length,  $l_{dh}$ , not less than the largest of  $8d_b$ , 6 inches or  $l_{dh} = f_y d_b / (65\sqrt{f'_c})$  where  $f_y$  is the yield strength of the beam bar,  $d_b$  is the diameter of the beam bar and  $f'_c$  is the compressive strength of the concrete. Typically,  $l_{dh}$  is measured from the face of the column to the outer edge of the hook. Joints were included in the data set which had a value of plus or minus 50% of the code value.
3. The ACI Code defines the nominal shear strength of joints confined on one face, as is the case for exterior beam-column building joints with no out-of-plane beams or slabs, to be  $12\sqrt{f'_c}A_j$  psi where  $f'_c$  is the concrete compressive strength in psi, and  $A_j$  is the cross-sectional area of the joint in square inches, defined as equal to the cross-sectional area of the column. Following the ACI Code specified design procedure, it is required that the design joint shear strength exceed the joint shear stress demand, which is computed using the recommendations of ACI Committee 352 (2002). Joints were included in the data set that had shear stress demands equal to the code defined strength plus or minus 50%.

Second, laboratory test configuration was used to identify specimens. Only laboratory tests with the same basic sub-assembly configuration and load pattern were used. Sub-assemblages from two-dimensional building frames, comprising the joint, the beam framing into the joint and extending to mid-span, and the columns framing into the joint and extending to mid-height were included in the study. Joints with out-of-plane framing members and slab-beam-column joints were not included in the study. Lateral loading was applied as a shear load at the top of the column and reacted by shear loads at the base of the column and beam end. If, under earthquake loading, the beam and columns develop a point of contra-flexure at mid-span, then this laboratory load distribution is representative of earthquake loading in a real building. Simulated earthquake load was applied pseudo-statically by forcing the top of the column through a prescribed cyclic displacement history (relative to the beam end and column base) consisting of one or more cycles at increasing maximum displacement demands. In some cases, a constant axial load was applied at the top of the column to represent gravity load.

Third, the availability of damage data was used to identify test specimens for inclusion in the study. A specimen was included in this study only if the researchers provided sufficient data characterizing the progression of damage in the joint. In many cases, researchers did not publish data characterizing maximum concrete crack widths, the extent of cracking, or the extent of spalling, nor did they provide pictures from

which these damage measures could be determined. In many cases the lack of sufficient damage data eliminated joint specimens from use in the study.

Table 4.3 Design Details and Load Data for Exterior Experimental Test Specimens

Specimen	$f'_c$ (psi)	Trans. Steel Ratio Req'd (%)	Ratio of Provided to Required Trans. Steel	$l_{dh}$ provided/ $l_{dh}$ required	Max. Shear Stress Demand/ $\sqrt{f'_c}$	Col. Axial Load / $f'_c A_g$	Beam to Col. Width Ratio
Karayannis-EJ1	3664	2.43	0.62	N/A	N/A	0	1.00
Karayannis-EJ5	2364	1.57	0.64	N/A	N/A	0	1.00
Karayannis-EJ6	2837	1.88	0.53	N/A	N/A	0.10	1.00
Milburn-Unit 4	5584	1.44	0.51	1.4	10.6	0.10	0.75
Penelis-A1	3770	0.51	1.32	1.1	10.0	0.20	1.00
Penelis-A2	4490	0.60	1.39	1.3	11.7	0.20	1.00
Penelis-A3	4960	0.67	1.01	1.1	10.4	0.20	1.00
Penelis-A4	4900	0.66	1.02	1.1	12.7	0.20	1.00
Penelis-C1	3700	0.50	1.35	1.1	11.3	0.20	1.00
Penelis-C2	4060	0.55	1.54	1.2	13.1	0.20	1.00
Penelis-C3	4930	0.66	1.01	1.1	12.7	0	1.00
Penelis-C4	4900	0.66	1.02	1.1	12.7	0	1.00
Penelis-M1	3620	0.49	1.38	1.1	12.0	0	1.00
Penelis-M2	4930	0.66	1.27	1.2	13.7	0	1.00
Penelis-M3	3910	0.53	1.28	1.1	14.9	0	1.00
Penelis-M4	4860	0.65	1.03	1.1	17.0	0	1.00
Penelis-MS3	3770	1.22	0.50	1.1	18.4	0.40	0.85
Penelis-MS4	4880	1.15	0.88	1.1	14.9	0.10	1.00
Renton-Unit 1	3730	1.40	0.71	0.9	11.0	0.18	0.80
Renton-Unit 2	5570	2.01	0.66	1.1	10.3	0.12	0.80
Renton-Unit 3	3440	1.28	1.29	0.8	11.4	0.19	0.80
Renton-Unit 4	4220	1.57	1.05	1.0	13.5	0.16	0.80
Smith-Unit 4	2970	1.42	0.79	0.9	4.4	0.00	0.77
Tsonos-A1	5076	2.19	0.44	1.0	8.8	0.14	1.00
Tsonos-E1	5076	2.19	0.46	0.7	8.3	0.14	1.00
Min.	2364	0.49	0.44	0.7	4.4	0.00	0.67
Max.	10000	2.43	1.54	1.4	18.4	0.40	1.00
Ave.	4470	1.15	0.95	1.1	11.9	0.11	0.93

Note: N/A implies data are not available

#### 4.2.6 Experimental Data Used in the Study – Exterior Joints

Four test programs and 20 test specimens were found that met the criteria employed to identify exterior beam-column building joint test specimens for the study. Test specimens are listed in Table 4.3. Following is a brief discussion of the test programs and test specimens:

- *Karayannis et al.* (1995) tested five full-scale exterior joints under cyclic loading and then repaired the joints by injecting the cracks with a resin paste and replaced the damaged concrete with high strength cement paste. The joints were then retested and found to perform as well or better than the originals maintaining as many full load cycles as the original joints without significant loss of strength or stiffness. In this test program, EJ1, EJ5 and EJ6 had typical detailing and were used in the current study. Only data from load cycles prior to repair were used.
- *Milburn and Park* (1982) investigated the impact on earthquake response of relocating the beam plastic hinge away from the column face and of varying joint transverse reinforcement volume. The results of the study verified the adequacy of NZS 3101:1982 (Standards Association of New Zealand) and showed that hinge relocation resulted in reduced congestion in joint reinforcing steel. Data from the one exterior joint (Unit 4) test that did not have the hinge relocated and had regular configuration was used.
- *Renton* (1972) tested four full-scale exterior joints and studied the failure mechanisms and stiffness degradation. The main parameters in the study were the



amount of transverse reinforcement in the joint, anchorage of the beam reinforcing steel in the joint, and the amount of transverse reinforcement in the column. Renton concluded that the anchorage length should at least meet ACI 318-71 requirements and that the inclusion of cross ties in the joint transverse reinforcement layout would forestall yielding and aid the earthquake resistance of the joint. All four joints (Unit 1, Unit 3 and Unit 4) were used in the current study.

- *Tsonos et al.* (1994) tested fourteen exterior joints to study the effect of variable axial loading in comparison to constant axial loading. The main variables for the study were the axial load, ratio of column flexural capacity to that of the beam, the joint shear stress level, and the amount of transverse reinforcement in the joint. The researchers concluded that increased axial load contributed to major deterioration in the earthquake resistance of the joints. All fourteen joints (A2 – A4, C1 – C4, M1 – M4, MS3 and MS4) were used in the current study.

#### **4.2.7 Factors that Determine Earthquake Performance - Exterior Joints**

The specimens listed in Table 4.3 have design details representative of modern construction and were subjected to similar simulated earthquake loads in the laboratory. As was the case for interior joint specimens, there are differences in specimen design and load characteristics that might be expected to result in variability in the observed damage patterns. The impact of these parameters on damage progression is presented in Section 4.4.2.1.

### **4.3 ENGINEERING DEMAND PARAMETERS, DAMAGE STATES AND METHODS OF REPAIR FOR JOINTS**

#### **4.3.1 Engineering Demand Parameters (EDP)**

EDPs for development of fragility functions for RC components are introduced in Section 2.2. The results of Pagni and Lowes (2006) were used as a basis for identifying potential EDPs for beam-column joints for this study. These include:

- Inter-story drift: Drift is a simple demand measure provided by all researchers, and there is consensus among engineers that drift is a measure of earthquake demand. However, in a building frame inter-story drift comprises the deformation of beams and columns joints. Thus, it is an imperfect measure of joint demand.
- Number of load cycles: Like drift, the number of load cycles is a simple demand measure provided by all researchers. Additionally, previous experimental research indicates that the number of load cycles may affect the performance of reinforced concrete components (El-Bahy et al. 1999, Walker 2001, Alire 2003). The number of load cycles was computed from the displacement history and a cycle counting algorithm was employed in which the contribution of a specific displacement cycle was weighted by the ratio of the maximum displacement demand of the cycles to the maximum historic displacement demand (Pagni 2003).
- Drift in combination with the number of load cycles for joints: The results of previous research suggest that earthquake demand may be characterized as a function of deformation demand and dissipated hysteretic energy (Park and Ang 1985). Since

hysteretic energy cannot be computed efficiently from non-digital data and is a function of the number of load cycles, Pagni (2003) propose a functional EDP that includes inter-story drift and number of load cycles:

$$F = aD^b + cN^d \quad 4.4$$

where  $D$  is the maximum drift demand,  $N$  is the number of load cycles computed from the drift history. Empirical parameters are defined in Table 4.4; computation of these parameters is discussed in Section 4.4.2.

Table 4.4 Empirical parameters for Eq. 4.4

	All Modern Interior Joints	Reduced Set of Modern Interior Joints	Pre-1967 Designed Joints	All Exterior Joints
a	0.159	0.026	0.252	0.014
b	0.781	1.780	0.645	1.158
c	0.099	0.217	0.018	0.245
d	0.277	0.181	0.819	0.396

Note: Empirical parameters for Pre-1967 designed joints taken from Pagni (2003)

- Joint shear strain: Maximum joint shear strain is a direct measure of joint deformation and thus represents an improvement over inter-story drift. However, joint shear strain may be measured in multiple ways in the laboratory, and these data are provided by few researchers. Both of these factors may increase the dispersion of the data.
- Joint shear strain in combination with the number of load cycles: A functional EDP that includes both maximum joint shear strain and number of load cycles is considered the most desirable EDP. Here this functional EDP is defined:

$$F = a\gamma^b + cN^d \quad 4.5$$

where  $\gamma$  is the maximum joint shear strain,  $N$  is the number of load cycles. Empirical parameters are defined in Table 4.5; computation of these parameters is discussed in Section 4.4.2.

Table 4.5 Empirical Parameters for Eq. 4.5

	All Modern Interior Joints	Reduced Set of Modern Interior Joints	Pre-1967 Designed Joints	All Exterior Joints
a	3.327	3.327	1.457	1.220
b	0.522	0.522	0.481	480.2
c	0.039	0.039	0.200	0.208
d	0.863	0.863	0.309	0.624

Note: Empirical parameters for Pre-1967 designed joints taken from Pagni (2003)

#### 4.3.2 Damage Measure (DM)

A series of fifteen damage states was used to characterize the progression of damage in joints with modern detailing. Table 4.6 lists these damage states as well as those employed by Pagni and Lowes (2006) for older beam-column joints. Damage states for modern joints are identical to those employed by Pagni and Lowes for older joints (2006) with three exceptions. First, a new DS was added (Damage State 4) that is defined by yielding of joint transverse reinforcement. Since older joints typically do not have transverse reinforcement, this damage state was not included in the previous study. Second, the previous study included a damage state characterized by yielding of the longitudinal reinforcement (Damage State 4 in the previous study); this damage

state was removed in the current study. For joints with modern detailing, yielding of beam longitudinal reinforcement was not found to correlate well with demand. Third, Damage State 6, defined as the onset of beam bar slippage in the joint, was added. For joints with modern detailing, initial slip of beam reinforcement typically was not substantial and was accompanied by moderate concrete cracking. This damage state was not included for older joints; for older joints, observed bar slip typically was substantial and was associated with joint failure (Damage State 13).

Table 4.6 Description of DSs for Joints

Description of the Damage State	Damage State	
	Modern Interior and Exterior Joints	Older Joints (Pagni and Lowes)
Initial hairline cracking at the beam-column interface.	0	0
Initial hairline cracking within the joint area.	1	1
Maximum crack width within the joint is measurable but less than 0.02 in. (0.5 mm)	2	2
Crack width within the joint is greater than 0.02 in. (0.5 mm)	3	3
Beam longitudinal reinforcement yields	-	4
Transverse reinforcement yields	4	-
Maximum crack width within the joint is greater than 0.05 in. (1.3 mm)	5	5
Initiation of beam bar slippage	6	-
Spalling of at least 10% joint surface concrete	7	6
Joint shear strength begins to deteriorate	8	7
Spalling of more than 30% joint surface concrete	9	8
Cracks extend into the beam and/or column	10	9
Spalling of more than 80% joint surface concrete	11	10
Crushing of concrete extends into joint core	12	11
Failure due to a) buckling of longitudinal steel reinforcement, b) loss of beam longitudinal steel anchorage within the joint core, or c) pull-out of discontinuous beam longitudinal steel reinforcement	13 (pull-out does not occur)	12

### 4.3.3 Method of Repair (MOR)

MORs are used to restore damaged components to their pre-earthquake condition. Table 4.7 links MOR with DS for the different sets of joint data considered in the study. Figure 4.1 shows representative damage for each of the MORs. An in depth description of the MOR and linkages between MOR and DSs can be found in Section 2.4.

Table 4.7 Methods of Repair for Joints

Method of Repair	Activities	DS for Modern Joints (Interior & Exterior)	DS for Older Interior Joints (Pagni & Lowes)
0. Cosmetic Repair	Replace and repair finishes	0 to 2	0 to 2
1. Epoxy Injection	Inject cracks with epoxy and replace finishes	3 to 6	3 to 5
2. Patching	Patch spalled concrete, epoxy inject cracks and replace finishes	7 to 9	6 to 8
3. Replace Concrete	Remove and replace damaged concrete, and replace finishes	10 to 12	9 to 11
4. Replace Joint	Replace damaged reinforcing steel, remove and replace concrete, and replace finishes	13	12

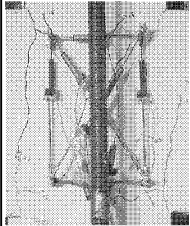
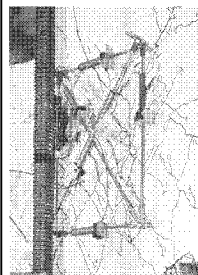
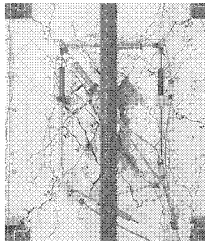
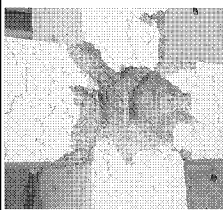
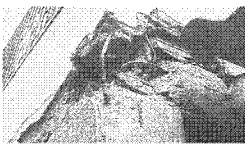
MOR 0 Cosmetic Repair	MOR 1 Epoxy Injection	MOR 2 Patching	MOR 3 Replace Concrete	MOR 4 Replace Joint
				
Spec. PEER 22 (Walker 2001)	Spec. CD30 22 (Walker 2001)	Spec. PEER 22 (Walker 2001)	Spec. CD 1514 (Walker 2001)	Existing joint in Caracas, Venezuela 1967
Replace and repair finishes.	Inject cracks with epoxy and replace finishes.	Patch spalled concrete, epoxy inject cracks and replace finishes.	Remove and replace damaged concrete, and replace finishes.	Replace damaged reinforcing steel, remove and replace concrete, and replace finishes.

Figure 4.1 Pictures and descriptions of DMs associated with MORs

## 4.4 DAMAGE VERSUS ENGINEERING DEMAND PARAMETER

### 4.4.1 Introduction

With EDPs and DSs identified, the relationship between EDPs and DSs were investigated to determine 1) the EDPs that most efficiently predict the progression of damage and 2) joint design parameters that may affect the EDP-DS relationship.

### 4.4.2 Interior Joints

Experimental data characterizing the progression of damage for the test specimens were used to generate data sets linking the fifteen damage states with the potential EDPs. The functional EDPs, defined by Eqs. 4.4 and 4.5, were calibrated to minimize the dispersion of the data about a line extending through all of the damage states and

spanning a range of functional EDP values from 0 to 1.0. Figure 4.2 shows the damage-EDP data for the full and reduced data sets and provides correlation coefficients, computed assuming a linear relationship between damage and EDPs, for the data.

The data in Figure 4.2 support several conclusions. First, the data indicate that drift and the functional EDPs are the most efficient predictors of damage. Similar results were obtained for older joints (Pagni and Lowes 2006). Second, the data suggest that there is not a significant difference in damage progression for the full and reduced data sets. Third, the scatter of the data in the full and reduced sets is approximately the same; though, correlation coefficient for the reduced data set are slightly larger for EDP defined by drift or number of load cycles. This is supported by the EDP-damage sets for which demand is defined by drift, number of load cycles or a function drift and number of load cycles, since these data sets have approximately equal correlation coefficients for the full and reduced data sets.



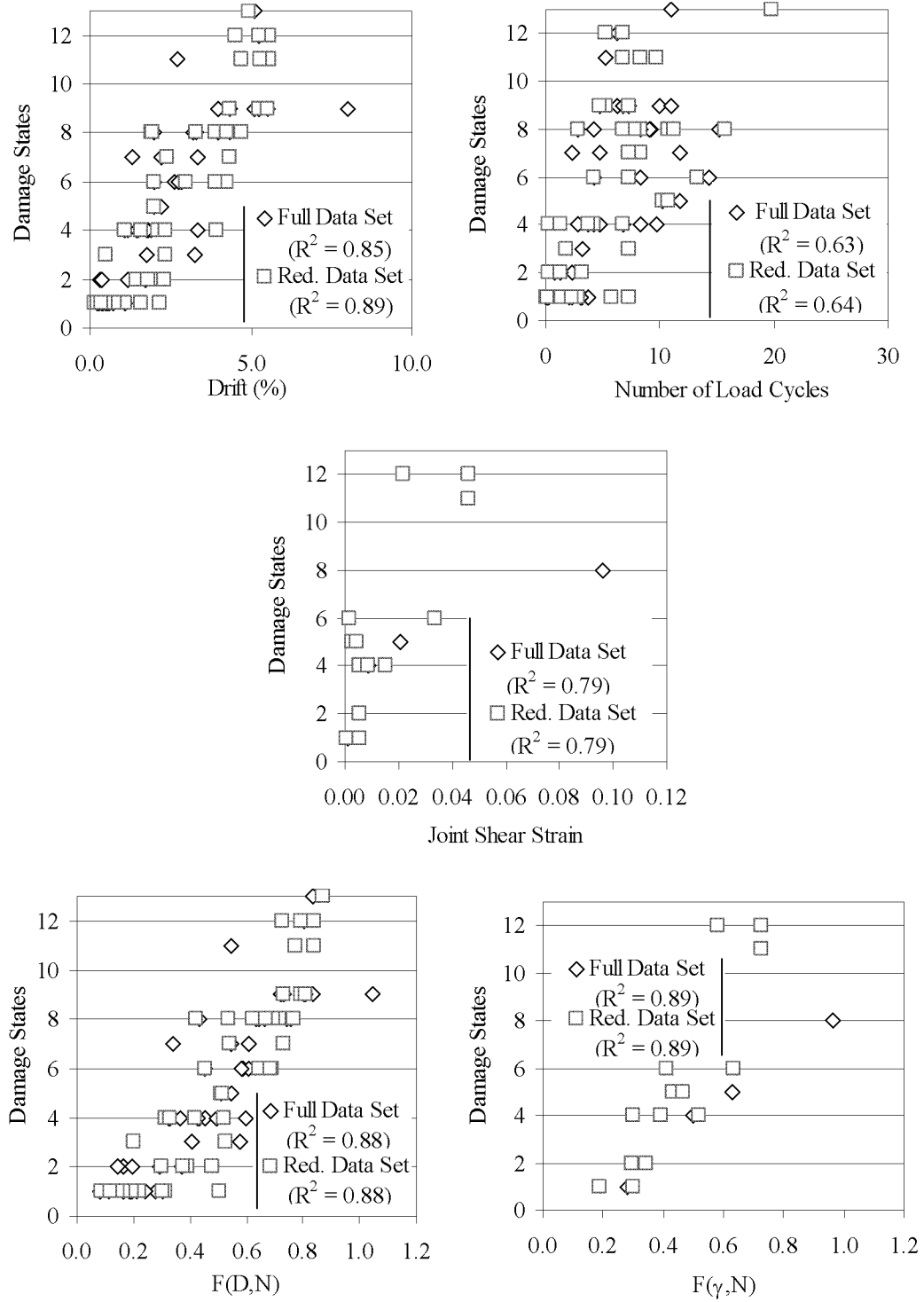
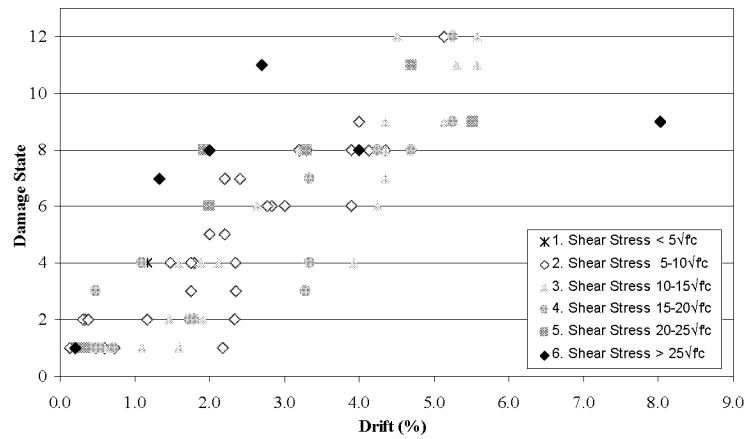


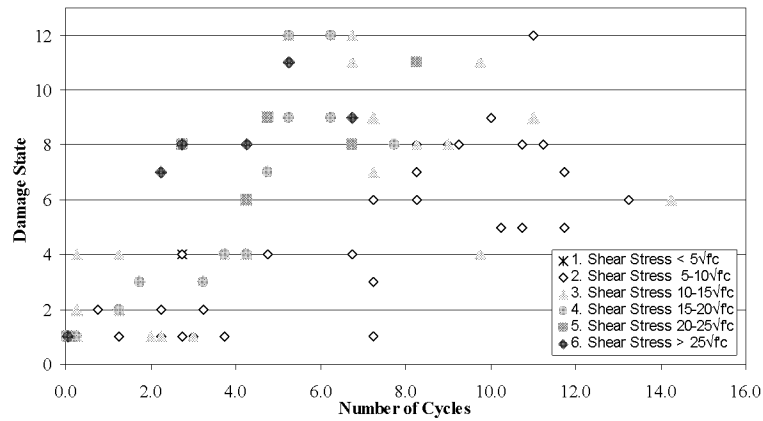
Figure 4.2 Damage State vs. EDPs

#### ***4.4.2.1 Impact of Design Parameters on Damage Progression on Interior Joints***

The data in Figure 4.2, which show DS versus EDP for both the reduced and full data set, suggest that the design parameters listed in Table 4.1 and 4.2 do not affect the progression of damage in interior beam-column joints. However, to further investigate the impact of design parameters on response, DS versus EDP were plotted for the full data set, with data grouped on the basis of individual design parameters. Figure 4.3 through Figure 4.10 show these plots for each of the design parameters listed in Table 4.1 and 4.2 and for the EDPs of maximum drift, number of load cycles and the functional EDP defined by Eq. 4.4. Plots are not provided for the EDPs of maximum joint shear strain and the functional EDP defined by Eq. 4.5, because too few data were available for these EDPs for meaningful evaluation.



a) Earthquake demand defined by drift



b) Earthquake demand defined by number of drift cycles

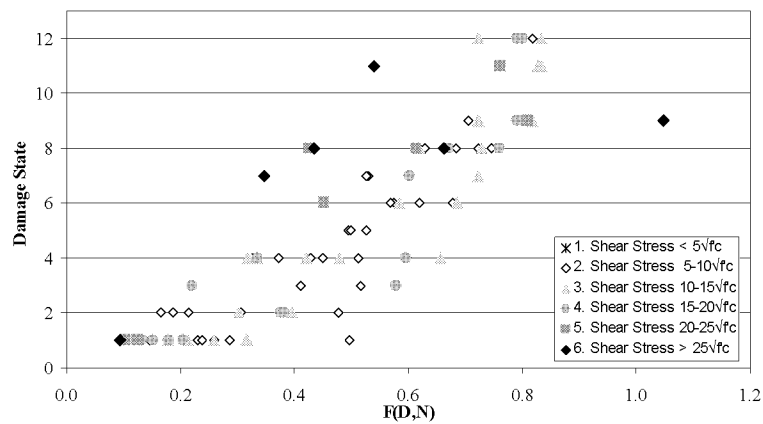
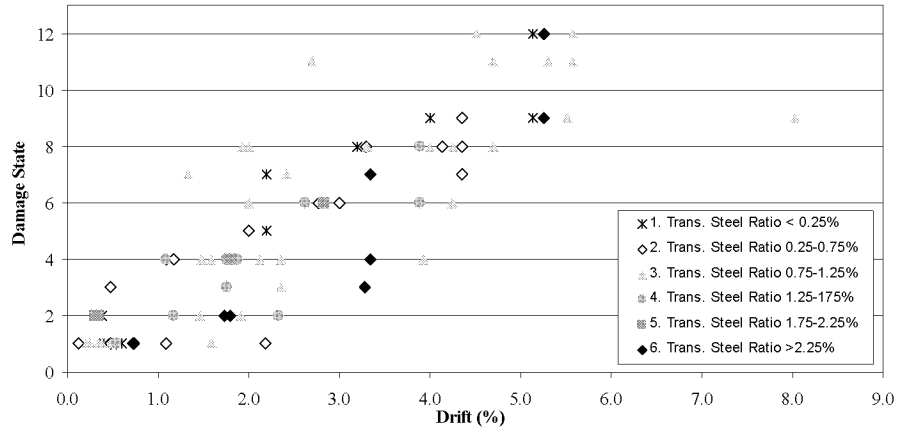
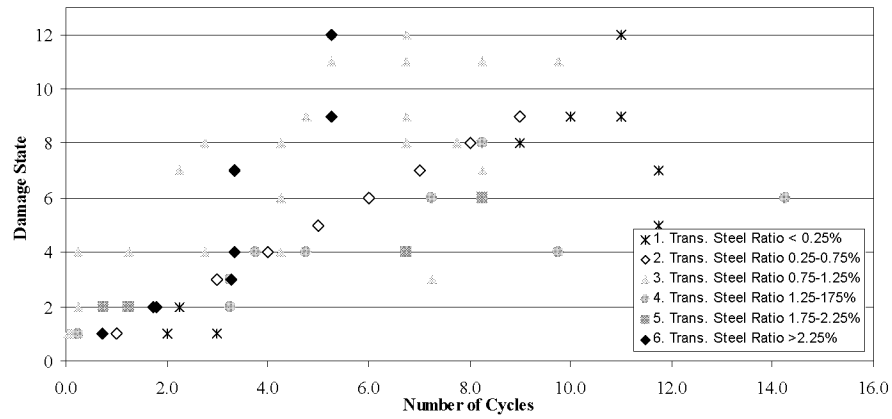


Figure 4.3 DS versus EDP for full data set with data grouped by shear demand

c) Earthquake demand defined as a function of drift and number of drift cycles



a) Earthquake demand defined by drift



b) Earthquake demand defined by number of drift cycles

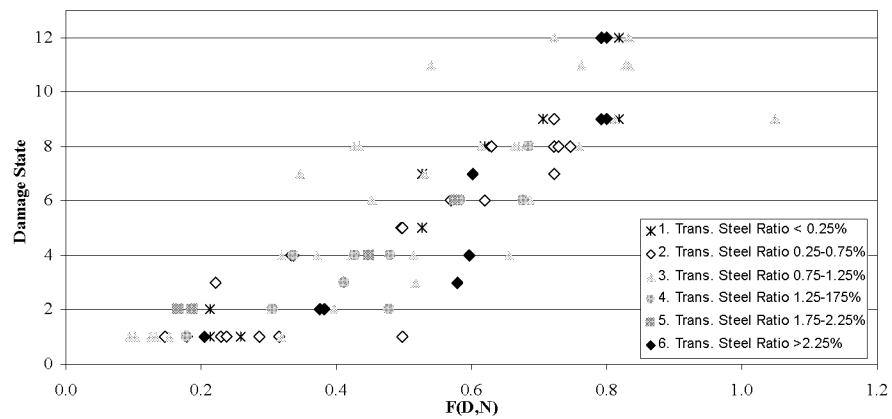
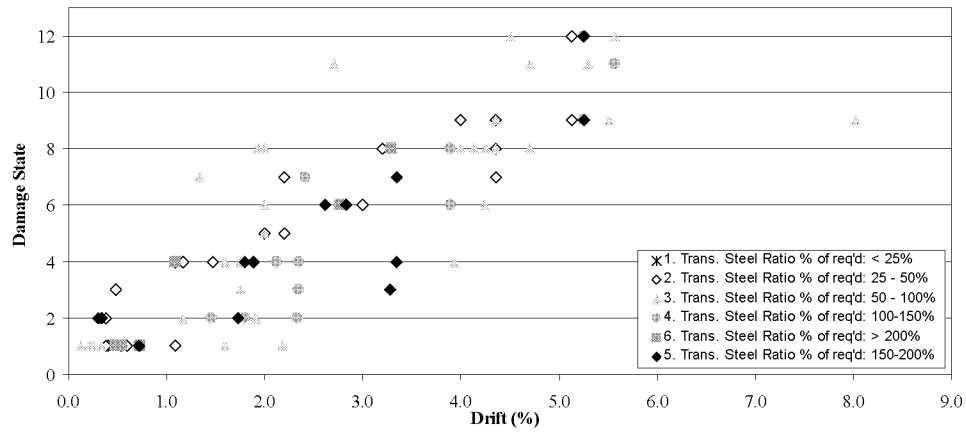
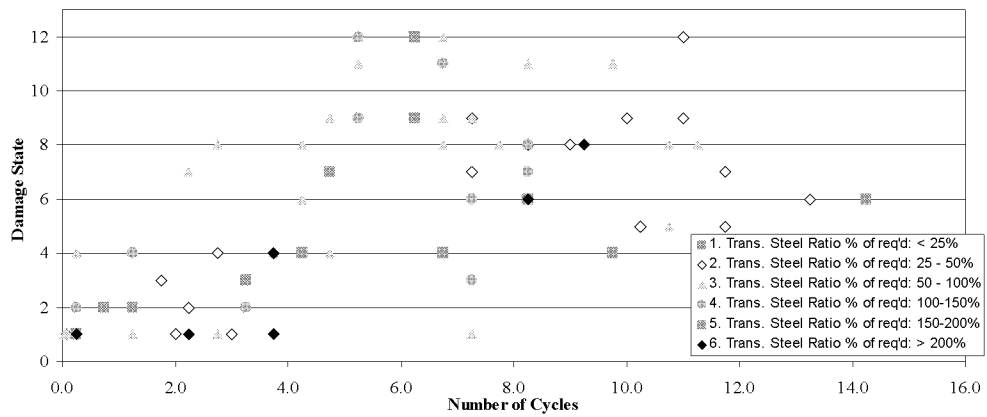


Figure 4.4 DS versus EDP for full data set with data grouped by transverse steel ratio

c) Earthquake demand defined as a function of drift and number of drift cycles



a) Earthquake demand defined by drift



b) Earthquake demand defined by number of drift cycles

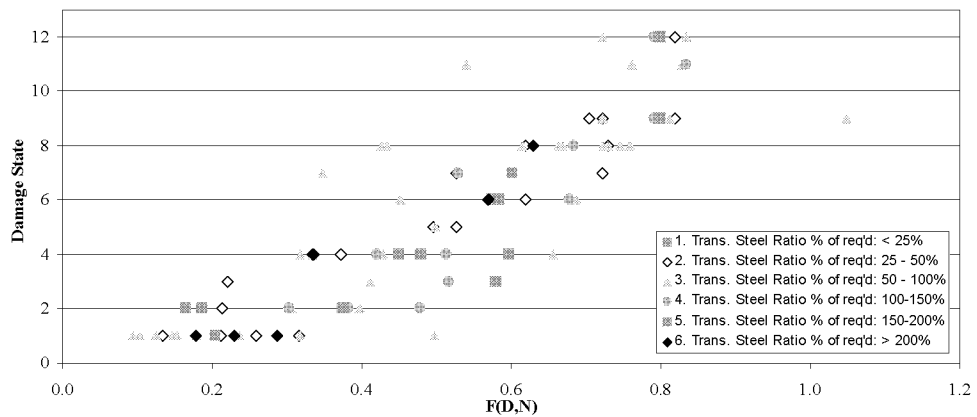
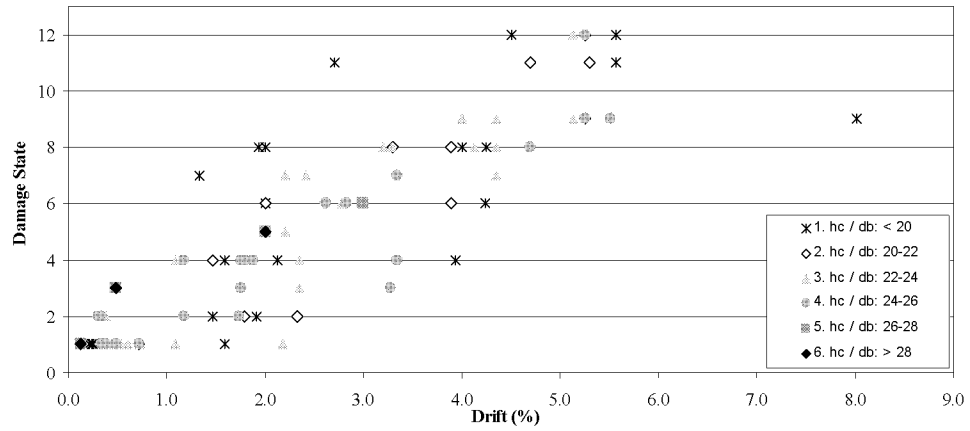
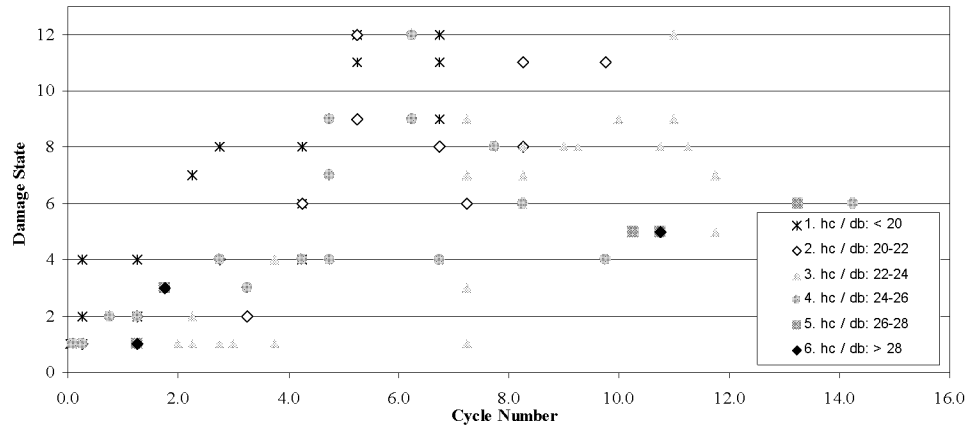


Figure 4.5 DS versus EDP with data grouped by % of req. transverse steel provided

c) Earthquake demand defined as a function of drift and number of drift cycles



a) Earthquake demand defined by drift



b) Earthquake demand defined by number of drift cycles

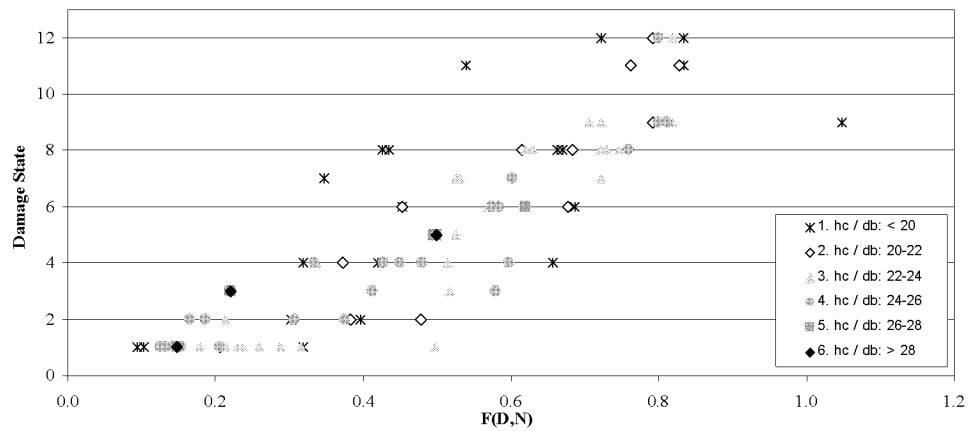
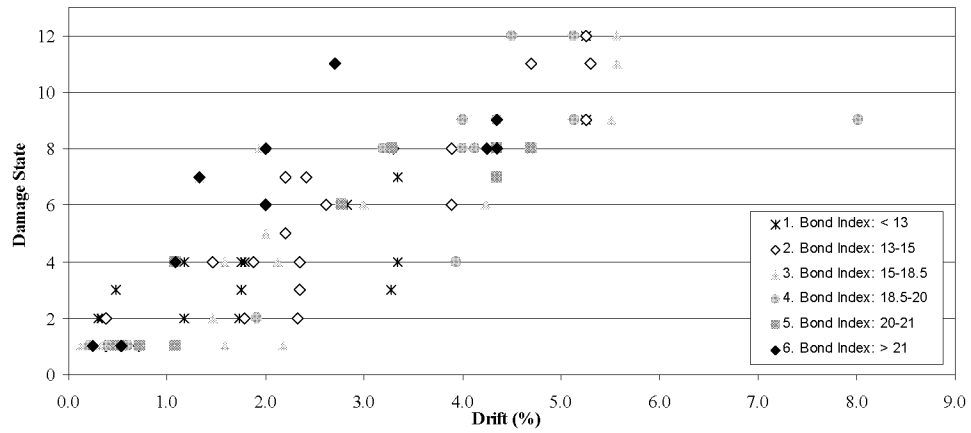
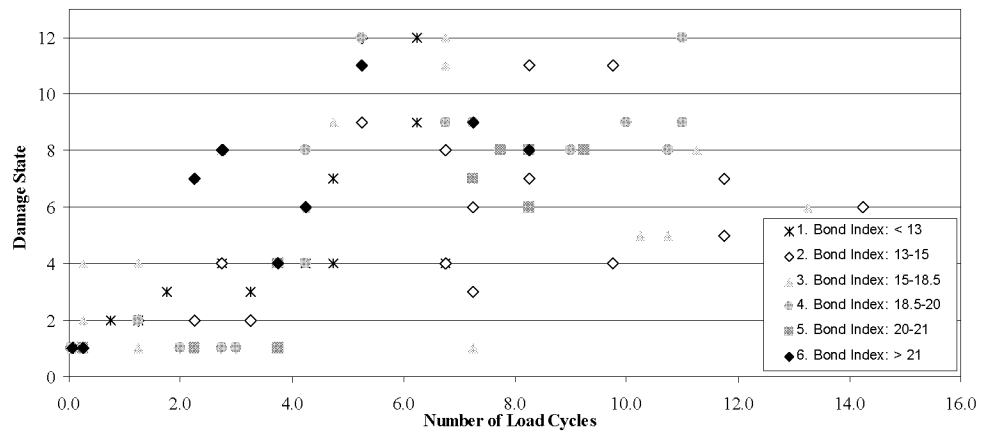


Figure 4.6 DS versus EDP with data grouped by column depth divided by bar diameter

c) Earthquake demand defined as a function of drift and number of drift cycles



a) Earthquake demand defined by drift



b) Earthquake demand defined by number of drift cycles

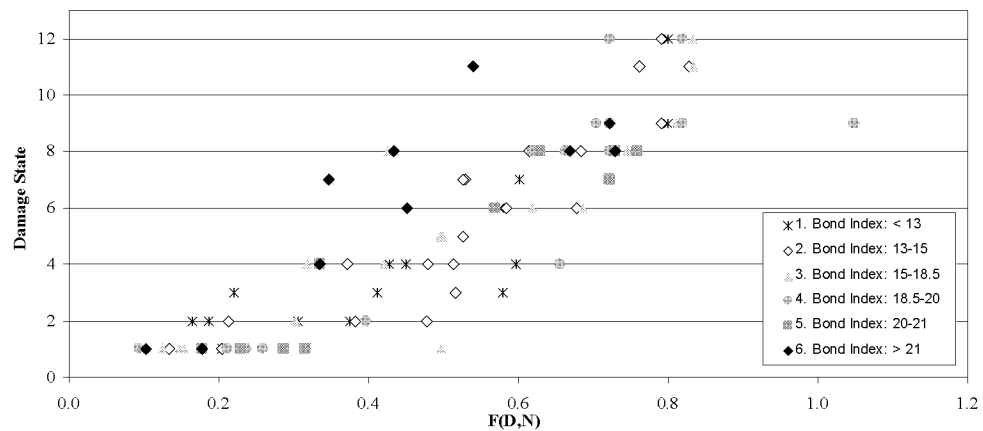
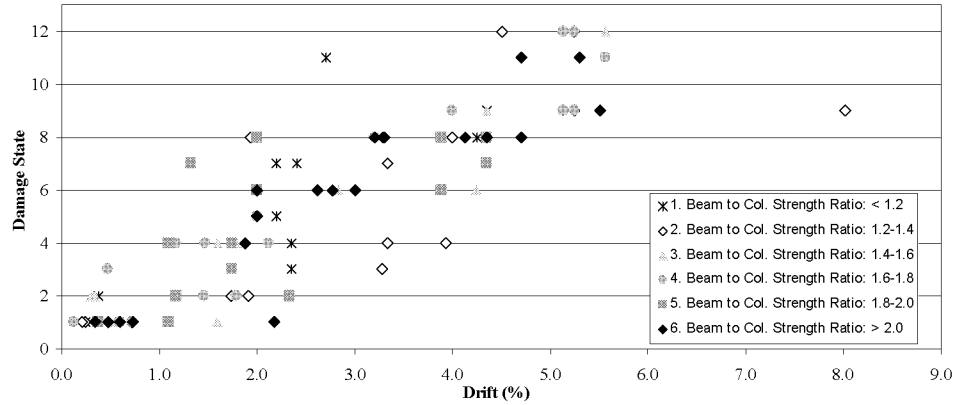
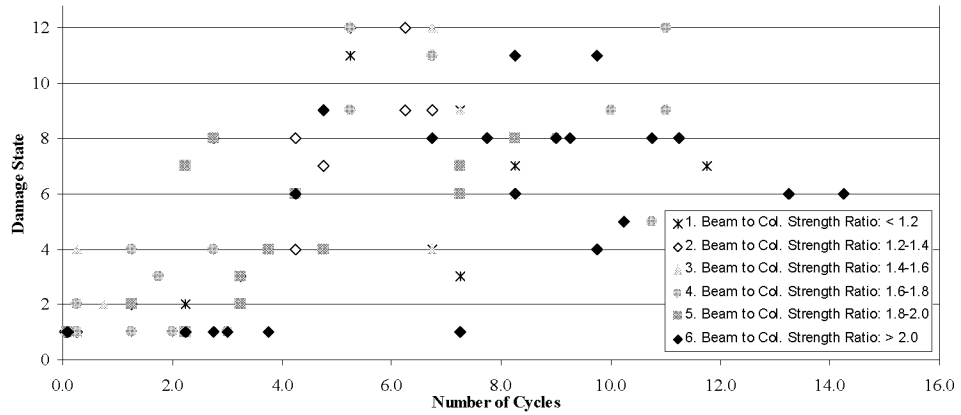


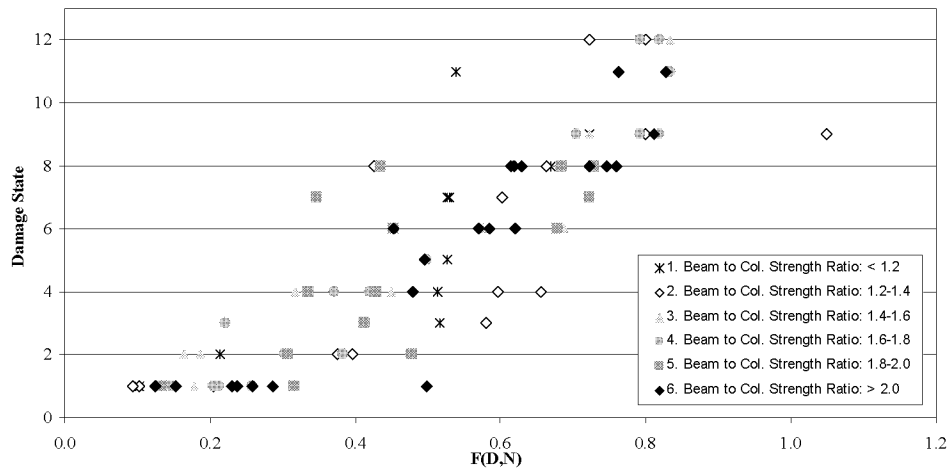
Figure 4.7 DS versus EDP for full data set with data grouped by bond index,  $\mu$   
 c) Earthquake demand defined as a function of drift and number of drift cycles



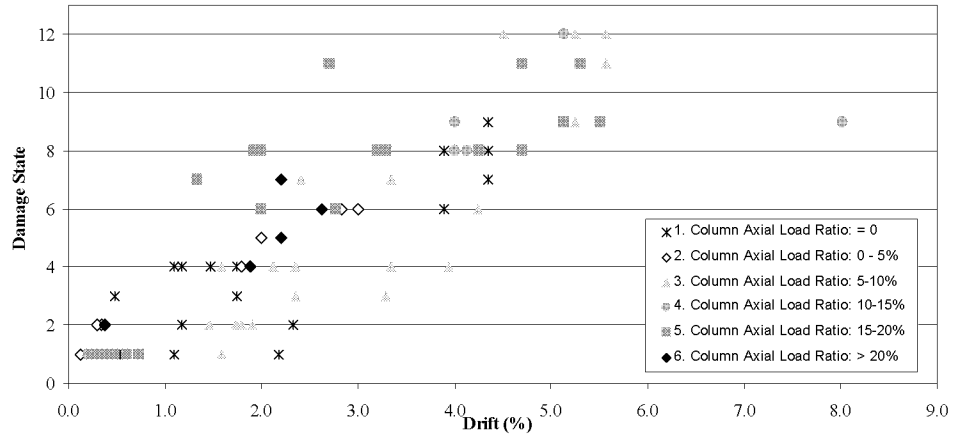
a) Earthquake demand defined by drift



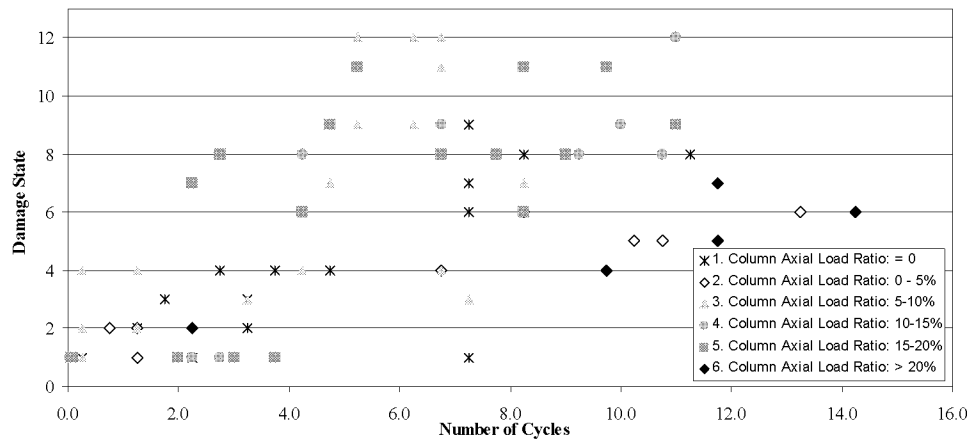
b) Earthquake demand defined by number of drift cycles

Figure 4.8 DS versus EDP with data grouped by beam to column strength ratio  
c) Earthquake demand defined as a function of drift and number of drift cycles





a) Earthquake demand defined by drift



b) Earthquake demand defined by number of drift cycles

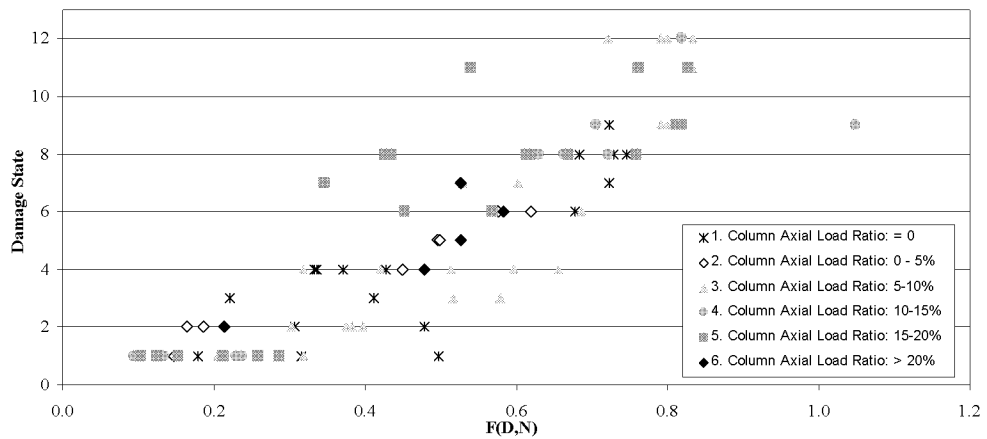
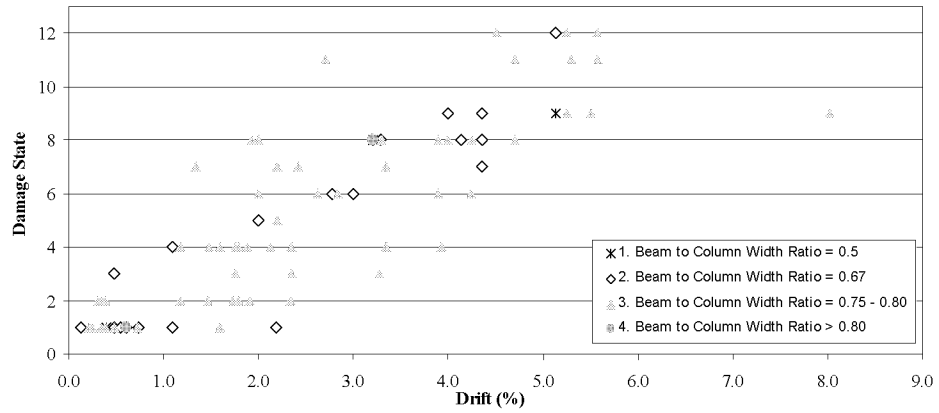
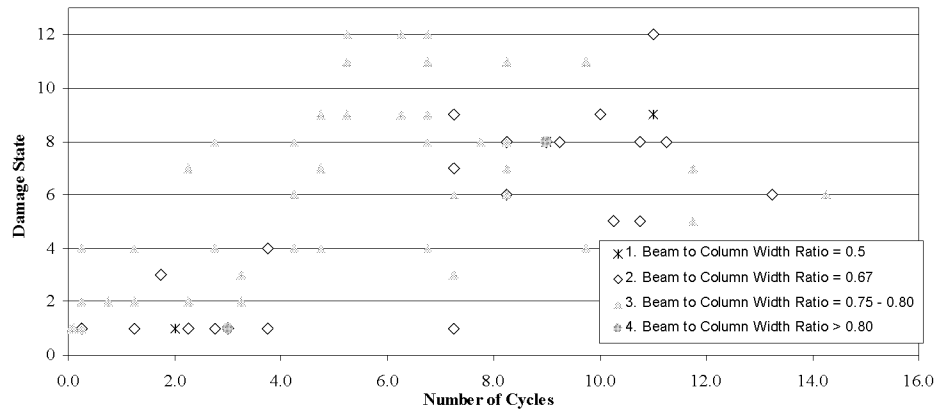


Figure 4.9 DS versus EDP for full data set with data grouped by column axial load

c) Earthquake demand defined as a function of drift and number of drift cycles



a) Earthquake demand defined by drift



b) Earthquake demand defined by number of drift cycles

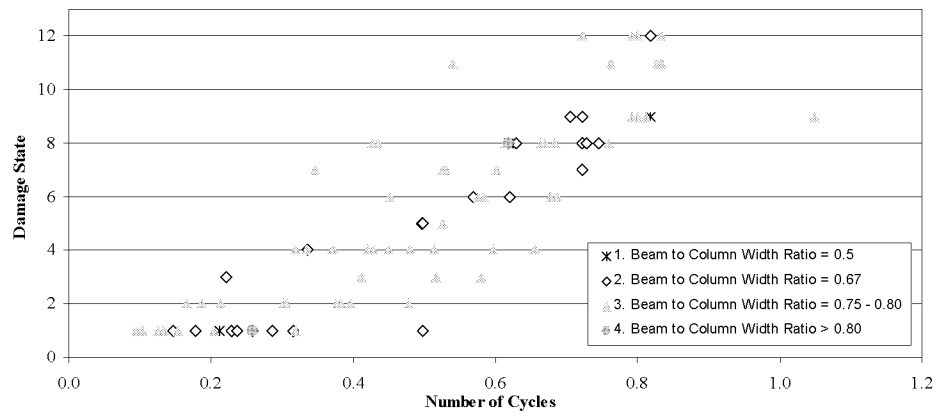


Figure 4.10 DS versus EDP with data grouped by beam to column width ratio

c) Earthquake demand defined as a function of drift and number of drift cycles

With a very few exceptions, the data in Figures 4.3 through 4.10 also support the conclusion that the joint design parameters listed in Table 4.3 do not affect the relationship between damage and earthquake demand for interior joints with 1) transverse reinforcement, 2) sufficient strength to enable development of the flexural yield strength of the beams framing into the joint, and 3) column-to-beam flexural strength ratios that ensure columns do not yield (see Section 4.2.2. for a detailed discussion of the criteria employed to identify joints for the current study). The one significant exception to this is that joints with higher shear stress demands require fewer load cycles to reach a given damage state (Figure 4.3b).

Evaluation of the data in Figure 4.3 through Figure 4.10 supports the following specific observations:

- Shear demand does not, in general, affect the relationship between damage and drift (Figure 4.3a). There are two exceptions to this: 1) initial spalling in the joint (DS 7 – spalling of at least 10% of the joint area) occurs at lower drift levels for joints with higher shear stress demands, 2) spalling of more than 30% of the joint area (DS 9) occurs at higher drift demands for joints with higher shear stress demand, and 3) initial cracking of the joint (DS 1) occurs at lower functional demand levels for joints with higher shear stress demands. This suggests that joints with higher shear demands exhibit more joint deformation, and thus greater inter-story drifts, once spalling initiates than do joints with lower shear stress demands.

- Shear demand does, in general, affect the relationship between damage and number of load cycles (Figure 4.3b); joints with higher shear stress demands reach a given damage state after fewer load cycles than do joints with lower shear stress demands.
- Shear demand does not, in general, affect the relationship between damage and the functional EDP defined by Eq. 4.4. The one exception to this is that initial joint cracking (DS 1) occurs at lower functional demand levels for joints with higher shear stress demands (Figure 4.3c).
- Neither joint transverse reinforcement ratio (Figure 4.4) nor joint transverse reinforcement ratio as a percentage of that required by the ACI Building Code (ACI 318 2002) (Figure 4.5) affects the progression of damage in the joint.
- Neither beam bar anchorage length defined as a function of the beam bar diameter (Figure 4.6) nor the average bond stress demand defined by the bond index,  $\mu$ , (Eq. 4.3) (Figure 4.7) affects the progression of damage in the joint. The one exception to this rule is that joints with longer beam-bar anchorage lengths exhibit initial cracking at lower drift demand levels (Figure 4.6a); however, this is counter intuitive, as longer anchorage lengths could be expected to reduce bond stress demand and delay the onset of damage.
- The ratio of beam to column flexural strength does not affect the progression of damage (Figure 4.8).
- Column axial load does not affect damage progression (Figure 4.9).

- The ratio of beam to column width does not affect the relationship between damage and drift (Figure 4.10a) or the relationship between damage and the functional EDP (Figure 4.10c) defined by Eq. 4.4. However, the data in (Figure 4.10b) do suggest that joints with lower beam to column width ratios require more load cycles than joints with width ratios to reach the more severe damage states of strength loss (DS 8), spalling of more than 30% of the joint area (DS 9) and crushing of joint core concrete (DS 12).

#### 4.4.3 Exterior Joints

As with the interior joints, experimental data characterizing the progression of damage in exterior joint test specimens were used to generate data sets linking the fourteen damage states with the potential EDPs. The functional EDPs defined by Eqs. 4.4 and 4.5 were calibrated to minimize the dispersion of the data about a line extending through all of the damage states and spanning a range of functional EDP values from 0 to 1.0.

The data in Figure 4.11 indicate that drift and the functional EDP,  $F(D,N)$  as defined by Eq. 4.4, are the best indicators of damage. The data also suggests that for exterior joints, the number of load cycles is almost as efficient an indicator of damage as drift. This was not the case for interior joints in which drift was a more efficient predictor than the number of load cycles. The difference between interior and exterior joints is most likely an artifact of the limited data sets; it is unlikely that the number of

load cycles would have a significantly different effect on interior versus exterior joints. The correlation coefficient for the strain data is both very low and negative which suggests that strain is a poor predictor of damage. This low correlation coefficient is likely due to the percentage of the total data contained in DS 1 and the high variability of data in DS 1. As with interior joints, the correlation of the data improves when drift and the number of cycles are combined in the functional EDP  $F(D,N)$  per Eq. 4.4.

|

#### ***4.4.3.1 Impact of Design Parameters on Damage Progression on Exterior Joints***

Due to the small size of the data set for exterior joints and the fact that design parameters were found to have limited impact on damage progression in interior joints, the impact of design parameters on damage progression in exterior joints was not investigated as was done for interior joints (Section 4.4.2.1).

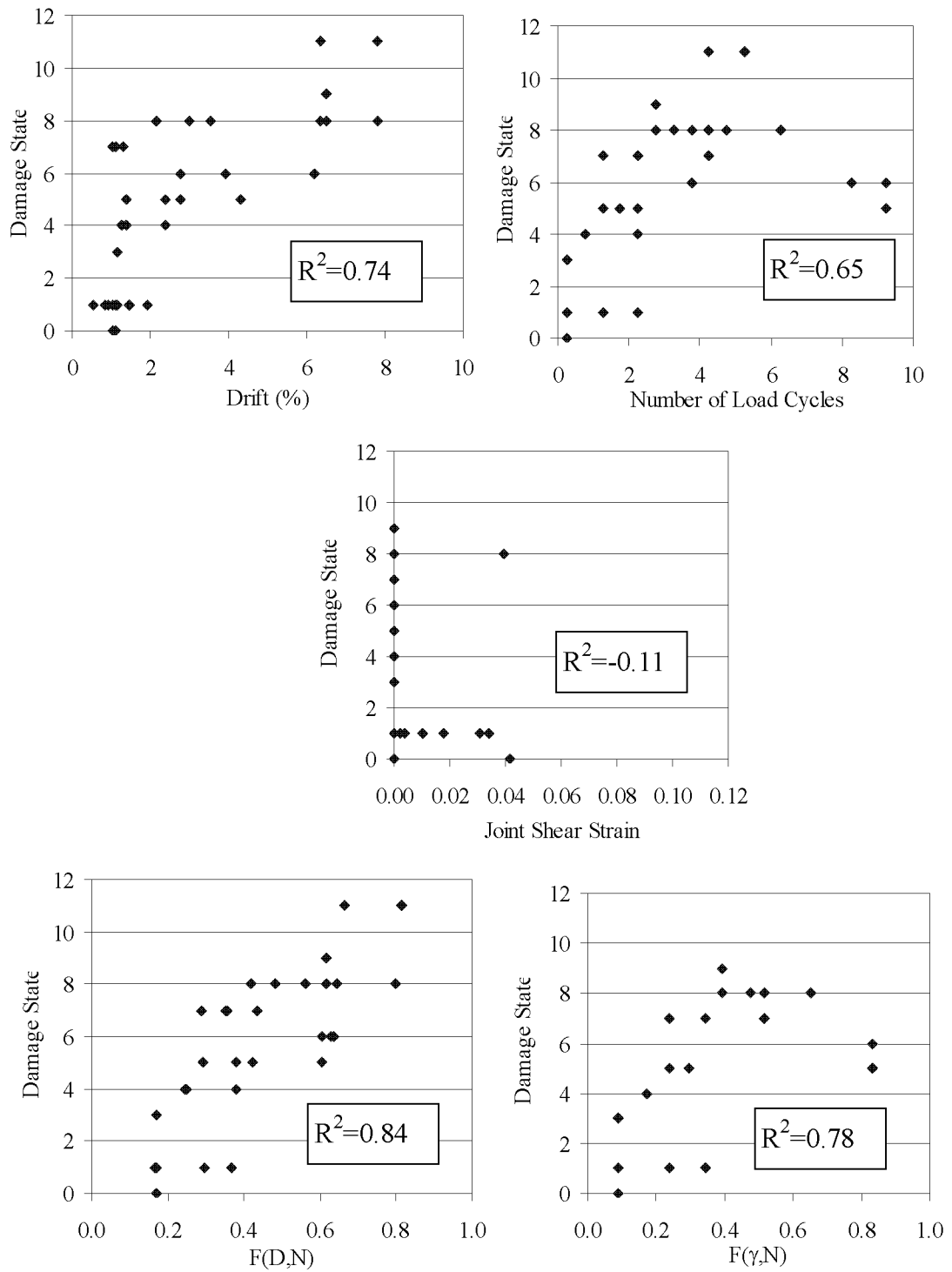


Figure 4.11 Damage State vs. EDP



#### 4.5 EDP VERSUS MOR

EDP-MOR data points are required to generate fragility functions defining the likelihood that a specific MOR will be required to restore an earthquake-damaged joint. For each individual specimen, the EDP-damage state pair for the lowest damage state associated with a specific method of repair is used, as discussed in Section 2.5.

Given a specific value of an EDP, the ideal family of fragility functions results in identification of a single method of repair that has a relatively high probability of being met or exceeded, with all more extensive methods having a relatively low probability of being met or exceeded. This requires that the EDP-method of repair data have well-spaced means and low variances. Table 4.8 shows the sample mean and coefficient of variation for each of the data sets, EDPs, and methods of repair. Several observations may be made regarding the data in Table 4.8:

- The functional EDPs result in the least variability of the data for each of the methods of repair.
- The functional EDPs result in well-spaced means across the range of methods of repair. The case of the full data set, Method of Repair 2, and EDP defined by Eq. 4.5 is not considered because insufficient data were available to construct a fragility function.
- Of the non-functional EDPs (inter-story drift, number of load cycles, joint shear strain), drift results in the least variability of the data for each of the methods of repair and the most uniformly spaced means across the range of methods.

- For EDP defined by drift and by number of load cycles, the data for Method of Repair 4 do not correlate well with data for the other methods.

On the basis of the data presented in Table 4.8, three preferred EDPs were identified: maximum inter-story drift,  $F(D,N)$  as defined by Eq. 4.4, and  $F(\gamma,N)$  and defined by eq. 4.5. Drift was included as a preferred EDP because the use of a functional EDP may not be viable for all applications. The functional EDP defined by Eq. 4.5 was included because it introduced dependence on joint shear strain and because of the relatively low coefficient of variation of the EDP-MOR data. Fragility functions are presented only for the three preferred EDPs.

Table 4.8 Statistical Characteristics of EDP-Method of Repair (MOR) Data.

	MOR	Drift		No. of Cycles		F(D,N)		Jt. Strain		F( $\gamma,N$ )	
		mean	c.o.v.	mean	c.o.v.	mean	c.o.v.	mean	c.o.v.	mean	c.o.v.
Interior Joints Full Data Set	0	0.77	0.78	1.44	1.12	0.23	0.44	4.18E-03	0.62	0.22	0.37
	1	1.93	0.42	5.09	0.57	0.44	0.24	7.41E-03	0.66	0.44	0.30
	2	3.66	0.32	6.91	0.41	0.64	0.20	N.A.	N.A.	N.A.	N.A.
	3	4.89	0.18	7.17	0.29	0.77	0.12	3.79E-02	0.37	0.84	0.19
	4	N.A.	N.A.	N.A.	N.A.	N.A.	N.A.	N.A.	N.A.	N.A.	N.A.
		max ave.	0.78 0.43	max ave.	1.12 0.60	max ave.	0.44 0.25	max ave.	0.66 0.55	max ave.	0.37 0.28
Interior Joints Reduced Data Set	0	0.95	0.79	1.30	1.51	0.25	0.39	4.18E-03	0.62	0.22	0.37
	1	1.98	0.48	4.75	0.63	0.41	0.28	7.41E-03	0.66	0.44	0.30
	2	4.06	0.25	7.02	0.37	0.68	0.21	N.A.	N.A.	N.A.	N.A.
	3	5.15	0.09	7.00	0.25	0.85	0.10	3.79E-02	0.37	0.84	0.19
	4	N.A.	N.A.	N.A.	N.A.	N.A.	N.A.	N.A.	N.A.	N.A.	N.A.
		max ave.	0.79 0.40	max ave.	1.51 0.69	max ave.	0.39 0.24	max ave.	0.66 0.55	max ave.	0.37 0.28
Exterior Joints	0	1.23	0.30	0.78	0.90	0.22	0.38	1.08E-02	1.40	0.20	0.50
	1	1.75	0.39	2.58	1.31	0.34	0.52	3.12E-05	0.53	0.13	0.47
	2	3.83	0.64	3.92	0.44	0.55	0.29	9.91E-03	2.00	0.55	0.23
	3	6.13	0.29	5.42	0.23	0.72	0.12	N.A.	N.A.	N.A.	N.A.
	4	N.A.	N.A.	N.A.	N.A.	N.A.	N.A.	N.A.	N.A.	N.A.	N.A.
		max ave.	0.64 0.40	max ave.	1.31 0.72	max ave.	0.52 0.33	max ave.	2.00 1.31	max ave.	0.50 0.40

#### 4.6 EVALUATION OF THE FRAGILITY FUNCTIONS

The lognormal, Weibull and Beta distributions (the normal distribution is omitted because it considers negative numbers and is therefore undesirable as discussed in Section 3.2.1) were fit to the EDP-MOR data using the Method of Maximum Likelihood for the full interior joint data set, reduced interior joint data set and exterior joint data set. The  $\chi^2$  and the K-S and, for the case of the lognormal distribution, Lilliefors goodness-of-fit tests were used to evaluate the results. Distribution parameters and  $\chi^2$  and the K-S goodness-of-fit test results are presented in Appendix C. Only the Lilliefors goodness-of-fit test applied to the lognormal distribution are presented here. The lognormal distribution was chosen as the preferred distribution because i) the lognormal distribution is commonly used for definition of fragility function, ii) the lognormal distribution was used by Pagni and Lowes (2006) for definition of fragility curves for older beam-columns joints, and iii) goodness-of-fit test results for all of the distributions considered did not indicate a preferred distribution. Results are present here for only Lilliefors test because only this test is considered exact for the current study in which the data sample is relatively small, potentially resulting in inaccurate results for the  $\chi^2$  test, and distribution parameters are estimate from the sample, potentially resulting in unconservative results for the K-S test. From the data in this table, it may be concluded that the lognormal distribution is acceptable for use in modeling approximately half of the empirical EDP-MOR data sets. The goodness-of-fit test results are worst for interior joints using the full data set, better for

interior joints using the reduced data set and best for the exterior joint. Note that for the full data set and Method of Repair 3, the Lilliefors tests probability is equal to the significance level, validating the hypothesis that the lognormal distribution is acceptable, when the data are rounded to two decimal places. The relatively poor results of the goodness-of-fit testing is attributed to the small size of the data set and wide dispersion of the data points.

Table 4.9 Results of the Lilliefors test for the lognormal distributions for the three preferred EDPs

MOR	Full Data Set						Reduced Data Set					
	Drift		F(D,N)		F( $\gamma$ ,N)		Drift		F(D,N)		F( $\gamma$ ,N)	
	P	correct CDF	P	correct CDF	P	correct CDF	P	correct CDF	P	correct CDF	P	correct CDF
0	> 0.20	TRUE	> 0.20	TRUE	0.03	FALSE	> 0.20	TRUE	> 0.20	TRUE	0.03	FALSE
1	0.04	FALSE	0.03	FALSE	> 0.20	TRUE	< 0.01	FALSE	NaN	TRUE	> 0.20	TRUE
2	< 0.01	FALSE	< 0.01	FALSE	N.A.	N.A.	< 0.01	FALSE	0.068	TRUE	N.A.	N.A.
3	0.04	FALSE	0.05	FALSE	N.A.	N.A.	0.19	TRUE	NaN	TRUE	N.A.	N.A.
4	N.A.	N.A.	N.A.	N.A.	N.A.	N.A.	N.A.	N.A.	N.A.	N.A.	N.A.	N.A.
MOR	Exterior Data Set											
	Drift		F(D,N)		F( $\gamma$ ,N)							
	P	correct CDF	P	correct CDF	P	correct CDF						
0	0.13	TRUE	0.00	FALSE	0.00	FALSE						
1	0.17	TRUE	> 0.20	TRUE	> 0.20	TRUE						
2	0.30	TRUE	> 0.20	FALSE	> 0.20	TRUE						
3	0.00	TRUE	0.00	TRUE	> 0.20	TRUE						
4	> 0.20	TRUE	> 0.20	TRUE	N.A.	N.A.						

Notes:  $P = P(D_n \leq D_n^\alpha)$  where  $D_n^\alpha$  is computed per Lilliefors (1967)

Figure 4.12, 4.13 and 4.14 show fragility functions for interior and exterior joints; both the theoretical fragility functions defined using the lognormal distribution and the empirical fragility functions are shown. Fragility functions for older interior

beam-column joints, as developed by Pagni and Lowes (2006), are provided for comparison. Table 4.10 lists the parameters defining the lognormal distribution (eq. 3.4) the 95% confidence interval on these parameters, normalized with respect to the value of the parameter; similar tables for all of the data sets and distributions are located in Appendix A. The confidence interval is

$$C.I. = 2t\sqrt{S} \quad 4.6$$

where  $t$  is the inverse of the Student's T CDF (Kottegoda and Rossa 1997) for the 95% confidence level and  $S$  is the diagonal of the covariance matrix for the coefficient estimates. The confidence interval was computed using the Matlab function **mle**. Fragility functions and distribution parameters are not provided where the empirical data sets are too small to support statistical evaluation.

The theoretical fragility functions presented in Figure 4.12, 4.13 and 4.14 are appropriate for use in predicting the probability that a particular method of repair will be required, given an earthquake demand as defined by one of three EDPs. However, comparison of the theoretical and empirical fragility functions as well as evaluation of the confidence interval data in Table 4.10 indicates that there is significant uncertainty in the parameters that define these models. This uncertainty is due primarily to the sparsity of the data sets used to construct the models.

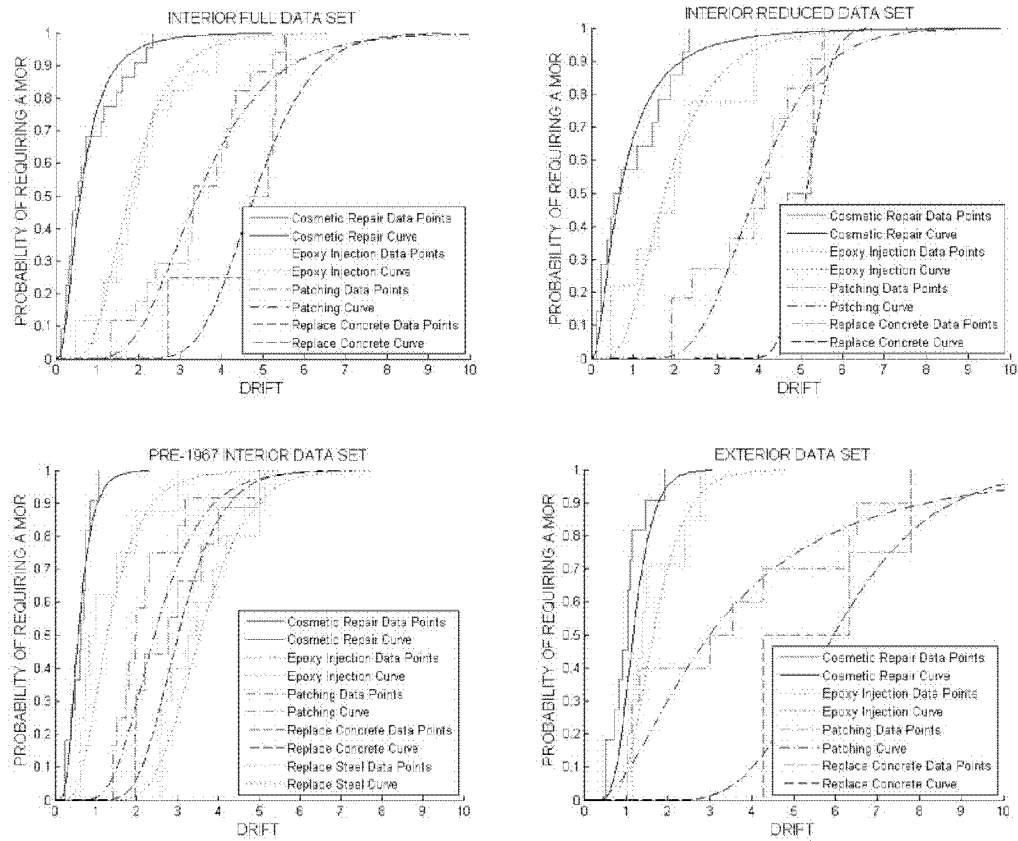


Figure 4.12 Fragility functions defining the probability of requiring, at least, a method of repair for earthquake demand defined by drift. Pre-1967 interior data set from Pagni (2003)

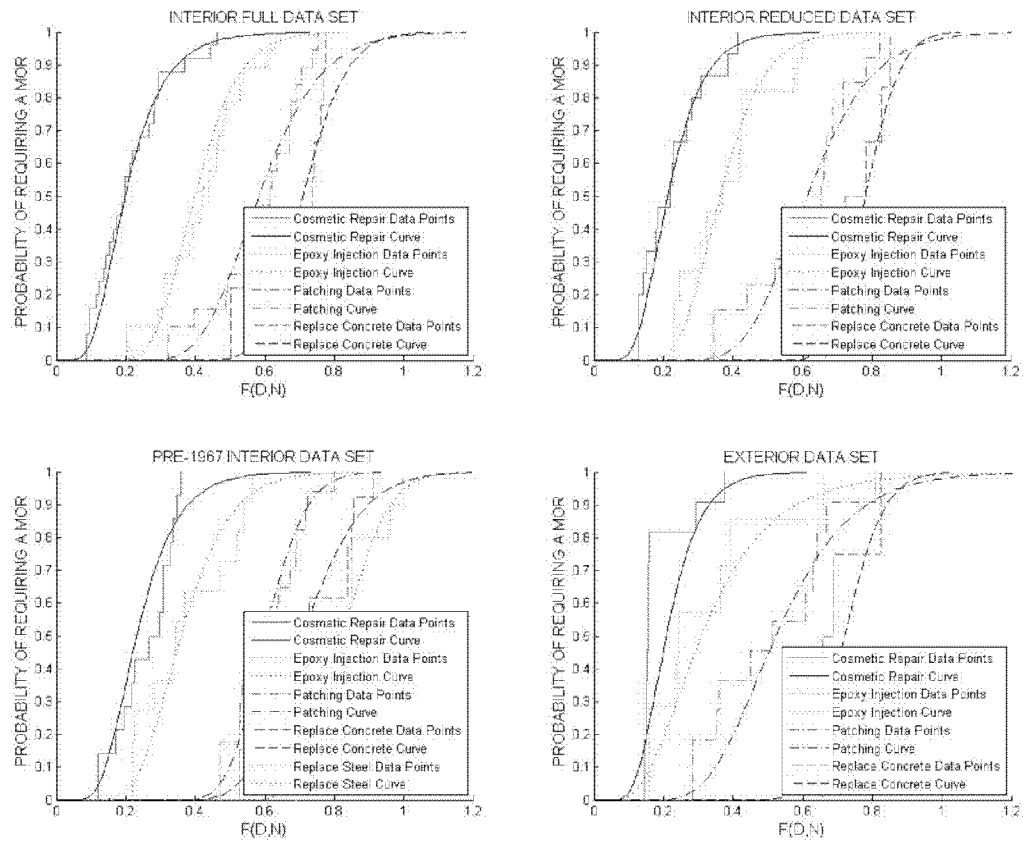


Figure 4.13 Fragility functions defining the probability of requiring, at least, a method of repair for earthquake demand defined by the  $F(D,N)$  per eq. 4.4. Pre-1967 interior data set from Pagni (2003).

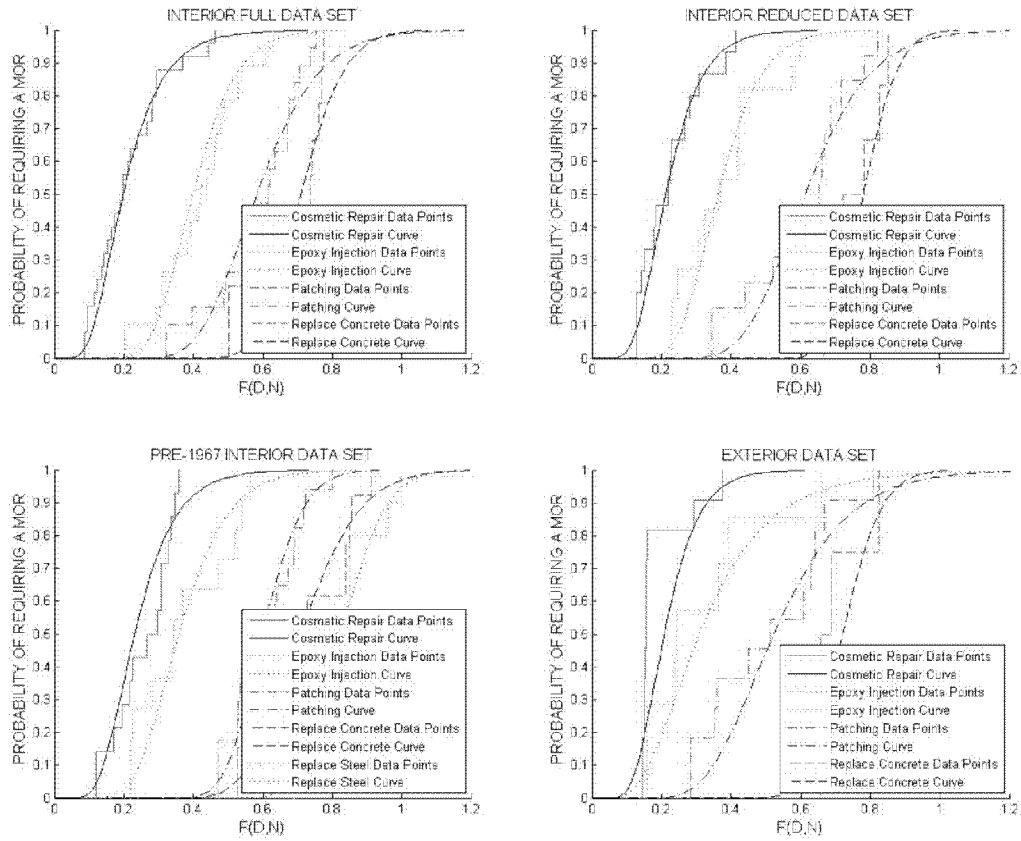


Figure 4.14 Fragility functions defining the probability of requiring, at least, a method of repair for earthquake demand defined by the  $F(\gamma, N)$  per eq. 4.5. Pre-1967 data set taken from Pagni (2003).



Table 4.10 Lambda and Zeta for the Three Preferred EDPs for Modern Joints (Full and Reduced Data Sets) and, for Comparison, Joints with Detailing Typical of Older Construction.

		MOR	Drift				F(D,N)				F( $\gamma$ ,N)			
			lambda		zeta		lambda		zeta		lambda		zeta	
			value	95% C.I.	value	95% C.I.	value	95% C.I.	value	95% C.I.	value	95% C.I.	value	95% C.I.
Modern Joints	Full Interior Data Set	0	-0.528	1.054	0.732	0.559	-1.544	0.215	0.436	0.559	-1.575	0.953	0.471	3.162
		1	0.569	0.599	0.440	0.571	-0.845	0.225	0.246	0.571	-0.871	0.955	0.335	2.274
		2	1.232	0.271	0.396	0.626	-0.465	0.429	0.237	0.626	N.A.	N.A.	N.A.	N.A.
		3	1.567	0.222	0.226	1.240	-0.269	0.792	0.139	1.240	N.A.	N.A.	N.A.	N.A.
		4	N.A.	N.A.	N.A.	N.A.	N.A.	N.A.	N.A.	N.A.	N.A.	N.A.	N.A.	N.A.
	Reduced Interior Data Set	0	-0.382	2.593	0.894	0.845	-1.472	0.281	0.373	0.845	-1.575	0.953	0.471	3.162
		1	0.565	1.031	0.526	0.845	-0.937	0.316	0.268	0.845	-0.871	0.955	0.335	2.274
		2	1.365	0.263	0.297	0.934	-0.413	0.698	0.239	0.934	N.A.	N.A.	N.A.	N.A.
		3	1.636	0.114	0.089	1.828	-0.171	1.221	0.100	1.828	N.A.	N.A.	N.A.	N.A.
		4	N.A.	N.A.	N.A.	N.A.	N.A.	N.A.	N.A.	N.A.	N.A.	N.A.	N.A.	N.A.
	Exterior Data Set	0	0.158	1.971	0.322	0.723	-1.573	0.222	0.363	0.723	-1.760	0.391	0.570	0.934
		1	0.499	1.524	0.363	1.828	-1.178	0.884	0.496	1.828	N.A.	N.A.	N.A.	N.A.
		2	1.098	0.907	0.784	0.989	-0.649	0.620	0.317	0.989	-0.615	1.263	0.244	3.162
		3	1.784	0.852	0.306	5.764	-0.328	1.829	0.121	5.764	N.A.	N.A.	N.A.	N.A.
		4	N.A.	N.A.	N.A.	N.A.	N.A.	N.A.	N.A.	N.A.	N.A.	N.A.	N.A.	N.A.
	Pre-1967 Design Data Set	0	-0.562	0.887	0.467	0.809	-1.464	0.282	0.387	0.809	-1.291	0.634	0.329	2.274
		1	0.242	2.340	0.491	0.886	-1.025	0.338	0.300	0.886	-0.867	0.551	0.334	1.138
		2	0.891	0.386	0.367	0.700	-0.508	0.271	0.147	0.700	-0.603	0.560	0.236	1.138
		3	1.103	0.299	0.273	0.934	-0.343	0.650	0.185	0.934	-0.355	0.759	0.175	1.240
		4	1.265	0.317	0.261	1.240	-0.188	0.958	0.117	1.240	N.A.	N.A.	N.A.	N.A.

Notes:

\* Distribution parameters refer to the log of the EDP data. The 95% C.I. is the 95% confidence interval on the parameter, normalized with respect to the value of the parameter. The confidence interval is not symmetric with respect to the distribution parameter.

\* Pre-1967 Design Data Set was taken from Pagni and Lowes (2006).

#### **4.7 COMPARISON OF DAMAGE FOR OLDER AND MODERN INTERIOR JOINTS**

The data in Table 4.10 and Figure 4.12, Figure 4.13 and Figure 4.14 support several observations about damage progression in older versus modern interior joints.

- At low drift levels, modern and older joints exhibit similar vulnerability under earthquake loading. Cracking and initial spalling are not determined by the design parameters since they are resisted by the concrete not the reinforcing detail. The drift level at which there is a 50% probability of a joint requiring repair MOR 0 (Cosmetic Repair) is approximately the same for modern joints and older joints (0.7% versus 0.6%).
- For MOR 1 (Epoxy Injection), modern interior joints exhibit a 50% probability of requiring the repair at drift levels that are only moderately higher than those of older joints (1.8% versus 1.3%).
- As drift demands increase, the severity of the damage and required repair effort increases much more rapidly for older joints than for modern joints. For older joints, there is a 50% probability of requiring MOR 2 (Patching) at a drift demand of 2.4% and MOR 3 (Replace Concrete) at a drift demand of 3.0%. For modern joints these levels of vulnerability are not reached until the drift demand reaches 4.0% and 5.1%. The improved performance is due to the increased reinforcing steel and anchorage, which delays damage.

- At moderate drift levels, older joints have a significant probability of exhibiting damage requiring MOR 4 (Replace Joint), and potentially causing structural collapse; while, modern interior joints typically do not exhibit this level of damage. Only 2 of 45 modern interior joint specimens exhibited damage requiring MOR 4, with the result that 1) it was not possible to create fragility functions for this method of repair and 2) it may be concluded that damage this severe is highly unlikely in joints with modern detailing. Older joints, however, exhibit a 50% probability of requiring MOR 4 at a drift demand of 3.5%.

#### **4.8 COMPARISON OF DAMAGE FOR EXTERIOR AND MODERN INTERIOR JOINTS**

The data in Table 4.10 and Figure 4.12, Figure 4.13 and Figure 4.14 support several observations about damage progression in exterior versus modern (reduced data set) interior joints.

- At low drift levels, exterior joints experience damage at a slightly higher drift level than the interior joints. The drift level at which there is a 50% probability of a joint requiring repair MOR 0 (Cosmetic Repair) is 0.7% for interior joints and about 1.1% drift for exterior joints.

- For MOR 1 (Epoxy Injection), exterior joints exhibit a 50% probability of requiring repair at approximately the same drift as interior joints (1.8% versus 1.7%).
- As drift demands increase, the severity of the damage and required repair effort increases much more rapidly for exterior joints than for interior joints. For exterior joints, there is a 50% probability of requiring MOR 2 (Patching) at a drift demand of 2.9% and MOR 3 (Replace Concrete) at a drift demand of 5.9% (It should be noted that MOR 3 for exterior joints contains very few data point). For modern joints these levels of vulnerability are not reached until the drift demand reaches 4.0% and 5.1%.
- Interior and exterior joints typically do not exhibit damage consistent with MOR 4 (Replace Joint). Only 2 of 65 modern interior joint specimens exhibited damage requiring MOR 4, with the result that 1) it was not possible to create fragility functions for this method of repair and 2) it may be concluded that damage this severe is highly unlikely in joints with modern detailing.

## **4.9 SUMMARY AND CONCLUSIONS**

### **4.9.1 Summary**

Fragility functions were developed that define the probability that a modern reinforced concrete interior or exterior beam-column joint subjected to a specific level of earthquake demand will require, at least, a specific method of repair to restore the

joint to pre-earthquake condition. For the two different joint configurations, data sets linking earthquake demand (EDP) with damage states (DS) were developed using data from previous experimental investigations. Damage states (DS) were linked directly with commonly employed methods of repair (MOR). Earthquake demand parameters (EDP), damage states (DS) and methods of repair (MOR), identified in a previous study (Pagni and Lowes 2006) were used, with modifications to improve characterization of damage progression in modern joints. The empirical demand-repair data were modeled using several probability distribution; these models are referred to a fragility functions. Standard hypothesis testing was used to assess the adequacy with which these distributions fit the empirical data. The lognormal distribution was chosen as the preferred distribution. Fragility functions for modern interior joints were compared with those for older interior and modern exterior joints.

#### **4.9.2 Conclusions**

The results of this study support a number of conclusions about damage progression in beam-column joints:

First, evaluation of demand-damage and demand-repair data for modern interior joints indicates that maximum inter-story drift, a function of maximum drift and number of load cycles, and a function of maximum joint shear strain and number of load cycles are more efficient predictors of damage and required repair technique than were joint shear strain or number of load cycles.

Second, to investigate the impact of different design parameters on damage progression in interior beam-column joints, a reduced data set was assembled of interior joints with design details approaching the requirements of the ACI Building Code (ACI Com. 318-02). Joints in the reduced data set had transverse reinforcement ratios, shear stress demands, and column depths equal to the ACI Code requirements  $\pm 50\%$ . Comparison of fragility functions for the full and reduced data set indicated that, within the ranges considered, design parameters considered do not affect the progression of damage.

Third, to further investigate the impact of design parameters on damage progression in modern interior joints, plots of damage versus earthquake demand were assembled with data grouped by eight design parameters, including maximum shear stress demand, transverse reinforcement ratio, beam bar anchorage length, and column axial load. Evaluation of these plots indicates that for joints meeting the criteria used initially to define modern (having transverse reinforcement, having sufficient joint strength to develop the flexural yield strength of beams, and beam-column strength ratios that ensure columns do not yield), the design parameters considered do not, in general, affect damage progression. The one significant exception to this was that joints with higher shear stress demands reach a given damage state after fewer cycles of loading than do joints with lower shear stress demands. A few additional exceptions to this conclusion were found for specific damage states and design parameters.

Fourth, to investigate damage progression in older versus modern interior beam-column joints, fragility functions were compared for both data sets. These functions show that at low to moderate drift demands, the drift demand at which older and modern joints require a specific method of repair is similar. However, when more extensive damage and methods of repair are considered, the drift demand at which older joints require a specific method of repair is substantially smaller than that for modern joints. Further, while older joints exhibit a 50% probability of developing damage that requires replacement of the joint and, potentially, results in structural collapse at a drift demand of 3.5%, modern joints typically do not exhibit this type of damage. The addition of transverse reinforcement in the joints has substantially improved their performance under lateral loading.

Fifth, to investigate damage progression in modern exterior versus interior (reduced data set) beam-column joints, fragility functions were compared for both data sets. At the low to moderate drift levels, interior joints and exterior joints exhibited similar probabilities for requiring the five methods of repair. However, as drift demand increases, damage increases more rapidly in exterior joints than in interior joints.

#### **4.9.3 Recommendations for Future Research**

Additional experimental research is required to expand EDP-DS data. The EDP-DS data used to develop fragility functions have very large coefficients of variation, and the fragility function parameters generated using these data have very

large confidence intervals. Both of these observations suggest that additional data are required to reduce the scatter of the EDP-DS data and improve the accuracy of damage predictions.



## **5 Structural Walls**

### **5.1 INTRODUCTION**

Structural walls are a key component of the lateral force resisting system of most modern reinforced concrete structures. To facilitate PBEE of walls, models are required to enable prediction of the economic impact of earthquake damage in walls. This chapter documents the development of fragility functions that define the probability that a planar reinforced concrete wall, subjected to a specific level of earthquake demand will require a specific method of repair to restore the wall to pre-earthquake conditions. Given a required method of repair, the cost of the repair and the time required to accomplish the repair can be computed using standard cost-estimating techniques.

The results of previous research provided a basis for developing fragility functions for walls. The results of previous experimental investigation of walls and previous research to develop fragility functions for joints were used to identify 1) a series of potential engineering demand parameters (EDPs) for walls, 2) a set of damage states (DS) characterizing the progression of damage in walls subjected to earthquake loading, and 3) methods of repair (MOR) that could be expected to restore earthquake-

damaged walls to pre-earthquake conditions. With potential EDPs, DSs and MORs defined, the results of experimental testing of planar walls were used to generate an EDP-DS-MOR data set. These data were evaluated to determine 1) the demand parameters that are the most efficient predictors of damage and 2) the design parameters that correlate with damage and could be used to group EDP-DM data to improve the accuracy of fragility functions. Finally, the statistical methods presented in Chapter 3 were used with the EDP-DS-MOR data to generate a suite of fragility functions that define the probability that, at a minimum, a specific method of repair will be required, given a measure of earthquake demand. Evaluation of these fragility functions provides a basis for conclusions about damage progression in walls and recommendation for additional research to be done to advance PBEE of structural walls.

In addition to developing models predicting the likelihood that a particular MOR will be required to restore an earthquake-damaged wall, the results of previous experimental testing of walls were used also to develop models predicting the loss of flexural stiffness in a wall resulting from earthquake damage. Here the results of previous experimental data were used to generate an EDP-effective flexural stiffness data set. These data were evaluated to determine the impact of wall design parameters on stiffness loss under earthquake loading. Ultimately, an exponential relationship between flexural stiffness and inter-story drift of the walls was developed.

The develop processes and resulting fragility functions and stiffness-prediction models are presented in the following sections.

## **5.2 PREVIOUS EXPERIMENTAL RESEARCH**

### **5.2.1 Introduction**

The results of previous experimental investigation into the cyclic response of planar walls were reviewed to develop a data set for use in the current study. Appendix B provides information about the wall test programs reviewed to generate data for the current study, including wall test programs that were reviewed but not used in the current study because the wall specimens did not meet the criteria for inclusion in the current study. The following sections define the criteria for inclusion in the study and present the test programs and specimens employed in the current study.

### **5.2.2 Experimental Data**

Four criteria were used to select the wall test specimens for inclusion in the current study. First, only planar walls, with either a rectangular or barbell configuration were considered. Second, only walls with design details representative of modern construction in zones of high seismicity were included in the study. In particular, only walls with transverse reinforcement in the boundary element were included. Third, specimens subjected to pseudo-static, cyclic or monotonic loading were included. Fourth, only tests for which sufficient damage data were available in published papers

and research reports were included in the study. Lack of sufficient damage data eliminated many tests from inclusion in the current study.

### 5.2.3 Characteristics of Wall Specimens

Ten test programs and 45 test specimens were found that met the above criteria (Table 5.1). For each of these specimens, lateral load was applied at the top of the wall under displacement control. Displacement was increased monotonically or multiple cycles with increasing maximum displacements were imposed. Following is a brief discussion of the test programs and test specimens:

- *Wang et al. (1975)* tested two 1/3-scale walls (SW1 and SW2 as labeled by the researcher) under monotonic and cyclic loading with the objective of studying the behavior of the walls under seismic loading. SW1 was monotonically loaded to a maximum drift demand of 3.0%, and SW2 was subjected to cyclic loading to a maximum drift level of 2.3%. Both walls were subsequently repaired and then subjected to monotonic loading. Only damage data collected prior to repair are used for the current study; data from the repaired specimens are used to validate repair techniques for walls (Section 5.6). Repair included epoxy injection of cracks, replacement of damaged concrete, and straightening of buckled longitudinal reinforcement. The researchers concluded that the maximum stiffness of the repaired walls was approximately 90% of the original walls.

- *Oesterle et al. (1976)* investigated the impact of wall configuration, volume of flexural reinforcement, volume of transverse reinforcement in the boundary element, and load history on the response of slender and squat walls. Seven of nine walls (B1 - B5, R1 and R2 as labeled by the researcher) were used in this study. With the exception of specimen B4, lateral load was applied to the top of the wall to produce a cyclic displacement history. The researchers concluded that wall performance was determined by shear stress demand and that stiff boundary elements greatly improved performance.
- *Oesterle et al. (1979)* investigated the impact of wall configuration and the volume of flexural reinforcement on earthquake response. Five of seven barbell wall specimens (B6 – B10) tested by Oesterle et al. were included in the current study. Two specimens were rejected due to irregular shape (F1 and F2) and the use of repair materials (B9R). All of the included specimens were subjected to cyclic, pseudo- static lateral loading. Variables considered in the experimental program included wall shape, longitudinal and horizontal reinforcement ratio, axial load, load history, concrete strength, and confinement of the boundary element. The researchers found that the wall performance is governed by shear stress demand, the maximum shear stress that can be developed is limited by web crushing, the presence of confined boundary elements improves inelastic behavior, and wall performance is a function of load history.
- *Vallenas et al. (1979)* tested four 1/3-scale wall specimens (SW4 - SW7). The walls were loaded to a maximum drift of 5.5% and then repaired by replacing concrete

(MOR 3 as discussed in Section 5.6). Only data from the initial phase of testing is used to develop fragility functions. Data characterizing the response of repaired walls were used to validate repair methods (Section 5.6). Specimens had different boundary-element confinement ratios and were subjected to different moment-shear demand ratios and displacement histories. The researchers found that slender rectangular walls exhibited out-of-plane instability.

- *Lefas et al. (1990)* investigated the effect of slenderness ratio, axial load, concrete strength, and the volume of web horizontal reinforcement on wall response through testing of 13 rectangular walls with scale factors of 0.3 and 0.4 (SW11 - SW17 and SW21 - SW26). The walls were tested under constant axial load and monotonically increasing lateral load. It was found that shear resistance was determined by concrete triaxial compressive strength, as a triaxial stress state develops in the compressive zone at the base of the wall, rather than concrete tensile strength. Thus, the researchers concluded that the ACI Building Code (318-83) is in conflict with observed structural behavior since
- *Pilakoutas et al. (1991)* tested six walls (SW4 - SW9 as labeled by the researcher) to evaluate previously developed analytical models. The walls were 0.4 scale and subjected to cyclic and monotonic lateral loads. The researchers found reasonable agreement between the analytical and experimental limit states and concluded that discrepancies were due to the expansion of the wall and imperfect crack closure.

- *Yanez et al. (1992)* tested six walls. The one specimen without openings (S1) was used in this study. The researchers concluded that properly designed walls with staggered openings could exhibit the same performance and ductility capacity as continuous walls.
- *Zhang and Wang (2000)* tested four walls (SW7 - SW9 and SW12 as labeled by the researcher) to investigate the impact on response of axial load ratio and shear ratio,  $\lambda_v = V_{\max} / (f_c A_g)$ , where  $V_{\max}$  is the maximum shear acting on the wall section,  $f_c$  is the concrete compression strength, and  $A_g$  is the gross area of wall section. Specimen SW12 was not used in the current study because of atypical construction details. The researchers concluded that the axial load ratio had a major effect on the cracking pattern, flexural strength, failure mode and the ductility.
- *Sittipunt et al. (2001)* tested four walls to investigate the impact of diagonal versus traditional reinforcement layout on seismic performance. The two walls with traditional reinforcement layouts (W1 and W2) were used in the current study. The researchers concluded that the walls with the diagonal reinforcement exhibited superior performance to those with traditional reinforcement layouts. Wall specimens W1 and W2 failed due to web crushing; while, the diagonally reinforced walls had smaller cracks in the web. The researchers also found that the choice of web reinforcement had little impact on the maximum lateral load resisted by the walls.
- *Thomsen and Wallace (2004)* tested two rectangular walls (RW1 and RW2), which differed by the volume of transverse reinforcement placed in the boundary

elements. Walls were subjected to cyclic loading. The researchers found good agreement between predicted and measured strain (curvature) distributions for drift levels up to 2.2% verifying that the ACI 318-99 recommendations for displacement-based design is a powerful and flexible tool.

#### **5.2.4 Wall Specimen Properties and Damage Data**

Table 5.1 lists the 45 wall specimens from nine test programs from which data were collected for the current study. Table 5.1 lists also basic design characteristics for the specimens that could be expected to impact earthquake response. A detailed list of specimen geometric, material and design parameters is provided in Appendix B. For each wall, Table 5.1 includes the following design parameters that could be expected to determine wall performance:

- **Scale:** Most experimental testing is conducted using small-scale models. If the scale is too small, then it might be expected to have an impact on the observed response and progression of damage. Since not all researchers specify specimen scale and since researchers may define scale using different approaches, wall scale was defined for the current study as the test specimen wall thickness divided by a typical full-scale wall thickness of 12 in. Review of existing structures suggests that 12 in. represents a lower bound on typical wall thickness.
- **Aspect Ratio** is defined as the height of the wall divided by the length of wall in the plan view. Walls with small aspect ratios could be expected to have higher base



shear-to-moment ratios and, as a result, exhibit larger shear deformations. Walls with large aspect ratios could be expected to have smaller base shear-to-moment ratios and exhibit small shear deformations.

- **Reinforcement ratios,  $\rho$** , define the area of longitudinal reinforcing steel relative to a specific area of the concrete wall. This parameter could be expected to determine wall performance. For the current study,  $\rho$  is defined as the ratio of the area of reinforcing steel to the area of the concrete perpendicular to the direction of the steel. This definition is used for the horizontal reinforcing steel ratio,  $\rho_{\text{horiz}}$ , the longitudinal steel ratio for the web of the wall,  $\rho_{\text{long,web}}$ , and the longitudinal reinforcement ratio for the boundary element,  $\rho_{\text{long,BE}}$ .
- $V_{\text{max}}/V_n$  is the shear demand-capacity ratio.  $V_{\text{max}}$  is the maximum shear demand as measured in the laboratory. Shear capacity is defined per the ACI Building Code (ACI Com. 318 2002):

$$V_n = A_{cv}(\alpha_c \sqrt{f'_c} + \rho_n f_y) \quad 5.1$$

where  $A_{cv}$  is the total cross sectional area,  $f'_c$  is the compressive strength of the concrete,  $\rho_n$  is the ratio of steel area (parallel to the plane of  $A_{cv}$ ) to concrete area, and  $f_y$  is yield strength of the reinforcement. The factor  $\alpha_c=3.0$  when the aspect ratio is less than or equal to 1.5,  $\alpha_c=2.0$  when the aspect ratio is great than or equal to 2.0 and varies linearly between. Shear demand-capacity ratio could be expected to determine

wall performance, with walls with higher shear demand exhibiting increased shear deformation and damage.

- $V_{\max}/(A_g f_c^{1/2})$ : The average shear stress corresponding to the maximum measured shear normalized by the gross area of the wall and the square root of  $f_c$ . Shear demand-capacity ratio could be expected to determine wall performance, with walls with higher shear demand exhibiting increased shear deformation and damage.

Table 5.1 Experimental details for structural walls

Specimen ID	Shape	Scale: Thickness /12"	Aspect Ratio	Load History	$f_c$ (psi)	$\rho_{horiz}$ (%)	$\rho_{long, BE}$ (%)	$\rho_{long, web}$ (%)	$V_{max}/V_n$	$V_{max}/$ $(A_g * f_c^{1/2})$	Axial Load (% $A_g f_c$ )
Lefas SW11	rectangular	0.23	1.0	M	6134	1.10	3.10	2.40	0.80	8.83	0
Lefas SW12	rectangular	0.23	1.0	M	6322	1.10	3.10	2.40	1.07	11.65	10.0
Lefas SW13	rectangular	0.23	1.0	M	4676	1.10	3.10	2.40	1.08	13.34	20.0
Lefas SW14	rectangular	0.23	1.0	M	4812	1.10	3.10	2.40	0.87	10.56	0
Lefas SW15	rectangular	0.23	1.0	M	4921	1.10	3.10	2.40	1.03	12.42	10.0
Lefas SW16	rectangular	0.23	1.0	M	6047	1.10	3.10	2.40	1.14	12.62	20.0
Lefas SW17	rectangular	0.23	1.0	M	5554	0.37	3.10	2.40	1.67	9.16	0
Lefas SW21	rectangular	0.21	2.0	M	4876	0.80	3.30	2.50	0.73	6.25	0
Lefas SW22	rectangular	0.21	2.0	M	5887	0.80	3.30	2.50	0.85	6.72	10.0
Lefas SW23	rectangular	0.21	2.0	M	5481	0.80	3.30	2.50	1.03	8.35	20.0
Lefas SW24	rectangular	0.21	2.0	M	5554	0.80	3.30	2.50	0.69	5.53	0
Lefas SW25	rectangular	0.21	2.0	M	5075	0.80	3.30	2.50	0.86	7.23	20.0
Lefas SW26	rectangular	0.21	2.0	M	3635	0.40	3.30	2.50	1.25	7.01	0
Oesterle B1	barbell	0.33	2.4	C	7685	0.31	1.47	0.25	0.74	2.36	0
Oesterle B2	barbell	0.33	2.4	C	7775	0.31	4.00	0.25	1.83	5.86	0
Oesterle B3	barbell	0.33	2.4	C	6860	0.31	1.11	0.29	0.80	2.50	0
Oesterle B4	barbell	0.33	2.4	M	6530	0.31	3.67	0.29	0.98	3.22	0
Oesterle B5	barbell	0.33	2.4	C	6570	0.31	1.11	0.29	2.10	6.83	0
Oesterle R1	rectangular	0.33	2.4	C	6490	0.31	1.11	0.29	0.26	1.14	0
Oesterle R2	rectangular	0.33	2.4	C	6735	0.63	3.67	0.29	0.29	2.05	0
Oesterle B6	barbell	0.33	2.4	C	3165	0.63	3.67	0.29	1.66	11.61	13.4
Oesterle B7	barbell	0.33	2.4	C	7155	0.63	3.67	0.29	1.73	8.59	7.6
Oesterle B8	barbell	0.33	2.4	C	6085	0.63	3.67	0.29	1.78	9.23	9.0
Oesterle B9	barbell	0.33	2.4	C	6395	0.63	3.67	0.29	1.95	9.63	8.5
Oesterle B10	barbell	0.33	2.4	C	6615	0.63	3.67	0.29	1.42	7.09	8.2
Pilakoutas SW4	rectangular	0.20	2.0	C	5351	0.39	6.86	0.49	1.16	5.79	0
Pilakoutas SW5	rectangular	0.20	2.0	C	4612	0.31	12.75	0.59	1.87	6.96	0
Pilakoutas SW6	rectangular	0.20	2.0	C	5598	0.31	6.86	0.49	1.62	5.71	0
Pilakoutas SW7	rectangular	0.20	2.0	C	4641	0.39	12.75	0.59	1.57	8.26	0
Pilakoutas SW8	rectangular	0.20	2.0	C	6642	0.31	7.14	0.49	1.64	5.51	0
Pilakoutas SW9	rectangular	0.20	2.0	C	5642	0.31	7.14	0.49	1.49	5.23	0
Sittipunt W1	barbell	0.33	1.3	C	5307	0.52	2.29	0.39	1.28	6.52	0
Sittipunt W2	barbell	0.33	1.3	C	5191	0.79	2.29	0.52	1.21	8.17	0
Thomsen RW1	rectangular	0.33	3.1	C	4580	0.33	2.93	0.33	0.59	2.54	10.0
Thomsen RW2	rectangular	0.33	3.1	C	4925	0.33	2.93	0.33	0.64	2.67	7.0
Vallenas SW3	barbell	0.33	1.3	M	5075	0.82	3.53	0.82	1.02	9.16	7.7
Vallenas SW4	barbell	0.33	1.3	C	5075	0.82	3.53	0.82	0.90	8.15	7.7
Vallenas SW5	rectangular	0.38	6.6	M	5020	0.54	5.58	0.54	0.91	6.24	6.0
Vallenas SW6	rectangular	0.38	6.6	C	5020	0.54	5.58	0.54	0.94	6.47	6.0
Wang SW1	barbell	0.33	1.4	M	4653	0.82	3.52	0.82	1.05	9.67	8.5
Wang SW2	barbell	0.33	1.4	C	4800	0.82	3.52	0.82	1.03	9.40	8.2
Zhang SW7	rectangular	0.33	2.1	C	4307	1.01	6.16	0.67	1.01	6.36	24.0
Zhang SW8	rectangular	0.33	2.1	C	4640	1.01	4.52	0.67	1.12	6.82	35.0
Zhang SW9	rectangular	0.33	2.1	C	5133	1.01	12.57	0.67	1.49	8.78	24.0
min	-	0.20	1.0	-	3165	0.31	1.11	0.25	0.26	1.14	0.0
max	-	0.38	6.6	-	7775	1.10	12.75	2.50	2.10	13.34	35.0
average	-	0.28	2.1	-	5528	0.64	3.78	1.05	1.16	7.23	6.8

Note: In the Load History column 'M' represents monotonic loading and 'C' represents cyclic loading.

### 5.3 ENGINEERING DEMAND PARAMETERS SPECIFIC TO WALLS

Engineering demand parameters (EDP) quantify the earthquake loading of a wall and can be used to predict the damage state of the wall. The preferred EDP can be computed using available structural analysis software, reliably predicts damage, and results in fragility functions with low coefficients of variation. Evaluation of research results and previous efforts to develop fragility functions for concrete components, provided guidance in selecting potential EDPs for structural walls. The potential EDPs included the following:

- **Inter-story drift:** Drift is a simple demand measure provided by all researchers, and there is consensus among engineers that drift determines damage in RC components.
- **Number of load cycles:** Like drift, the number of load cycles is a simple demand measure provided by all researchers. Additionally, previous experimental research indicates that the number of load cycles may affect the performance of reinforced concrete components (El-Bahy et al. 1999, Walker 2001, Alire 2003). Here, the number of load cycles was computed from the displacement history and a cycle counting algorithm was employed in which the contribution of a specific displacement cycle was weighted by the ratio of the maximum displacement demand of the cycle to the maximum historic displacement demand.
- **Displacement ductility:** defined as the ratio of maximum displacement demand to the yield displacement. Yield displacement is defined as the displacement at first

yield of the longitudinal reinforcement. Displacement ductility could be expected to be good predictor of damage because it defines the extent of yielding and progressive yielding could be expected to result in widening of cracks and more extensive damage.

- **Plastic rotation:** defined as the maximum displacement demand minus the yield displacement divided by the height of the wall:

$$\theta_p = \frac{\Delta_{\max} - \Delta_{\text{yield}}}{\text{height}} \quad 5.2$$

The plastic rotation indicates how far beyond yield the component has been loaded. As with displacement ductility, plastic rotation could be expected to be a good measure of demand because it defines the extent of flexural yielding. Note that a plastic rotation was computed for all displacement demands using Eq. 5.2; thus, if the wall displacement was less than the yield displacement a negative plastic rotation was computed.

The correlation between damage and each of the above EDPs was investigated (Section 5.7) to determine a set of preferred EDPs for use in developing fragility functions.

#### 5.4 DAMAGE STATES FOR WALLS

Damage in structural walls was characterized by six damage states (DS) that describe the extent of concrete cracking, spalling, crushing, and loss of lateral strength. To

develop this set of DS, the results of previous research to develop repair-specific fragility functions (Pagni and Lowes 2006, Pagni 2003) were reviewed. Additionally, the experimental data were reviewed to determine the extent of available damage data.

These DS used for walls are a subset to the DS used for modern joints presented in Section 4.3.2. For walls, the available damage data were substantially more limited damage than was the case for joints. For example, research reports documenting wall tests typically did not include maximum or residual crack width measurements, but provided only descriptions of the extent of cracking. Thus, it was necessary to define relatively broad damage states, so that as much of the available damage data as possible could be used. These broad damage states were defined primarily on the basis of the repair techniques. These six damage states employed to characterize the progression of was data were as follows:

- **DS 0.** First recorded horizontal crack.
- **DS 1.** First recorded diagonal crack.
- **DS 2.** Recorded and/or measured yield of extreme reinforcement.
- **DS 3.** Initial spalling of concrete cover as specified within the research document.
- **DS 4.** Crushing of the web concrete recorded in the report.
- **DS 5.** Extreme damage including a) buckling of the reinforcement or b) damage resulting in the reduction of lateral strength by 20%.

## **5.5 PREDICTING DAMAGE AS A FUNCTION OF DEMAND**

### **5.5.1 Introduction**

With specific EDPs and DSs identified, documentation of previous experimental tests was reviewed to generate EDP-DS data sets. The EDP-DS data set was used to determine preferred EDPs and parameters that determine damage progression in structural walls.

### **5.5.2 Identification of a Preferred EDP**

Figure 5.1 shows plots of damage versus EDP for each of the proposed EDPs: drift, number of cycles, displacement ductility and plastic rotation. Figure 5.1 provides also correlation coefficients for each data set. Numbers of cycles, displacement ductility and plastic rotation all have similar correlation coefficients of approximately 0.7 while drift has a correlation coefficient of 0.83. Thus, drift is a slightly more efficient predictor of damage than are the other potential EDPs considered. Note that Figure 5.1 shows negative plastic rotations at low damage states. This is due to the fact that plastic rotation was computed using Eq. 5.2 for all displacement levels, resulting in negative plastic rotations for displacements less than the yield displacement.

Review of the data in Figure 5.1 shows that data points are in a tight cluster for the lower damage states and that the dispersion of the data increases as the DS increases. This might be expected since all the walls could be expected to exhibit initial

cracking at approximately the same drift level, while variation in design parameters could be expected effect development of higher DSs, such as crushing of the concrete.



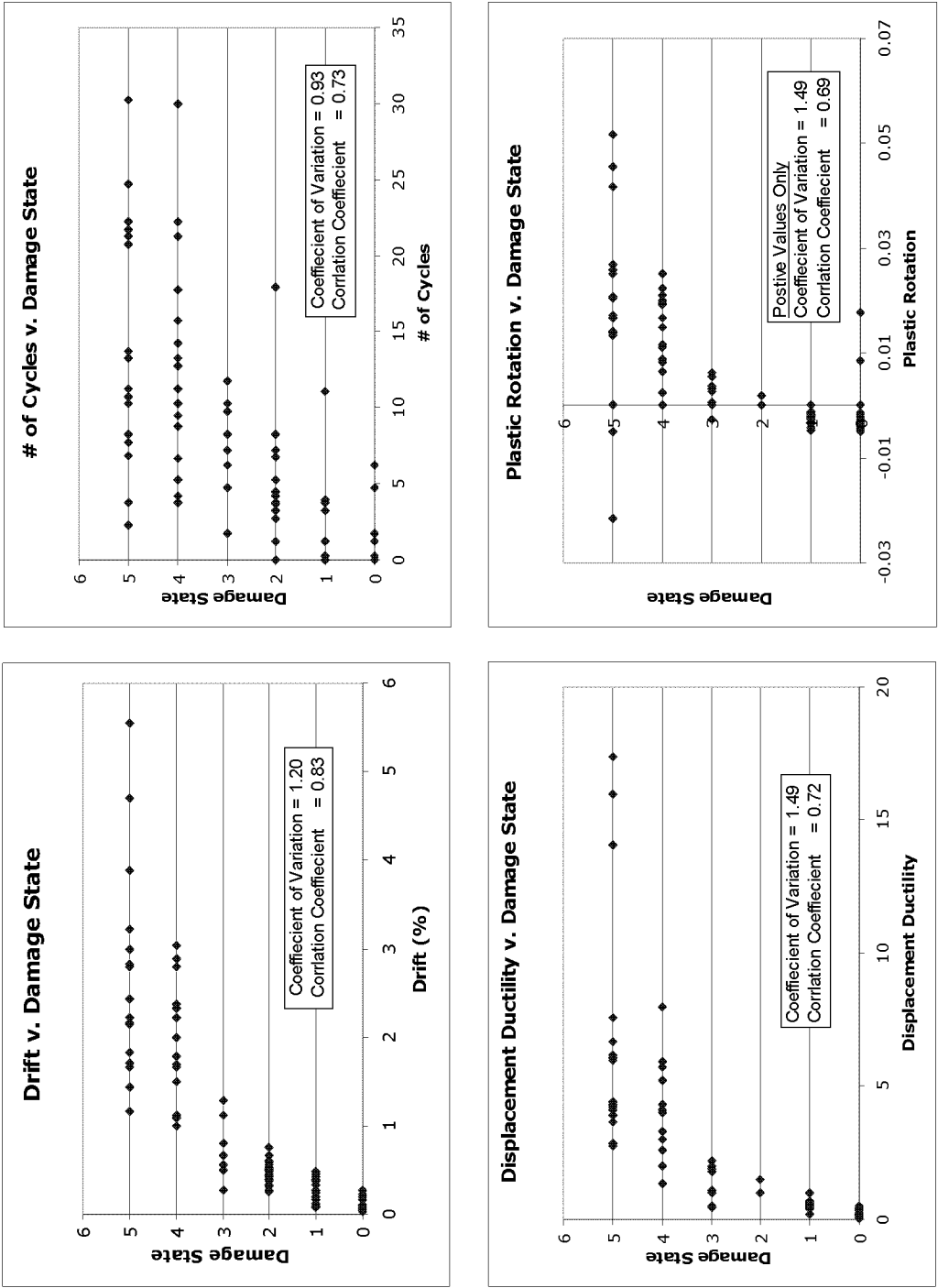


Figure 5.1 DSs versus EDPs

### **5.5.3 Identification of a Design Characteristics that Determine Damage Progression**

With drift identified as the preferred EDP, the drift-damage data were evaluated to determine if damage progression was dependent on specific design parameters. Wall shape, aspect ratio, and shear demand-capacity ratios were considered.

#### ***5.5.3.1 Damage States versus Drift – Wall Shape***

Two wall shapes were considered in this study, rectangular and barbell. The rectangular walls have a constant thickness throughout the entire length of the wall while the barbell walls have an increased thickness at the ends of the walls. The reduced thickness of the web of a barbell wall might be expected to result in more rapid yielding of web reinforcement and more rapid deterioration of web concrete, which in turn reduces the strength of the wall.

Figure 5.2 shows damage versus drift for the walls in the experimental data set with rectangular and barbell walls identified by different symbols. Table 5.2 lists, for each DS and each shape, the mean drift at initiation of the DS and the coefficient of variation on the mean drift. The rectangular and barbell walls have similar damage progression until DS 4 when rectangular walls experience damage at a much lower drift levels than do the barbell walls, drifts of 1.28% and 2.20%, respectively. This trend continues to DS 5; the average drift required to achieve DS 5 in rectangular walls was 1.92% and it was 3.25% in the barbell walls.

Thus, the data indicate that rectangular and barbell walls experience cracking, yielding of longitudinal reinforcement, and spalling of cover concrete at similar drift levels; however, rectangular walls experience web crushing and extreme damage at significantly lower drift levels than do barbell walls.

Ultimately, fragility functions were developed for the combined data set that included both barbell and rectangular walls. Individual fragility functions were not developed for the barbell and rectangular walls because there were too few data points in the lower damage states for individual wall data sets.

#### ***5.5.3.2 Damage States versus Drift – Impact of Aspect Ratio***

Aspect ratio is defined as the ratio of wall height to length. For this study it was defined as the height from the fixed base of the wall to point at which lateral load was applied divided by the total length of the wall. Aspect ratio could be expected to determine damage progression since squat walls (low aspect ratio walls) could be expected to develop higher shear demands and exhibit more shear deformation while slender walls could be expected to response entirely in flexure. For the current study, an aspect ratio of 1.5 was considered to represent the upper limit on squat wall behavior; while walls with aspect ratios in excess of 2.0 were considered to exhibit behavior dominated by flexure. Figure 5.2 shows damage versus drift for the walls in the experimental data set with aspect ratios less than or equal to 1.5, between 1.5 and 2, and greater than 2 identified by different symbols as defined in the legend. Table 5.2

lists, for each DS and aspect ratio grouping, the mean drift at which the DS initiates and the coefficient of variation for the mean drift. With one exception, all three divisions of the aspect ratio exhibit similar damage progression and each aspect ratio division has approximately the same mean drift at which each DS initiates. The one exception is for walls with aspect ratios between 1.5 and 2; these walls exhibit DS 4 and 5 at much lower drift levels than the other aspect ratio divisions. However, for walls with aspect ratios between 1.5 and 2, the data set includes only two data points for DS 4 and three data points for DS 5. Thus, it is likely that the atypical behavior is due to the limited size of the data set. Thus, the damage prediction model is not dependent on the aspect ratio.

#### ***5.5.3.3 Damage States versus Drift – Shear Demand-Capacity Ratio***

Damage progression in a wall could also be expected to be dependent on the shear demand-capacity ratio. Walls with higher demand-capacity ratios could be expected to exhibit increased shear deformation. Additionally, analyses of walls using continuum models shows that interaction of flexure and shear demands results in early yielding of longitudinal reinforcement. Finally, concrete cracking due to flexural yielding can reduce the shear capacity of the wall and ultimately produce a shear failure.

For the current study, shear demand-capacity ratio was defined as the maximum applied lateral load divided by the nominal shear strength (Eq. 5.1). Walls

were classified as having low shear demand, with shear demand-capacity ratios less than 1.0 or high shear demand with demand capacity ratios greater than 1.0 as shown in Figure 5.2. Table 5.2 lists, for each DS and shear demand-capacity ratio grouping, the mean and coefficient of variation for the drift divided by shear demand capacity ratio. Both divisions of the shear demand capacity ratio have similar damage progression with the exception of DS 4. This anomaly in the data is attributed to the sparsity of the available data. Thus, the damage prediction model is not dependent on shear-demand capacity ratio.

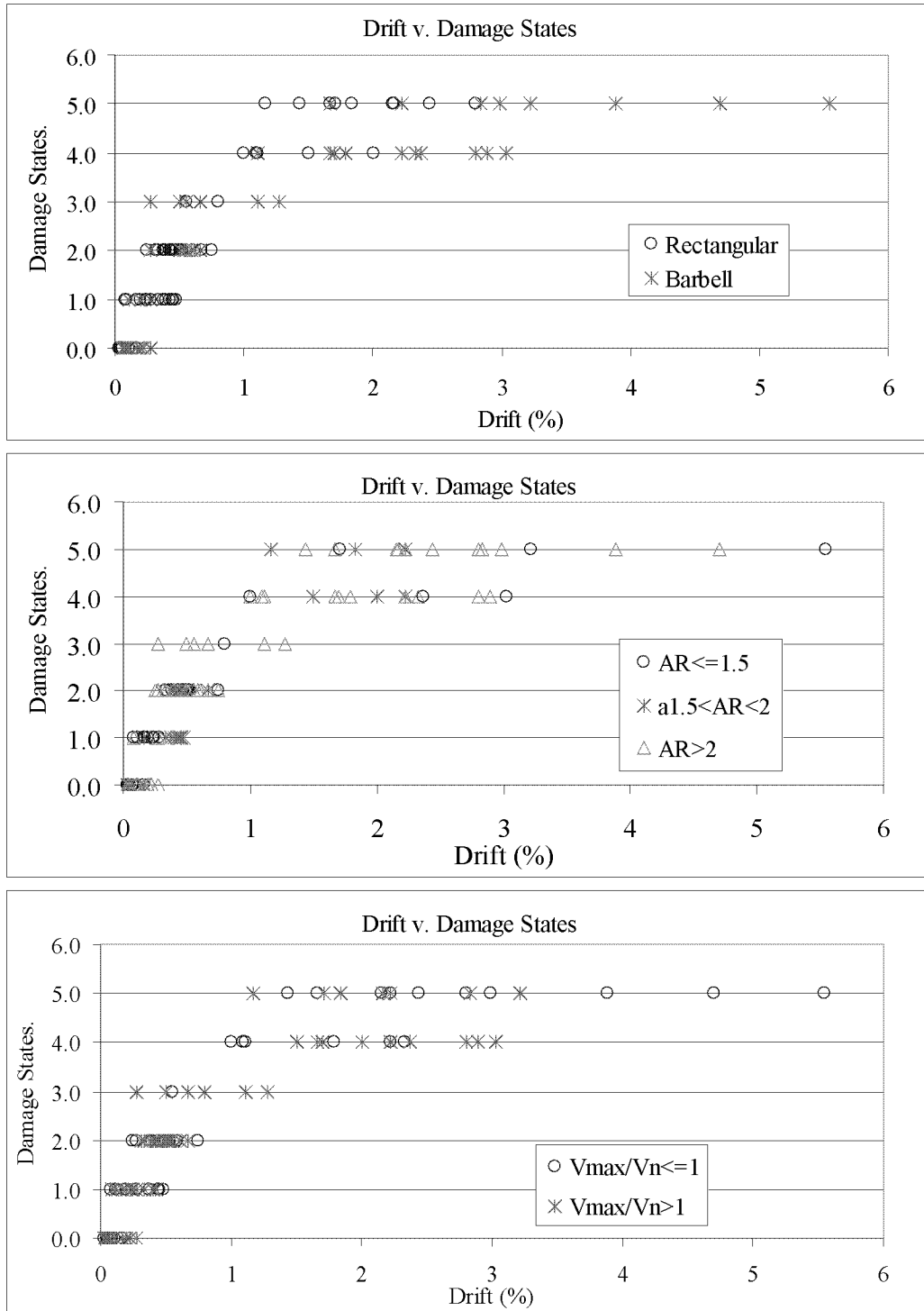


Figure 5.2 DS versus Drift

Table 5.2 Mean and Coefficient of Variation for drift separated by wall shape, aspect ratio and shear capacity demand ratio

Drift				
Wall Shape				
	Rectangular		Barbell	
Damage State	mean, $\mu$	Coefficient of Variation	mean, $\mu$	Coefficient of Variation
DS 0	0.08	0.75	0.14	0.55
DS 1	0.29	0.43	0.17	0.44
DS 2	0.47	0.25	0.49	0.27
DS 3	0.64	0.64	0.75	0.49
DS 4	1.28	0.31	2.20	0.24
DS 5	1.92	0.25	3.25	0.39

Drift						
Aspect Ratio						
	AR<1.5		1.5<AR<=2		AR>2	
Damage State	mean, $\mu$	Coefficient of Variation	mean, $\mu$	Coefficient of Variation	mean, $\mu$	Coefficient of Variation
DS 0	0.06	0.35	0.10	0.69	0.14	0.64
DS 1	0.20	0.28	0.37	0.23	0.18	NA
DS 2	0.48	0.17	0.48	0.16	0.47	0.34
DS 3	No Data	No Data	No Data	No Data	0.72	0.44
DS 4	2.35	0.19	1.75	NA	2.61	0.27
DS 5	3.08	0.50	1.75	0.24	3.25	0.31

Drift				
Shear Demand-Capacity Ratio				
	$V_{max}/V_n \leq 1$		$V_{max}/V_n > 1$	
Damage State	mean, $\mu$	Coefficient of Variation	mean, $\mu$	Coefficient of Variation
DS 0	0.06	0.54	0.13	0.62
DS 1	0.30	0.51	0.25	0.41
DS 2	0.45	0.35	0.49	0.19
DS 3	0.62	NA	0.78	0.49
DS 4	1.41	0.42	2.20	0.23
DS 5	2.54	0.42	2.56	0.49

Note: NA indicates only two data points which can give misleading results for the standard deviation. No Data indicates that no data was available for the design parameter DS

## 5.6 METHODS OF REPAIR FOR WALLS

The results of previous research indicate that the MORs described in Section 2.4 are appropriate for use in repairing earthquake-damaged walls. For example, Lefas and Kostovos (1990) used epoxy injection, concrete replacement and straightening of buckled reinforcement bars to repair damaged walls and return them to 80% of their pre-earthquake strength. Oesterle et al. (1976) removed and replaced the damage concrete from the web which returned the wall to 80% of its pre-earthquake strength.

To develop repair-specific fragility functions for walls, it is necessary to link DSs with MORs to generate EDP-MOR data pairs. Figure 5.3 displays pictures of the DSs and Table 5.3 lists the specific DSs that are associated with each MOR for the current study. These linkages were developed on the basis of similar linkages developed for joints. For DS 3-5 and MOR 2-4, each DS is associated with a single MOR; determination of these linkages followed directly from the previous research. For the cases of MOR 0, cosmetic repair and MOR 1, epoxy injection, the primary issue that must be addressed in linking damage states with methods of repair is the maximum crack width for which epoxy injection is required. Review of the experimental data indicated that at the initiation of flexural cracking (DS 0), cracks width typically were not sufficiently wide as to require epoxy injection, but that at the initiation of diagonal cracking (DS 1) damage was typically more severe and cracks likely to be sufficiently wide as to require epoxy injection. Thus, DS 1 (initiation of



diagonal cracking) and DS 2 (yield of longitudinal reinforcement) were linked with MOR 1.

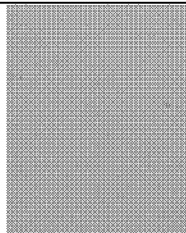
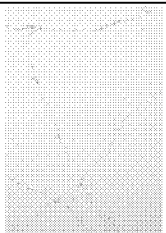
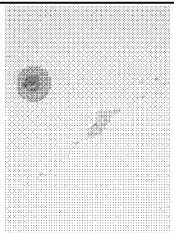
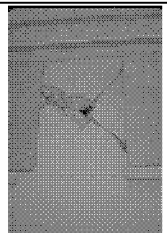
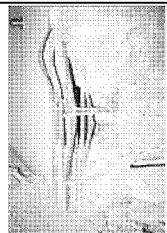
MOR 0 Cosmetic Repair	MOR 1 Epoxy Injection	MOR 2 Patching	MOR 3 Replace Concrete	MOR 4 Replace Joint
 <a href="http://nisee.berkeley.edu/libRARY">http://nisee.berkeley.edu/libRARY</a> Replace and repair finishes.	 <a href="http://nisee.berkeley.edu/libRARY">http://nisee.berkeley.edu/libRARY</a> Inject cracks with epoxy and replace finishes.	 <a href="http://nisee.berkeley.edu/libRARY">http://nisee.berkeley.edu/libRARY</a> Patch concrete, epoxy inject cracks, and replace finishes.	 <a href="http://nisee.berkeley.edu/libRARY">http://nisee.berkeley.edu/libRARY</a> Remove and replace damaged concrete and replace finishes.	 <a href="http://nisee.berkeley.edu/libRARY">http://nisee.berkeley.edu/libRARY</a> Replace damaged steel, remove and replace damaged concrete and replace finishes.
DS 0	DS 1 - 2	DS 3	DS 4	DS 5

Figure 5.3 Pictures and Descriptions of DMs Associated with MORs for Structural Walls

Table 5.3 Methods of Repair for Walls

Method of Repair	Activities	DS for Structural Walls
0. Cosmetic Repair	Replace and repair finishes.	0
1. Epoxy Injection	Inject cracks with epoxy and replace finishes.	1-2
2. Patching	Patch spalled concrete, epoxy inject cracks and replace finishes.	3
3. Replace Concrete	Remove and replace damaged concrete, replaces finishes	4
4. Replace steel	Replace damaged reinforcing steel, remove and replace concrete, and replace finishes.	5

## 5.7 FRAGILITY FUNCTIONS FOR WALLS

With drift identified as the preferred EDP for prediction of damage in walls, fragility functions were generated defining the probability that given a specific level of

earthquake demand, as defined by maximum drift ratio, a specific MOR would be required to restore the wall to pre-earthquake conditions. The process used to generate the fragility functions was 1) use EDP-DS data and the DS–MOR associations listed in Table 5.3 to generate drift versus MOR data, 2) use the Method of Maximum Likelihood to fit a standard probability distribution to the empirical data, and 3) use goodness of fit testing to evaluate the adequacy of the probability distribution.

Table 5.4 lists statistics for the EDP-MOR data for the wall specimens. These data were generated from the EDP-DS data using the deterministic relationships between DSs and MORs listed in Table 5.3. Given a specific value of an EDP, the ideal family of fragility functions results in identification of a single MOR that has a relatively high probability of being met or exceeded, with all more extensive MORs having a relatively low probability of being met or exceeded. This requires that the EDP-MOR data have well-spaced means and low variances. Table 5.4 shows the sample mean and coefficient of variation (c.o.v.) for each of the EDP-MOR data sets. Drift result in well-spaced means across the range of MORs, but relatively large c.o.v.s for each MOR. The large c.o.v.s are a direct measure of the scatter of the data. MOR 0, which was the most difficult MOR to accurately gather damage data for due to the lack of crack width information presented in the reports. Given the diversity of methods used to report damage in the wall reports the c.o.v. are of a reasonable magnitude.

Table 5.4 Statistical Characteristics of EDP-Method of Repair Data

MOR	drift	
	Mean	c.o.v.
0	0.1	0.65
1	0.5	0.47
2	1.0	0.55
3	1.9	0.34
4	2.6	0.48
	max	0.65
	avg.	0.50

### 5.7.1 Use of Empirical Data to Calibrate Fragility Functions

Empirical fragility functions defining the probability of an earthquake damaged wall requiring a specific method of repair could be developed directly from the EDP-MOR data sets. However, to facilitate use of the fragility functions, it is desirable to fit a standard probability distribution to the empirical data. For the current study, only the lognormal distribution was considered as discussed in Section 3.2.2 and Section 4.6. This distribution has been used commonly to define fragility functions for structural components.

The lognormal distribution is recommended for use in predicting the probability that a specific method of repair will be required to restore a structural wall subjected to earthquake loading. Figure 5.4 shows the theoretical and empirical fragility functions developed for use in predicting the probability that a method of repair will be required given an earthquake demand on the modern joint. Table 5.5 provides the parameters defining the lognormal distribution as well as the 95%

confidence interval on these parameters, normalized with respect to the value of the parameter. The confidence interval is

$$C.I. = 2t\sqrt{S} \quad 5.3$$

where  $t$  is the inverse of the Student's T CDF (Kottagoda and Rossa 1997) for the 95% confidence level and  $S$  is the diagonal of the covariance matrix for the coefficient estimates. The confidence interval was computed using the Matlab function **mle**.

The theoretical fragility functions presented in Figure 5.3 are appropriate for use in predicting the probability that a particular method of repair will be required, given an earthquake demand as defined by one of three EDPs. However, comparison of the theoretical and empirical fragility functions as well as evaluation of the confidence interval data in Figure 5.4 indicates that there is significant uncertainty in the parameters that define these models. This uncertainty is due primarily to the sparsity of the data sets used to construct the models.

Table 5.5 Lognormal distribution parameters

MOR	Drift			
	$\ln(\mu)$		$\sigma$	
	value	95% C.I.	value	95% C.I.
	value	95% C.I.	value	95% C.I.
0	-2.455	0.175	0.634	0.493
1	-1.091	0.371	0.641	0.458
2	-0.166	3.861	0.580	0.845
3	0.586	0.610	0.370	0.723
4	0.868	0.469	0.423	0.723

Notes: Distribution parameters refer to the log of the EDP data. The 95% C.I. is the 95% confidence interval on the parameter, normalized with respect to the value of the parameter. The confidence interval is not symmetric with respect to the distribution parameter.  $\mu$  is the mean of the data and  $\sigma$  is the standard deviation of the data

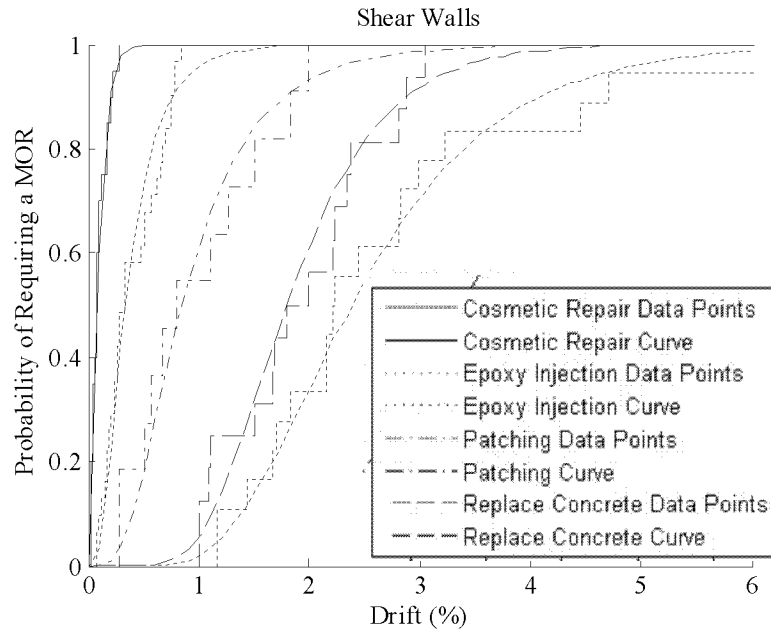


Figure 5.4 Fragility functions for structural walls.

Table 5.6 shows the results of the hypothesis test. From the data in this table, it may be concluded that the lognormal distribution is acceptable for use in modeling. According to the Lilliefors test the lognormal distribution is acceptable for all but MOR 0; damage data associated with MOR 0 was difficult to consistently record due to the lack of crack width information presented in the wall reports.

Table 5.6 Results of the goodness-of-fit tests for structural wall lognormal distribution

	Drift	
	Lilliefors Test	
MOR	P	correct CDF
2	0.01	FALSE
3	0.11	TRUE
4	>0.20	TRUE
5	0.06	TRUE
0	> 0.20	TRUE

## 5.8 EVALUATION OF THE FRAGILITY FUNCTIONS

The fragility functions presented in Figure 5.4 show a relatively smooth progression of increasing damage under increasing drift demand. Though, there is a noticeable jump in the progression as the required method of repair progresses from the relatively simply patching of concrete (MOR 2) to the more extensive replacement of concrete (MOR 3). Evaluation of the fragility function plots in Figure 5.4 emphasizes the increased scatter of the data at higher demand-damage levels. A likely explanation for this is that the impact of the variation in design parameters has more of an impact for more severe damage states.

## 5.9 EFFECTIVE STIFFNESS VERSUS DRIFT

In addition to developing damage-prediction models, for structural walls, experimental data were used also to develop models for predicting effective flexural

stiffness. These models may be used in analysis to improve prediction of load and deformation demands on walls subjected to earthquake loading. To develop these models, data were collected for each of the experimental tests specimens listed in Table 5.1, relating earthquake demand, as defined by drift, with effective flexural stiffness. These data were evaluated to determine the impact of design parameters on stiffness. Finally, functional relationships were calibrated using the data.

### 5.9.1 Earthquake Demand and Effective Stiffness Data

Ideally, in developing effective stiffness models for walls, one would develop models for predicting both effective flexural and shear stiffness. However, for most of the wall specimens listed in Table 5.1, only load-displacement data were available. Thus, the walls were assumed to respond only in flexure, and effective flexural stiffness was determined using the data. For various levels of earthquake demand, the effective stiffness ratio,  $k_{eff}$ , was defined as the secant stiffness,  $k_{secant}$ , divided by the gross-section flexural stiffness,  $k_{gross}$ . At any point in the test history, the secant stiffness is defined

$$k_{secant} = \frac{\Delta_{max}}{P} \quad 5.4$$

where  $\Delta_{max}$  and  $P$  are the displacement demand and load at a point in the test history.

The gross stiffness is defined:

$$k_{gross} = \frac{3E_c I_{gross}}{h^3} \quad 5.5$$

where  $E_c$  is the concrete elastic modulus,  $I_{gross}$  is the moment of inertia of the gross wall section, and  $h$  is the height of the wall. Concrete elastic modulus was estimated using the equation recommended in the ACI Building Code (ACI 318 2002):

$$E_c = 57000\sqrt{f'_c} \text{ psi} \quad 5.6$$

where  $f'_c$  is the compressive strength of concrete in psi.

Since drift was found to be the most efficient predictor of damage, drift was the only EDP considered in developing stiffness-prediction models.

### 5.9.2 Investigation of the Impact of Design Parameters on Effective Stiffness

To determine if design parameters affect stiffness loss in walls, plots of effective stiffness ratio versus drift with data grouped by design parameters were reviewed. Figure 5.5 shows effective stiffness versus drift, with data grouped by wall shape, aspect ratio and shear capacity-demand ratio. The data in Figure 5.5 show effective stiffness ratio is determined by wall configuration, with rectangular walls exhibiting a higher effective stiffness ratio at lower drift levels than barbell walls. The data in Figure 5.5 suggest also that barbell walls are capable of sustaining higher drift levels than rectangular walls. When the data is grouped by aspect ratio or shear capacity-demand ratio there is no correlation between design parameters and change in effective stiffness ratio. These observations are consistent with the DS-EDP data (Section 5.5.3)



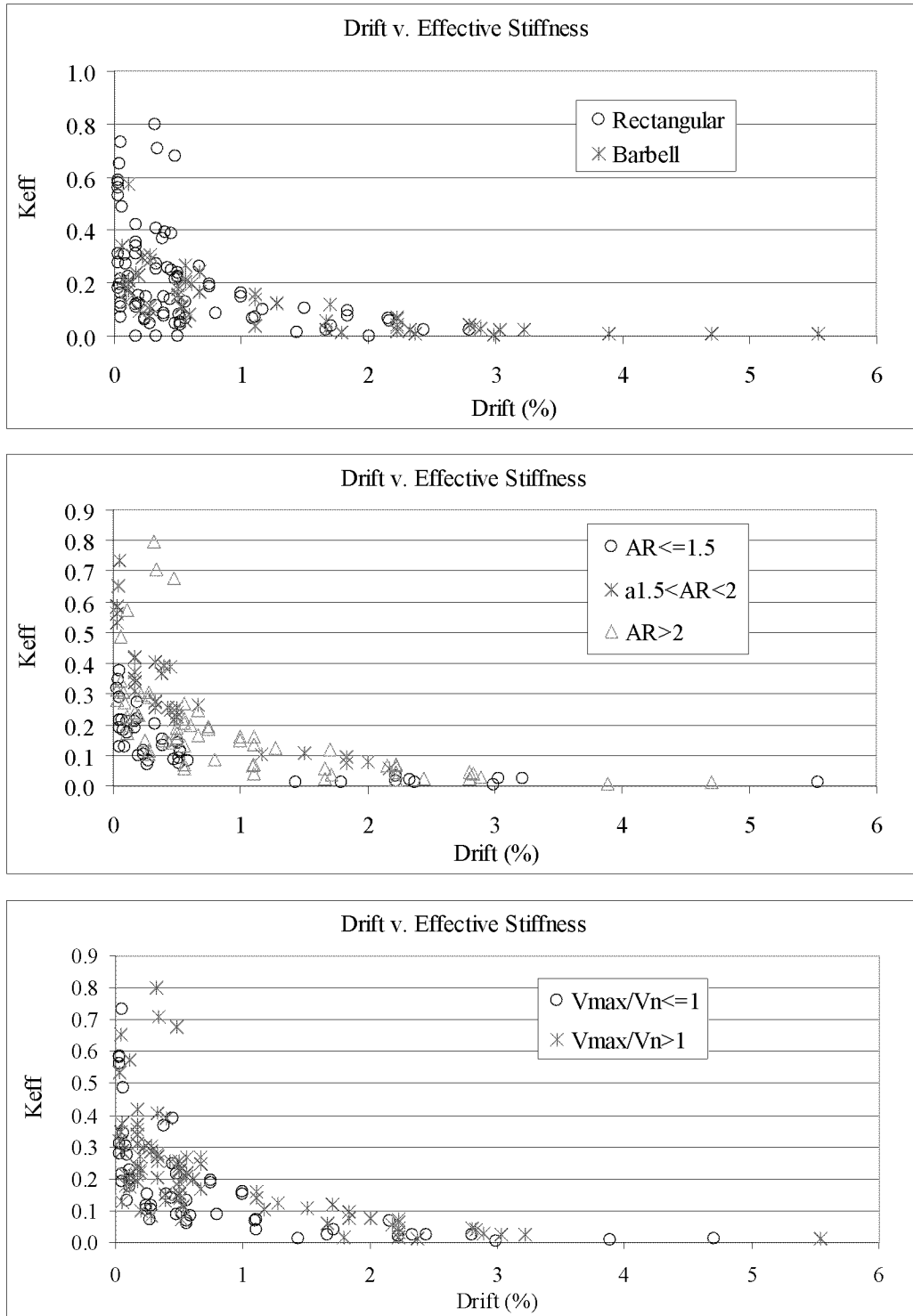


Figure 5.5 Effective Stiffness versus Drift

### 5.9.3 Development of an Effective Stiffness versus Drift Model

To facilitate use of the drift versus effective stiffness data, functional relationships were defined to fit the data. Functions were developed for the full data set and for a data set comprising only rectangular walls. No model was developed for barbell walls as this configuration is rarely found in modern construction.

Review of the effective stiffness versus drift suggested that the functional relationships should be exponential. Also, because of the relatively large scatter in the drift-effective stiffness data and the rapid change in effective stiffness at low drift levels; it was decided that the functional relationships should include a single average effective stiffness ratio for low drift demands. To determine the drift at which the effective stiffness ratio would plateau, the drift versus damage data were considered. For DS 0, the maximum drift at which initiation of the damage state was observed was 0.3%; for DS 1, the average drift at which initiation of the damage state was observed was 0.3%. Thus, a drift of 0.3% was chosen as the maximum drift for which effective stiffness would remain constant.

For each data set, a two step process was used to calibrate the model. First the average effective stiffness ratio for drift levels less than 0.3% was computed. Second, the matlab function **fminsearch** was used to determine the rate of decay in stiffness for drifts greater than 0.3%. Here an error function equal to the sum of the squares of the difference between the measured and predicted effective stiffnesses was used and only

the data for drifts greater than 0.3% were used. The resulting equations are, for the full data set:

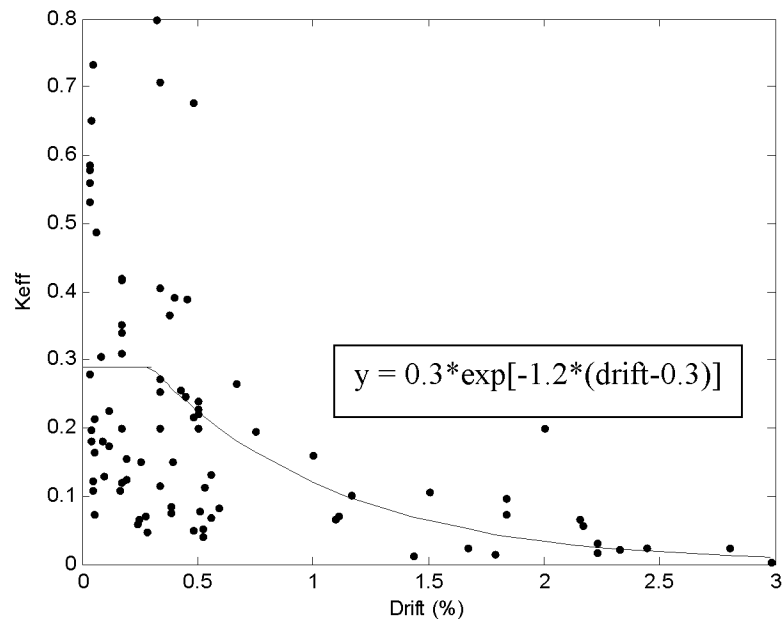
$$k_{eff} = 0.3 \exp(-1.2(drift - 0.3)) \leq 0.3 \quad 5.7$$

and for the data set comprising only rectangular walls:

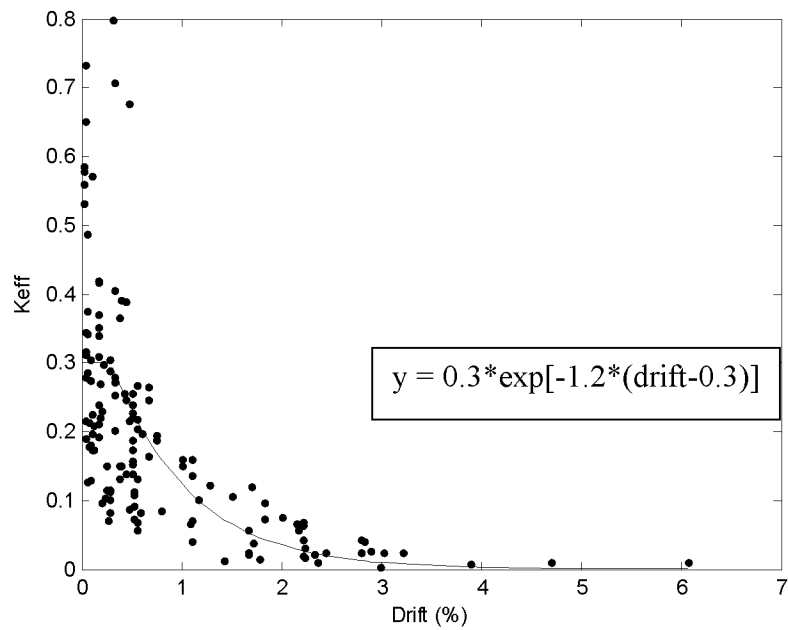
$$k_{eff} = 0.3 \exp(-1.2(drift - 0.3)) \leq 0.3 \quad 5.8$$

Figure 5.6 shows the functional relationships and experimental data for a) the data set comprising only rectangular walls and b) the full data set. Equations (Eq. 5.7 and 5.8) were determined to provide a best fit to the rectangular data set and to the full data set.

However, as shown, the resulting equations were the same for both data sets.



a) Rectangular walls only



b) Rectangular and barbell walls

Figure 5.6 Effective Stiffness Ratio versus Drift. Note that the same functional equation describes both data sets.

## **5.10 SUMMARY AND CONCLUSIONS**

### **5.10.1 Summary**

Fragility functions were developed that predict the probability that a structural wall will require, at least, a specific method of repair as a result of earthquake loading. An empirical data set linking earthquake demand with damage was assembled using data from previous experimental investigations; damage states were linked directly with commonly employed methods of repair. The empirical data were modeled using the lognormal probability distribution, and hypothesis testing was used to verify that the lognormal distribution is appropriate for use. Fragility function for the preferred EDP, drift, was created. Drift was only EDP that was found to adequately predict damage progression and effective stiffness in walls. Wall shape presented the only discernable trends in the damage versus drift relationship (Section 5.9.2)

Data from previous experimental studies were used also to develop effective stiffness versus drift relationships (Section 5.9.3). Given the results of the damage prediction model, drift was the only EDP considered in developing the stiffness prediction models. Wall shape, barbell versus rectangular, was the only design parameter found to affect the stiffness versus drift relationship. Effective stiffness versus drift data were used to calibrate models predicting an exponential decay in effective flexural stiffness. Two models were developed, one for planar walls and one for rectangular walls in which data from barbell walls were not used.

### 5.10.2 Conclusions

The results of this study support several conclusions about damage prediction for planar structural walls.

1. Drift is the most efficient predictor of damage for RC walls. In comparison with number of load cycles, plastic rotation and displacement ductility, drift is most highly correlated with damage. Additionally, fragility functions for walls that employ drift as the EDP have well-space means and relatively small coefficients of variation (less than 40% for all but one damage level).
2. Shear demand–capacity ratio, and aspect ratio do not affect damage progression in walls. Thus one set of fragility functions may be used for walls with different values of these parameters.
3. Wall shape does affect damage progression at higher drift demand levels, with barbell walls developing higher DS at much higher drift levels than rectangular walls. Fragility functions were developed for the full data set that included both barbell and rectangular walls; fragility functions were not developed individually for the barbell and rectangular walls because there were too few data points in the lower damage states for either wall on its own.
4. Wall shape also affects the decay of flexural stiffness, however we can conclude that the difference in flexural stiffness due to the wall shapes is minimal because the best fit equations (eq. 5.7 and eq. 5.8) are the same for both the full data set and the rectangular data set.

### **5.10.3 Recommendations for Future Work**

Additional experimental investigation of the seismic performance of structural walls must be done that increases the quantity and quality of the damage data available for this type of study; it is recommended that testing continue through to collapse so that a comprehensive data set could be assembled for the higher DS.

With additional damage data, it seems likely that it will be possible to generate fragility functions that account for variation in design parameters and wall type.

## **6 Summary and Conclusions**

### **6.1 SUMMARY**

This study used the results of previous experimental testing to develop fragility functions for three types of reinforced concrete components: interior and exterior beam-column joints with modern detailing, and planar structural walls. The fragility functions developed here define the probability that a component will require the use of specific method of repair, given a measure of earthquake demand on the component. These fragility functions are required to apply the PEER performance-based earthquake engineering framework equation (Cornell and Krawinkler 2000) to assess the economic impact of earthquake hazard for a structure.

To develop these fragility functions, the results of previous experimental investigations of the earthquake response of reinforced concrete components and the repair of earthquake damaged components were reviewed. On the basis of this review, a set of damage states (DS) was developed for each of the components that could be linked directly with the methods of repair (MOR) employed commonly to restore earthquake damaged components. Also from this review, a set of earthquake demand parameters (EDPs) was identified that could be expected to predict the progression of



damage. The EDP-DS data were analyzed to identify a preferred set of EDPs that most efficiently predicted the progression of damage in the components. These data were analyzed also to determine if different design parameters impact damage progression.

Once EDP-MOR data were collected, standard probability functions were calibrated using EDP-MOR data. For modern interior joints, lognormal, Weibull, and Beta distribution were considered and standard goodness-of-fit tests were used to identify a preferred distribution. For exterior joints and walls, only the lognormal distribution was considered. Standard goodness-of-fit tests were used to evaluate the adequacy of this distribution for modeling the data. The calibrated cumulative probability distribution is a fragility function, which defines the probability that the RC component will require, at least, a specific method of repair as a result of earthquake loading. To evaluate fragility functions for modern interior and exterior joints, these functions were compared with previously developed functions for older interior joints.

For modern interior beam-column joints, experimental data from eleven tests with a total of 45 specimens were reviewed for use in developing a suite of fragility functions. Initially, “modern” interior joints were considered to be joints with transverse reinforcement, sufficient joint strength to develop the beam flexural yielding and a column-to-beam flexural strength ratio that precluded column yielding. However, this data set included a number of specimens that deviated substantially from the ACI Code requirements for special moment frames. Thus, a reduced data set was

created that included joint specimens that more closely conformed to the Code requirements. These data were used to link EDPs with DSs and common MORs. The results of previous research by Pagni and Lowes (2006) were used as a basis for identifying appropriate EDPs, DSs and MORs for reinforced concrete beam-column joints. Evaluation of the EDP-DS data sets indicated that the most accurate predictors of damage in modern interior joints were found to be i) drift ii) a function of drift and number of load cycles, and iii) joint shear strain and number of load cycles. The impact of various design parameters on EDP-DS response was investigated and found to have little impact on damage progression, with the exception that joints with higher shear stress reached a damage state at a lower number of load cycles than joints with lower shear stresses. Design parameters considered included shear stress demand, bond stress demand, joint transverse reinforcement ratio, column-to-beam flexural strength ratio and column axial load. Thus, standard probability distributions were fit to the complete experimental EDP-MOR data sets using the method of maximum likelihood. Use of standard “goodness of fit” tests indicated that the lognormal distribution provided the best fit to the data for both the full and reduced data set. Ultimately, fragility functions for modern joints, developed using the full and reduced data sets, were compared as were fragility functions for exterior and older joints.

For modern exterior beam-column joints, experimental data from four tests with a total of 20 specimens were reviewed for use in developing a suite of fragility functions. Due to the limited size of the data set, here joints were considered

“representative of modern design” if they had sufficient strength to develop beam yield strength and design parameters that fell within 50% of the ACI Code requirements for special moment frames. The same EDPs, DSs and MORs were used for exterior joints as for modern interior joints. For exterior joints, the best predictors of damage progression were found to be story drift, number of load cycles and a function of drift and number of load cycles. However, the efficiency with which “number of load cycles” predicted damage was considered to be an artifact of the small data set as there was no evidence of this trend in for interior joints. Standard goodness of fit testing indicated that the lognormal distribution provided an adequate fit the EDP-MOR data sets for exterior joints. Comparison of fragility functions for modern interior and exterior joints indicated that damage and repair effort increased more rapidly for exterior joints as the drift increased.

For planar concrete walls, experimental data from nine tests with a total of 44 specimens, 16 barbell walls and 28 rectangular walls were reviewed for use in developing a suite of fragility functions. Evaluation of these data and the results of previous research resulted in consideration of four EDPs for walls: drift, number of cycles, displacement ductility, and plastic rotation. Evaluation of the available experimental data for walls resulted in characterization of damage using only the five MORs used for joints: cosmetic repair, epoxy injection, concrete patching, replace concrete and replace reinforcing steel. For walls, damage was characterized also using the effective stiffness ratio, which was defined as the effective flexural stiffness

computed from load-displacement data divided by the gross-section flexural stiffness. Evaluation of wall data indicated that drift was the only EDP that adequately predicted damage progression, defined by required MOR as well as effective stiffness, in walls. The impact of various design parameters on wall damage as defined by required MOR and effective stiffness was evaluated, and wall shape was found to be presented the only factor that impacted damage progression. Fragility functions were developed using the EDP-MOR data, the lognormal distribution and the method of maximum likelihood. Additionally, data were used to calibrate a model defining the effective stiffness ratio as a function of drift.

## **6.2 CONCLUSIONS**

Beyond providing repair-specific fragility functions for modern interior joints, exterior joints and planar walls, the results of this study provide improved understanding of damage progression in RC components

1. Comparison of fragility functions developed for modern and older joints shows that at low to moderate earthquake drift demands, the drift demand at which older and modern joints require a specific method of repair is similar. However, when more extensive damage and methods of repair are considered, the drift demand at which older joints require a specific method of repair is substantially smaller than that for modern joints. Further, while older joints exhibit a 50% probability of developing damage that requires replacement of the joint and,

potentially, results in structural collapse at a drift demand of 3.5%, modern joints typically do not exhibit this type of damage.

2. For joints with moderate volumes of transverse reinforcement and sufficient strength to develop beam yielding, the volume of transverse reinforcement, beam-bar anchorage length and shear stress demand has relatively little effect on damage progression. This contends the arguments of some researchers
3. Drift is an efficient predictor of damage for RC walls. This is demonstrated by the fact that fragility functions for walls that employ drift as the EDP have well-space means and relatively small coefficients of variation.
4. Shear demand–capacity ratio, aspect ratio, plastic rotation and displacement ductility are not highly correlated with damage. Thus one set of fragility functions may be used for walls with different values of these parameters.
5. Wall configuration is highly correlated with damage. Barbell walls reach the higher DS at much higher drift levels than do rectangular walls.

### **6.3 FUTURE WORK**

As a result of this study, several recommendations for future research may be made. First, additional experimental data are required to develop more accurate fragility functions and further evaluate the impact of design parameters on these functions. This requires additional testing of structural components to increase the quantity and quality of damage data available for this type of study. Additionally, a

standard method for defining damage states should be adopted so that data generated by different researchers can be combined easily. Finally, component testing should continue through to collapse, so that data are available for severe damage states.

Second, studies similar to this must be conducted for other types of components. This will provide a comprehensive suite of fragility functions for use in assessing the economic impact of the earthquake hazard as well as identifying where additional research must be done to generate damage data.

Third, additional damage data may permit generation of fragility functions that account for variation in design parameters. This will enable more accurate prediction of damage.

## 7 References

- ACI Committee 318 (2002). "Building Code Requirements for Structural Concrete (ACI 318-02) and Commentary (ACI 318-R02)." Farmington Hills, MI: American Concrete Institute.
- ACI-ASCE Joint Committee 352 (2002). "Recommendations for Design of Beam-Column Connections in Monolithic Reinforced Concrete Structures (ACI 352-R02)." Farmington Hills, MI: American Concrete Institute.
- ACI Com. 546 (1996). *ACI 546R-96: Concrete Repair Guide*. Farmington Hills: ACI.
- Applied Technology Council (1998). *FEMA 308: Repair of Earthquake Damaged Concrete and Masonry Wall Buildings*. Washington D.C.: FEMA.
- Alire, D. (2003). "Seismic Evaluation of Existing Unconfined RC Joints." *M.S. Thesis*. Seattle: University of Washington.
- Beckingsale, C. W., R. Park and T. Paulay (1980). "Post Elastic Behavior of Reinforced Concrete Beam-Column Joints." *Ph.D. Dissertation*. New Zealand: University of Canterbury.
- Birss, G.R., T. Paulay and R. Park (1978). "The Elastic Behavior of Earthquake Resistant Reinforced Concrete Interior Beam-Column Joints." *M.S. Thesis*. New Zealand: University of Canterbury.
- Cornell, A. and H. Krawinkler (2000). "Progress and Challenges in Seismic Performance Assessment." *PEER News*: April.

- Durrani, A. and J. Wight (1982). "Experimental and Analytical Study of Internal Beam to Column Connections Subjected to Reversed Cyclic Loading." *Report UMEE 82R3*.
- EERI (1994). *Northridge Earthquake January 17, 1994 Preliminary Reconnaissance Report*. Ed. J.F. Hall. Oakland, CA.: EERI.
- El-Bahy, A., S.K. Kunnath, W.C. Stone and A.W. Taylor (1999). "Cumulative Seismic Damage of Circular Bridge Columns: Benchmark and Low-Cycle Fatigue Tests." *ACI Structural Journal* 96 (4): 633-641.
- Endoh, Y., T. Kamura, S. Otani and H. Aoyama (1991). "Behavior of R/C Beam-Column Connections Using Light Weight Concrete." *Transaction of the Japan Concrete Institute* (13): 319-326.
- French, C.W., G.A. Thorp and W.J. Tsai (1990). "Epoxy Repair Techniques for Moderate Earthquake Damage." *ACI Structural Journal* 87 (4): 416-424.
- Haldar, A. and S. Mahadevan (2000). *Probability, Reliability and Statistical Methods in Engineering Design*. New York: John Wiley and Sons, Inc. 304 pp.
- Hayashi K., M. Teraoka, A.A. Mollick and Y. Kanoh (1993). "Bond Properties of Main Reinforcing Bars and Restoring Force Characteristics in RC Interior Beam-Column Subassemblages Using High Strength Materials." *Proceeding of the Japan Concrete Institute* 15 (2): 583-588.
- Joh, O., Y. Goto and T. Shibata (1991a). "Influence of Transverse Joint and Beam Reinforcement and Relocation of Plastic Hinge Region on Beam-Column Joint Stiffness Deterioration." *ACI SP-123: Design of Beam-Column Joints for Seismic Resistance*. Ed. J. Jirsa. Framington Hills: ACI: 187-223.
- Joh, O., Y. Goto and T. Shibata (1991b). "Behavior of Reinforced Concrete Beam-Column Joints with Eccentricity." *ACI SP-123: Design of Beam-Column Joints for Seismic Resistance*. Ed. J. Jirsa. Framington Hills: ACI: 317-357.
- Karayannis, C., K. Sideris and C. Economou (1995). "Response of Repaired RC Exterior Joints Under Cyclic Loading." *European Seismic Design Practice, Elnashai ed.*: 285-292



- Kottegoda, N. and R. Rosso (1997). "Probability, Statistics and Reliability for Civil and Environmental Engineers." *Boston: McGraw-Hill Custom Publishing*.: 735pp.
- Lefas, I., M. Kostovos and N. Ambraseys. (1990) "Behavior of Reinforced Concrete Structural Walls: Strength, Deformation Characteristics, and Failure Mechanism." *ACI Structural Journal* 87 (1): 23-31
- Lefas, I. and M. Kostovos. (1990) "Strength and Deformation Characteristics of Reinforced Concrete Walls under Load Reversal." *ACI Structural Journal* 87 (6): 716-726
- Leon, R.T. (1990). "Shear Strength and Hysteretic Behavior of Interior Beam-Column Joints." *ACI Structural Journal* 87 (1): 3-11.
- Lilliefors, H.W. (1967). "On the K-S Test for Normality with Mean and Variance Unknown." *Journal of the American Statistical Association* 62: 399-402.
- Mathworks (2005). *Matlab*. Version 7.0.1. <<http://www.mathworks.com>>.
- Meinheit, D. and J. Jirsa (1977). "The Shear Strength of Reinforced Concrete Beam-Column Joints." *CESRL Report*.
- Meinheit, D. and J. Jirsa (1981). "Shear Strength of R/C Beam-Column Connections." *Journal of the Structural Division* 107 (ST11): 2227-2243.
- Milburn, J.R. and R. Park (1982). "Behavior of Reinforced Concrete Beam-Column Joints Designed to NZS 3101." *M.S. Thesis*. New Zealand: University of Canterbury.
- Oesterle R., Fiorato A., Johal L., Carpenter J., Russell H. and Corley W. (1976) "Earthquake Resistant Structural Walls – Tests of Isolated Walls." *Technical Report, National Science Foundation*, Washington DC.
- Oesterle R., Aristizabal-Ochoa J., Fiorato A., Russell H. and Corley W. (1979) "Earthquake Resistant Structural Walls – Tests of Isolated Walls – Phase II." *Technical Report, National Science Foundation*, Washington DC.

- Otani, S., Y. Kobayashi and H. Aoyama (1984). "Reinforced Concrete Interior Beam-Column Joints Under Simulated Earthquake Loading." *Report 113*, Japan: University of Tokyo Bunkyo-Ku.
- Pagni, C.A. and L.N. Lowes (2006). "Fragility Functions for Older Reinforced Concrete Beam-Column Joints." *Earthquake Spectra*. In press.
- Pagni, C.A. and L.N. Lowes (2004). "Predicting the Economic Impact of Earthquake Damage in Older Reinforced Concrete Beam-Column Joints." *PEER Report 2003/17*. Berkeley: University of California, Pacific Earthquake Engineering Research Center. 78 pp.
- Pagni, C.A. (2003). "Modeling of Structural Damage of Older Reinforced Concrete Components." *MS Thesis*. Seattle: University of Washington.
- Park, Y.J. and A.H.S. Ang (1985). "Mechanistic Seismic Damage Model for Reinforced Concrete." *Journal of Structural Engineering ASCE* 111(4): 722-739.
- Park, R. and D. Ruitong (1988). "A Comparison of the Behavior of Reinforced Concrete Beam-Column Joints Designed for Ductility and Limited Ductility." *Bulletin of the New-Zealand National Society for Earthquake Engineering* 21 (4): 255-278.
- Pessiki, S.P., C. Conley, R.N. White and P. Gergely (1990). "Seismic Behavior of the Beam-Column Connection Region in Lightly-Reinforced Concrete Frame Structures." *Proceedings of Fourth National Conference on Earthquake Engineering May 20-24, Palm Springs California*. Oakland: EERI. 707-716.
- Pilakoutas K., A. Elnashai and Ambraseys A. (1991) "Earthquake Resistant Design of Reinforced Concrete Walls." *Ph.D Dissertation*. Imperial College of Science Technology and Medicine
- Renton, G. (1972). "The Behavior of Reinforced Concrete Beam-Column Joints Under Cyclic Loading." *Master of Engineering Report*

- Shinozuka, M., M.Q. Fend, J. Lee and T. Naganuma (2000). "Statistical Analysis of Fragility Curves." *Journal of Engineering Mechanics* 126 (12): 1224-1231.
- Sittipunt C., Wood S., Lukkunaprasit P. and Pattarattanak (2001). "Cyclic Behavior of Reinforced Concrete Structural Walls with Diagonal Web Reinforcement." *ACI Structural Journal* 98 (4): 554-562
- Smith, B. (1973). "Exterior Reinforced Concrete Joints with Low Axial Load Under Seismic Loading." *Master of Engineering Report*
- Standards Association of New Zealand (1982). "*New Zealand Standard Code of Practice for the Design of Concrete Structures, NZS 3101 Part 1: 1982 and Commentary on the Design of Concrete Structures, NZS 3101 Part 2:1982.*" Wellington: Standards Association of New Zealand.
- Teraoka, M., Y. Kanoh, K. Tanaka and K. Hayashi (1990). "Strength and Ductility Behavior of RC Interior Beam-Column Joint Using High Strength Concrete." *Proceeding of the Japan Concrete Institute* 12 (2): 633-638.
- Teraoka, M., Y. Kanoh, K. Hayashi and S. Sasaki (1997). "Behavior of Beam-and-Column Subassemblages in an RC Frame." *Proceedings of the First International Conference on High Strength Concrete July 13-18, Kona Hawaii.*
- Thomsen J. and J. Wallace (2004). "Displacement-Based Design of Slender Reinforced Structural Walls – Experimental Verification." *Journal of Structural Engineering* 130 (4): 618-630.
- Tsonos, A., I. Tegos and G. Penelis (1994) "Influence of Axial Force Variations on the Seismic Behavior of Exterior Beam-Column Joints." *European Earthquake Engineering* IX (3): 51-63
- Tsonos, A. (2002). "Seismic Repair of Reinforced Concrete Beam-Column Subassemblages of Modern Structures by Epoxy Injection Techniques." *Structural Engineering and Mechanics* 14 (5): 543-563
- Vallenas J., Bertero V. and Popov E. (1979) "Hysteretic Behavior of Reinforced Concrete Structural Walls." *Ph.D Dissertation*. University of California, Berkeley.

- Walker, S. (2001). "Seismic Performance of Existing RC Beam-Column Joints." *MS Thesis*. Seattle: University of Washington.
- Wang T., V. Bertero and E. Popov. (1975) "Hysteretic Behavior of Reinforced Concrete Framed Walls." *Ph.D Dissertation*. University of California, Berkeley.
- Yanez F., Park R. and Paulay T. (1992) "Seismic Behavior of Walls with Irregular Openings." *Earthquake Engineering, Tenth World Conference*: 3303-3308
- Zaid, S.S.S., S. Otani and H. Shiohara (2001). "Behavior of Reinforced Concrete Beam-Column Connections Under Earthquake Loading." *Ph.D. Dissertation*. Japan: University of Tokyo.
- Zhang Y. and Wang Z. (2000). "Seismic Behavior of Reinforced Concrete Shear Walls Subjected to High Axial Loading." *ACI Structural Journal* 97 (5): 739-750

## A. Appendix – Joints

### Interior Joints

#### Definition of Column Titles in Table A.1

- Researcher – Author of the report
- Specimen – Specimen under consideration
- Ref # per Researcher – cycle count per author of report
- Cycle # Algorithm –
- $\Delta_{\max}$  in cycle – the maximum displacement during the current cycle
- Max history drift – the maximum drift experienced by the joint up to that point in the test
- Max history drift – the maximum negative drift experienced by the joint up to that point in the test
- Response characteristics – description of damage during current cycle

Table A.1 Damage Data for Modern Interior Joints

Researcher	Specimen	Ref # per Researcher	Cycle # algorithm	$\Delta$ max cycle (in)	Max history drift	Min history drift	Response Characteristic
Beckingsale	B11	3.00	1.2	-0.5		-0.003	*max crack width<0.02in (0.55mm) P.107
		5.00	2.1	-1.2		-0.009	begin beam bar yield P.81;
		14.00	5.9	2.4	0.018		transverse reinforcement yields P.109
		17.00	6.6	-3.7		-0.028	initiation of beam bar slip in joint P.73
		22.00	9.0	3.4		-0.028	joint cover separation of 30% but no spalling P.107
Beckingsale	B12	2.00	0.8	0.3		-0.003	*max crack width<0.02in (0.55mm) P.154
		5.00	2.1	-1.2		-0.009	Beam bar yields P.124
		14.00	5.8	2.4	0.018		transverse reinforcement yields (one bar only) P.109
		17.00	6.5	-3.7		-0.028	initiation of beam bar slip in joint P.146
		22.00	8.9	3.8	0.029		joint cover separation of 30% but no spalling P.154
Beckingsale	B13	5.00	2.3	-0.8		-0.006	beam bar yields P.171
		20.00	8.3	2.5		-0.019	transverse reinforcement yields
		29.00	12.1	-3.5		-0.026	failure-beam bar slippage P.224,225
		30.00	12.6	3.4		-0.026	less than 10% of cover separated (approximation by researcher) P.210
Birss	Unit B1	11.00	5.1	0.9	0.007		Residual cracks = 0"; top beam bar yield in joint?P.54
		12.00	5.6	-1.7		-0.013	first yield of joint transverse reinforcement; begin core deterioration P. 69
		15.00	7.1	3.2		-0.024	Residual cracks = 0.047";
		16.00	7.6	-3.3		-0.024	Spalling = 7%
		17.00	8.1	3.3		-0.024	Spalling = 12%
Birss	Unit B2	1.00	0.3	0.5	0.004		cracks = 0.01' (0.33mm)
		11.00	5.3	0.5	0.004		top beam bar yield ?P.58
		20.00	9.7	-1.6		-0.012	all joint transverse reinforcement yielded P.74
		23.00	11.2	2.9	0.022		top beam bar yield ?P.57
		24.00	11.7	-2.9	0.022		spalled area = 27%; max crack width = 0.05" (1.27mm)
Durrani	X1	0.25	0.3	1.5	0.016		*Max joint crack width<0.02" P.40 Beam long. reinf. yields P.41 Transverse reinf. yields P.44
		4.25	4.3	4.0	0.042		initiation of beam bar slip in joint P.42
		6.75	6.8	-5.3	0.056		Vj begins to deteriorate (load carrying capacity 74% of max) P.151 joint surface spalling 10%+ (21%) P.162 crushing of conc. extend into joint core P.40
Durrani	X2	0.25	0.3	1.4	0.015		*Max joint crack width<0.02" P.44 Beam long. reinf. yields P.45
		1.25	1.3	2.0	0.021		Transverse reinf. yields P.46
		6.75	6.7	-5.3	0.056		joint surface spalling 80%+ (89%) P.170

Table A.1 Damage Data for Modern Interior Joints

Researcher	Specimen	Ref # per Researcher	Cycle # algorithm	$\Delta$ max cycle (in)	Max history drift	Min history drift	Response Characteristic
Durrani	X3	1.25	1.3	1.8	0.019		*Max joint crack width<0.02" P.48 Beam long. reinf. yields P.49
		4.25	4.3	3.7	0.039		Transverse reinf. yields P.50
		5.25	5.3	4.3	0.045		*crushing of conc. extend into joint core P.47 *anchorage failure in joint P.49
Endoh	HC	-2.00	1.8	-0.3	0.005		*0.02"<max joint crack width<0.05" P.322 (initial shear crack at drift of 0.00498, requires epoxy injection?)
		7.00	6.3	0.6	0.011		Beam long. reinf. Yields P.321
Endoh	LA1	-2.00	1.8	-0.3	0.005		*0.02"<max joint crack width<0.05" P.322 (initial shear crack at drift of 0.00454)
Endoh	HLC	-2.00	1.8	-0.3	0.005		*0.02"<max joint crack width<0.05" P.322 (initial shear crack at drift of 0.00437)
		7.00	6.3	0.6	0.011		Beam long. reinf. Yields P.321
Endoh	A1	-2.00	1.8	-0.3	0.005		*0.02"<max joint crack width<0.05" P.322 (initial shear crack at drift of 0.00328)
Hayashi	NO 43	0.50	0.1	0.3	0.004		Beam long. reinf. Yields P.23
Hayashi	NO 46	1.00	0.3	0.6	0.008		Beam long. reinf. Yields P.23
Hayashi	NO 47	0.50	0.1	0.3	0.004		Beam long. reinf. Yields P.23
		20.00	9.8	4.1	0.053		joint surface spalling 80%+ (93%) P. 24
Hayashi	NO 49	1.00	0.3	0.6	0.008		Beam long. reinf. Yields P.23
Joh	B8-HH	-4.00	3.8	0.5	0.007		Hairline crack joint surface P. 205
		9.00	8.3	1.9	0.028		initiation of beam bar slip in joint P.196
Joh	B8-HI	3.00	2.3	0.4	0.005		Hairline crack joint surface P. 205
		10.00	9.3	2.7	0.033		Vj begins to deteriorate (77%) P. 212
Joh	B8-MH	-3.00	2.8	0.4	0.005		Hairline crack joint surface P. 205
		-11.00	10.8	3.3	0.041		Vj begins to deteriorate (79%) P. 212
Milburn	Unit 1	1.00	0.3	0.9	0.007		Hairline crack joint surface P. 55
		3.00	1.3	2.3	0.017		Max joint crack width<0.02" (0.38mm, 0.015") P. 51
		4.00	1.8	-2.3	0.017		Beam long. reinf. Yields P.49
		7.00	3.3	4.3	0.033		0.02"<max joint crack width<0.05" (0.75mm, 0.03") P.51
		9.00	4.3	4.4	0.033		*Transverse reinf. Yields P.52 (text on P.52 states yield occurs in load run 9 while fig. 5.1.4 P.54 shows that yield occurs in load run 11)
		10.00	4.8	-4.4	0.033		joint surface spalling 10%+ (22%) P.56
		13.00	6.2	6.3	0.053		crushing of conc. extend into joint core P.59 joint surface spalling 30%+ (76%) P.57

Table A.1 Damage Data for Modern Interior Joints

Researcher	Specimen	Ref # per Researcher	Cycle # algorithm	$\Delta$ max cycle (in)	Max history drift	Min history drift	Response Characteristic
Milburn	Unit 2	1.00	0.3	0.9	0.007		Hairline crack joint surface P. 55
		3.00	1.3	2.4	0.018		Max joint crack width<0.02" (0.3mm, 0.012") P. 60
		4.00	1.8	-2.4	0.018		Beam long. reinf. Yields P.49
		7.00	3.2	4.7	0.036		Transverse reinf. Yields P.65
		12.00	5.7	-6.5	0.053		joint surface spalling 30%+ (33%) P.68
		13.00	6.1	6.9	0.053		crushing of conc. extend into joint core P.59
Otani	J1	1.00	0.3	0.3	0.005		Hairline crack joint surface P.12 (diagonal shear crack @ story displacement of 5.60 mm - epoxy injection)
		-4.00	3.8	-0.6	0.011		Transverse reinf. Yields P.12
		8.00	6.8	2.5	0.044		joint surface spalling 10%+ (20%) P.44
		9.00	7.8	2.5	0.044		*Vj begins to deteriorate (79% of max) P.45
Otani	J2	1.00	0.3	0.3	0.005		Hairline crack joint surface P.12 (diagonal shear crack @ story displacement of 5.48 mm - epoxy injection)
		-4.00	3.8	-0.6	0.011		Transverse reinf. Yields P.12
		8.00	6.8	2.5	0.044		joint surface spalling 30%+ (47%) P.44
		9.00	7.8	2.5	0.044		*Vj begins to deteriorate (79% of max) P.45
Otani	J3	1.00	0.3	0.3	0.005		Hairline crack joint surface P.12 (diagonal shear crack @ story displacement of 7.92 mm - epoxy injection)
		-4.00	3.8	-0.6	0.011		Transverse reinf. Yields P.12
Otani	J4	3.00	2.3	0.6	0.011		Hairline crack joint surface P.12 (diagonal shear crack @ story displacement of 9.02 mm - epoxy injection)
		-4.00	3.8	-0.6	0.011		Transverse reinf. Yields P.12
		8.00	6.8	2.5	0.044		joint surface spalling 10%+ (27%) P.44
		9.00	7.8	2.5	0.044		*Vj begins to deteriorate (57% of max) P.45
Otani	J5	3.00	2.3	0.6	0.011		Hairline crack joint surface P.12 (diagonal shear crack @ story displacement of 8.15 mm - epoxy injection)
		-4.00	3.8	-0.6	0.011		Transverse reinf. Yields P.12
		8.00	6.8	2.5	0.044		joint surface spalling 30%+ (51%) P.44
		9.00	7.8	2.5	0.044		*Vj begins to deteriorate (73% of max) P.45
Otani	J6	8.00	6.8	1.3	0.022		Hairline crack joint surface P.12 (diagonal shear crack @ story displacement of 31.96 mm - epoxy injection)
		12.00	10.0	2.5	0.044		*Vj begins to deteriorate (70% of max) P.45
Park	Unit 1	3.00	1.3	1.2	0.012		Max joint crack width<0.02" P.267
		7.00	3.3	1.8	0.017		*0.02"<max joint crack width<0.05" P.268
		10.00	4.8	-1.8	0.017		Transverse reinf. Yields P.269
Park	Unit 2	7.00	3.3	2.4	0.023		*Max joint crack width<0.02" P.268
		15.00	7.3	3.9	0.039		initiation of beam bar slip in joint P. 268
		17.00	8.3	3.9	0.039		Vj begins to deteriorate (76%) P.267



Table A.1 Damage Data for Modern Interior Joints

Researcher	Specimen	Ref # per Researcher	Cycle # algorithm	$\Delta$ max cycle (in)	Max history drift	Min history drift	Response Characteristic
Park	Unit 3	6.00	2.8	-1.2	0.012		Transverse reinf. Yields P.269
Park	Unit 4	6.00	2.8	-1.5	0.015		Transverse reinf. Yields P.270
Teraoka	HJ-2	17.00	9.3	4.1	0.047		Vj begins to deteriorate (80%) P.98 Fig. 3
Teraoka	HJ-4	10.00	5.8	1.8	0.020		initiation of beam bar slip in joint P.99
		15.00	8.3	3.0	0.033		Vj begins to deteriorate (80%) P.98 Fig. 3
		18.00	9.8	4.1	0.047		joint surface spalling 80%+ (94%) P. 98 Fig.3
Teraoka	HJ-5	10.00	5.8	1.8	0.020		initiation of beam bar slip in joint P.99
Teraoka	HJ-6	10.00	5.8	1.8	0.020		initiation of beam bar slip in joint P.99
Teraoka	HJ-7	10.00	5.8	1.8	0.020		initiation of beam bar slip in joint P.99
Teraoka	HJ-8	10.00	5.8	1.8	0.020		initiation of beam bar slip in joint P.99
Teraoka	HJ-9	10.00	5.8	1.8	0.020		initiation of beam bar slip in joint P.99
Teraoka	HJ-12	6.00	2.8	1.2	0.013		joint surface spalling 10%+ ('concrete crush') P. 99
		7.00	4.3	1.8	0.020		Vj begins to deteriorate (71%) P.98 Fig. 3
		12.00	6.8	2.4	0.027		joint surface spalling 80%+ (100%) P. 98 Fig.3
Teraoka	HJ-14	6.00	2.8	1.2	0.013		joint surface spalling 10%+ ('concrete crush') P. 99
		7.00	4.3	1.8	0.020		Vj begins to deteriorate (79%) P.98 Fig. 3
Teraoka	HNO-1	0.39	0.1	0.4	0.005		Hairline crack joint surface P.14
		0.54	0.1	0.6	0.007		Beam long. reinf. Yields P.10
		10.00	4.7	4.9	0.055		joint surface spalling 30%+ (54%) P.12
Teraoka	HNO-2	0.28	0.1	0.3	0.003		Hairline crack joint surface P.14
		0.78	0.2	0.9	0.010		Beam long. reinf. Yields P.10
		10.00	4.7	4.9	0.055		joint surface spalling 30%+ (63%) P.12
Teraoka	HNO-3	0.19	0.0	0.2	0.002		Hairline crack joint surface P.14
		0.52	0.1	0.6	0.006		Beam long. reinf. Yields P.10
		6.00	2.7	1.7	0.019		Vj begins to deteriorate (72%) P.12
Teraoka	HNO-4	0.19	0.0	0.2	0.002		Hairline crack joint surface P.14
		0.83	0.2	0.9	0.010		Beam long. reinf. Yields P.10
		9.00	4.2	2.4	0.028		Vj begins to deteriorate (71%) P.12
Teraoka	HNO-5	0.31	0.1	0.3	0.004		Hairline crack joint surface P.14
		0.58	0.1	-0.6		-0.007	Beam long. reinf. Yields P.10
Teraoka	HNO-6	0.17	0.0	0.2	0.002		Hairline crack joint surface P.14
		0.87	0.2	-1.0		-0.011	Beam long. reinf. Yields P.10
		9.00	4.3	3.5	0.040		Vj begins to deteriorate (71%) P.12
		14.00	6.8	7.1	0.080		joint surface spalling 30%+ (56%) P.12
Zaid	S1	8.25	8.3	0.7	0.015		Beam long. reinf. Yields P.153
		10.25	10.3	0.9	0.020		Max joint crack width>0.05" P.158
		13.25	12.8	1.4	0.030		initiation of beam bar slip in joint P.158
Zaid	S2	1.25	1.3	0.1	0.001		Hairline crack joint surface P.158
		4.25	4.3	0.2	0.005		Beam long. reinf. Yields P.154
		10.75	10.8	-0.9	0.020		Max joint crack width>0.05" P.159

## Exterior Joints

### Definition of Column Titles in Table A.2

- Researcher – Author of the report
- Specimen – Specimen under consideration
- Ref # per Researcher – cycle count per author of report
- Cycle # Algorithm –
- $\Delta_{\text{max}}$  in cycle – the maximum displacement during the current cycle
- Max history drift – the maximum drift experienced by the joint up to that point in the test
- Max history drift – the maximum negative drift experienced by the joint up to that point in the test
- Response characteristics – description of damage during current cycle

Table A.2 Damage Data for Modern Exterior Joints

Researcher	Specimen	Ref # per Researcher	Cycle # algorithm	$\Delta$ max cycle (in)	max historic drift	min historic drift	Response Characteristic
Karayannis	EJ1	1	0.25	1.2598	0.00842		Formation of hairline cracks in joint region P.289
		5	2.125	1.5748		-0.0132	less than 80% of max load (70% of max) P.287
Karayannis	EJ5	1	0.25	0.7874	0.00526		Formation of hairline cracks in joint region P.289
		9	3.9199076	1.1811		-0.0103	less than 80% of max load (70% of max) P.288
Karayannis	EJ6	1	0.25	1.378	0.00921		Formation of hairline cracks in joint region P.289
		5	2.22	1.5354	0.01026		max) P.289
Milburn	Unit 4	1	0.25	0.9449	0.00716		Hairline crack joint surface P. 82
		3	1.17	1.9685	0.01493		Beam long. reinf. Yields P.84
		5	2.17	1.9685	0.01493		Transverse reinf. Yields P.84
		13	6.10	5.6299	0.04269		joint surface spalling 30%+ (31%) P.?
		14	6.60	-5.118	0.04269		core P.89
Penelis	A1	-11	10.75	-2.598	0.05077		P.59
Penelis	A2	-11	10.75	-2.598	0.05077		P.59
Penelis	A3	2	1.25	0.748	0.01462		Hairline crack joint surface P.59
		-11	10.75	-2.598	0.05077		P.59
Penelis	A4	1	0.25	0.5906	0.01154		Hairline crack joint surface P.59
Penelis	C1	2	1.25	0.748	0.01462		Hairline crack joint surface P.59
		5	4.25	1.4173	0.02769		Vj begins to deteriorate P.56
Penelis	C2	3	2.25	0.9843	0.01923		Hairline crack joint surface P.59
Penelis	C3	2	1.25	0.748	0.01462		Hairline crack joint surface P.59
		7	6.25	1.811	0.03539		Vj begins to deteriorate P.56
Penelis	C4	1	0.25	0.5906	0.01154		Hairline crack joint surface P.59
		5	4.25	1.4173	0.02769		Vj begins to deteriorate P.56

Table A.2 Damage Data for Modern Exterior Joints Continued

Researcher	Specimen	Ref # per Researcher	Cycle # algorithm	$\Delta$ max cycle (in)	max historic drift	min historic drift	Response Characteristic
Penelis	M1	2	1.25	0.748	0.01462		Hairline crack joint surface P.59
Penelis	M2	3	2.25	0.9843	0.01923		Hairline crack joint surface P.59
Penelis	M3	2	1.25	0.748	0.01462		Hairline crack joint surface P.59
Penelis	M4	1	0.25	0.5906	0.01154		Hairline crack joint surface P.59
Penelis	MS3	2	1.25	0.748	0.01462		Hairline crack joint surface P.59
Penelis	MS4	1	0.25	0.5906	0.01154		Hairline crack joint surface P.59
Renton	Unit 1	1	0.25	1.25	0.01042		Hairline crack B-C interface, Hairline crack joint surface P.38
		2	0.75	1.5	0.0125		yield of transverse reinforcement P.18
		4	1.65	5.2	0.04333		Max joint crack width>0.05" P.39 (estimate from picture)
		6	2.6067308	7.8	0.065		Vj begins to deteriorate (57%) P.37 joint surface spalling 30%+ (34%) P.26
Renton	Unit 2	1	0.25	0.8	0.00667		Hairline crack B-C interface, Hairline crack joint surface P.64
		4	1.65	4.85	0.04042		crack extend into the column P.51, yield of transverse reinforcement
		5	2.15	-4.45	0.04042		expansion (crushing?) of joint concrete P.51
Renton	Unit 3	1	0.25	1.3	0.01083		Hairline crack B-C interface, Hairline crack joint surface P.88
		2	0.75	1.7	0.01417		yield of transverse reinforcement P.78,
		3	1.25	-1.2	0.01417		Max joint crack width>0.05" P.70 (estimate from picture)
		8	2.7581136	7.6	0.06333		Vj begins to deteriorate (77% of max historic load) P.92 Table 6.1
		9	3.26	-7.6	0.06333		>80% spalled P.70, 93 (estimate from picture), beam bar bond failure P.94

Table A.2 Damage Data for Modern Exterior Joints Continued

Researcher	Specimen	Ref # per Researcher	Cycle # algorithm	$\Delta$ max cycle (in)	max historic drift	min historic drift	Response Characteristic
Renton	Unit 4	4	1.69	2.8	0.02333		yield of beam bars P.102,
		5	2.19	-2.9		-0.0242	yield of transverse reinforcement P.106, Max joint crack width>0.05" P.116 (estimate from picture)
		8	2.89	7.4	0.06167		initiation of beam bar slip in the joint P.101
		10	3.89	9.4	0.07833		Vj begins to deteriorate (72% of max historic load) P.113 table 7.1
		11	4.39	-9.4	0.07833		>80% spalled (100% spalled) P.117
Smith	Unit 4	3_12	3.92	0.7333	0.00698		beam bar yield P.27
		4_18	5.82	-3.667		-0.0349	transverse reinforcement yield P.35
		6_25	7.27	-3.667		-0.0349	hinge formed in joint P.42
		6_26	7.77	0		-0.0349	initiation of beam-bar slip in the joint P.34
		9_35	9.02	7.3333	0.06984		Vj begins to deteriorate (80% load) P.42 between 30 & 80% spalled (approx.) P.42
		13_50	13.27	11	0.10476		bond failure P.42 - beam bars @ joint fully exposed P.34
Tsonos	A1	7	3.25	1.1811	0.0214		Vj begins to deteriorate (80% of max load) P. 554 fig. 9
Tsonos	E1	17	8.25	2.1654	0.03923		initiation of beam-bar slip in the joint, partial spalling began (no ref. to how much, no picture of rear face of E1) P.551

## B. Appendix – Shear Walls

### Appendix B. 1 Damage data for shear walls

- Researcher – Author of the report
- Specimen – Specimen under consideration
- Ref # per Researcher – cycle count per author of report
- $\Delta_{\max}$  in cycle – the maximum displacement during the current cycle
- disp ductility,  $\mu_y$  – as defined in Section 5.3
- Load – the maximum load applied during the current cycle
- $V/V_n$  – the shear for the current cycle divided by the nominal shear as defined by eq. 5.1
- $\theta_p$  – Plastic rotation defined in Section 5.3
- Secant stiffness – is defined as (Load)/ ( $\Delta_{\max}$  in cycle)
- Response characteristics – description of damage during current cycle

Table B.1 Damage Data for Shear Walls

Researcher	Specimen	Ref # per Researcher (cycle)	$\Delta$ max cycle (in)	disp. ductility, $\mu_y$	Load (kips)	V/V <sub>n</sub>	$\theta_p$	Secant Stiffness (kip/in)	Response Characteristic
Lefas	SW11		0.01	0.1	7.9	0.11	-0.004	588.3	1st flexural cracking
			0.07	0.5	22.5	0.32	-0.002	322.9	1st inclined cracking
			0.14	1.0	38.3	0.54	0.000	270.6	1st yield of tension reinf
			0.32	2.3	56.3	0.80	0.006	173.2	ultimate (maximum load)
Lefas	SW12		0.01	0.1	10.1	0.14	-0.004	989.1	1st flexural cracking
			0.05	0.4	29.3	0.41	-0.002	599.2	1st inclined cracking
			0.11	1.0	47.3	0.67	0.000	413.8	1st yield of tension reinf
			0.35	3.1	75.4	1.07	0.008	216.1	ultimate (maximum load)
Lefas	SW13		0.01	0.1	11.3	0.16	-0.005	772.3	1st flexural cracking
			0.06	0.4	33.8	0.49	-0.003	591.2	1st inclined cracking
			0.15	1.0	56.3	0.82	0.000	374.0	1st yield of tension reinf
			0.35	2.3	74.3	1.08	0.007	212.4	ultimate (maximum load)
Lefas	SW14		0.01	0.1	7.9	0.11	-0.005	588.3	1st flexural cracking
			0.07	0.5	22.5	0.33	-0.003	314.0	1st inclined cracking
			0.15	1.0	38.3	0.56	0.000	249.1	1st yield of tension reinf
			0.44	2.9	59.6	0.87	0.010	135.1	ultimate (maximum load)
Lefas	SW15		0.01	0.1	10.1	0.15	-0.003	952.5	1st flexural cracking
			0.05	0.4	29.3	0.43	-0.002	580.4	1st inclined cracking
			0.11	1.0	47.3	0.69	0.000	415.3	1st yield of tension reinf
			0.32	2.8	70.9	1.03	0.007	223.6	ultimate (maximum load)
Lefas	SW16		0.02	0.2	18.0	0.26	-0.003	1143.0	1st flexural cracking
			0.06	0.6	47.3	0.67	-0.001	827.7	1st inclined cracking
			0.10	1.0	60.8	0.86	0.000	617.2	1st yield of tension reinf
			0.23	2.3	79.9	1.14	0.004	351.0	ultimate (maximum load)
Lefas	SW17		0.01	0.1	5.6	0.17	-0.005	376.0	1st flexural cracking
			0.08	0.5	20.3	0.61	-0.002	246.1	1st inclined cracking
			0.15	1.0	32.6	0.98	0.000	212.5	1st yield of tension reinf
			0.42	2.8	55.6	1.67	0.009	131.3	ultimate (maximum load)
Lefas	SW21		0.01	0.1	2.3	0.06	-0.004	178.6	1st flexural cracking
			0.23	1.0	18.0	0.46	0.000	78.7	1st inclined cracking
			0.23	1.0	18.0	0.46	0.000	78.7	1st yield of tension reinf
			0.81	3.5	28.6	0.73	0.011	35.2	ultimate (maximum load)
Lefas	SW22		0.02	0.1	3.2	0.08	-0.003	205.2	1st flexural cracking
			0.19	1.0	24.8	0.62	0.000	128.0	1st inclined cracking
			0.19	1.0	24.8	0.62	0.000	128.0	1st yield of tension reinf
			0.60	3.1	33.8	0.85	0.008	56.0	ultimate (maximum load)
Lefas	SW23		0.02	0.1	4.5	0.11	-0.004	219.8	1st flexural cracking
			0.20	1.0	27.0	0.69	0.000	131.9	1st inclined cracking
			0.20	1.0	27.0	0.69	0.000	131.9	1st yield of tension reinf
			0.52	2.5	40.5	1.03	0.006	78.0	ultimate (maximum load)
Lefas	SW24		0.01	0.0	2.3	0.06	-0.005	197.1	1st flexural cracking
			0.25	1.0	18.0	0.46	0.000	73.4	1st inclined cracking
			0.25	1.0	18.0	0.46	0.000	73.4	1st yield of tension reinf
			0.71	2.9	27.0	0.69	0.009	37.8	ultimate (maximum load)

Table B.1 Damage Data for Shear Walls Continued

Researcher	Specimen	Ref # per Researcher (cycle)	$\Delta$ max cycle (in)	disp. ductility, $\mu_y$	Load (kips)	V/V <sub>n</sub>	$\theta_p$	Secant Stiffness (kip/in)	Response Characteristic
Lefas	SW25		0.02	0.1	5.6	0.14	-0.004	238.1	1st flexural cracking
			0.23	1.0	29.3	0.75	0.000	126.6	1st inclined cracking
			0.23	1.0	29.3	0.75	0.000	126.6	1st yield of tension reinf
			0.37	1.6	33.8	0.86	0.003	90.5	ultimate (maximum load)
Lefas	SW26		0.02	0.1	2.3	0.10	-0.004	146.5	1st flexural cracking
			0.22	1.0	15.3	0.69	0.000	70.5	1st inclined cracking
			0.22	1.0	15.3	0.69	0.000	70.5	1st yield of tension reinf
			0.82	3.8	27.7	1.25	0.012	33.6	ultimate (maximum load)
Oesterle	B1	4	0.20	0.4	30.0	0.36	-0.002	150.0	flexural cracking first observed (P. B-67)
		crack	0.08	0.2	28.0	0.34	-0.002	350.0	first flexural crack as read from graph (P. B-69)
		10	0.50	1.0	44.0	0.53	0.000	88.0	first yielding (P. B-67)
		14	1.00	2.0	50.0	0.60	0.003	50.0	minor spalling and flaking along web cracks (P. B-67)
		19	2.00	4.0	60.0	0.72	0.008	30.0	significant increase in spalling and flaking along web cracks (P. B-67, 72), cracks remain open in compression column (P. B-72), BE's had slight reverse curvature in lower 3 ft of height (P. B-72)
		22	3.00	6.0	59.0	0.71	0.014	19.7	first indication of crushing at base (P. B-72), first flexural bar buckling (P. B-72)
		28	4.00	8.0	62.0	0.74	0.019	15.5	maximum load (P. B-72), end hooks of horizontal steel started to open (P. B-72)
		fracture	4.20	8.4	57.0	0.68	0.021	13.6	first bar fracture as read from graph (P. B-70)
		31	5.00	10.0	56.0	0.67	0.025	11.2	first bar fracture (P. B-74)
		33	5.00	10.0	48.0	0.57	0.025	9.6	load carrying capacity dropped below 80% of maximum, load at this stage was 70% of the maximum load (P. B-74)



Table B.1 Damage Data for Shear Walls Continued

Researcher	Specimen	Ref # per Researcher (cycle)	$\Delta$ max cycle (in)	disp. ductility, $\mu y$	Load (kips)	V/V <sub>n</sub>	$\theta_p$	Secant Stiffness (kip/in)	Response Characteristic
Oesterle	B2	4	0.30	0.3	62.0	0.73	-0.003	206.7	flexural cracking first observed (P. B-138)
		crack	0.06	0.1	30.0	0.35	-0.005	500.0	first flexural crack as read from graph (P. B-140)
		13	0.90	1.0	122.0	1.44	0.000	135.6	first yielding (P. B-138)
		14	0.90	1.0	118.0	1.39	0.000	131.1	first indication of spalling and flaking along diagonal cracks (P. B-142)
		19	2.00	2.2	145.0	1.71	0.006	72.5	residual cracks in compression columns noted (P. B-142)
		22	3.00	3.3	150.0	1.77	0.012	50.0	first indication of crushing (P. B-142)
		25	4.00	4.4	155.0	1.83	0.017	38.8	maximum load, crushing of columns increased significantly, first indication of reverse curvature in columns (P. B-142)
		26	4.00	4.4	152.0	1.79	0.017	38.0	two bars buckled, 10 more bars buckled in subsequent cycles, considerable spalling and flaking in web during cycles 25-27 (P. B-142)
		28	5.00		152.0			30.4	sudden web failure occurred, highest compression strut that intercepted base of column crushed and slipped along existing crack (P. B-142), eventual sliding failure (P. B-144)

Table B.1 Damage Data for Shear Walls Continued

Researcher	Specimen	Ref # per Researcher (cycle)	$\Delta$ max cycle (in)	disp. ductility, $\mu y$	Load (kips)	V/V <sub>n</sub>	$\theta_p$	Secant Stiffness (kip/in)	Response Characteristic
Oesterle	B3	4	0.20	0.4	32.0	0.41	-0.002	160.0	flexural cracking first observed (P. B-93)
		crack	0.06	0.1	30.0	0.39	-0.002	500.0	first flexural crack as read from graph (P. B-95)
		10	0.50	1.0	46.0	0.59	0.000	92.0	first yielding (P. B-93)
		28	4.00	8.0	61.0	0.79	0.019	15.3	significant crushing and grinding progressively deteriorated web after cycle 28 (P. B-93)
		34	6.00	12.0	62.0	0.80	0.031	10.3	maximum measured load (P. B-98)
		38	7.00	14.0	64.0	0.82	0.036	9.1	compression boundary element appeared to shear through (P. B-98)
		38	7.00	14.0	51.0	0.66	0.036	7.3	first bar fracture as read from graph (P. B-96)
		39	7.00	14.0	58.0	0.75	0.036	8.3	loading in positive direction: vertical bar fractured, no evidence of previous distress such as buckling (P. B-98), loading in negative direction: vertical bar fractured, evident that bar previously buckled (P. B-100)
		40	8.00	16.0	54.0	0.70	0.042	6.8	all vertical bars in web buckled in cycles 39 and 40 but only one fractured (P. B-100)
Oesterle	B4	4	0.10	0.2	27.0	0.34	-0.002	270.0	flexural cracking first observed (P. B-119), data read from graph (P. B-120)
		6	0.50	1.0	46.0	0.58	0.000	92.0	first yielding (P. B-119)
		7	0.70	1.4	54.0	0.68	0.001	77.1	full yield (P. B-120)
		9	2.00	4.0	64.0	0.81	0.008	32.0	slight crushing in outer shell of compression face first noted (P. B-119)
		10	3.00	6.0	68.0	0.86	0.014	22.7	one diagonal crack started to predominate (P. B-119)
		15.5	8.50	17.0	78.0	0.98	0.044	9.2	maximum load, vertical bar in web fractured (P. B-123)
		fracture	8.70	17.4	78.0	0.98	0.046	9.0	first bar fracture as read from graph (P. B-120)

Table B.1 Damage Data for Shear Walls Continued

Researcher	Specimen	Ref # per Researcher (cycle)	$\Delta$ max cycle (in)	disp. ductility, $\mu y$	Load (kips)	V/V <sub>n</sub>	$\theta_p$	Secant Stiffness (kip/in)	Response Characteristic
Oesterle	B5	4	0.35	0.4	64.0	0.81	-0.003	182.9	flexural cracking first observed (P. B-164)
		crack	0.10	0.1	35.0	0.44	-0.004	350.0	first flexural crack as read from graph (P. B-95)
		13	0.90	1.0	125.0	1.58	0.000	138.9	first yielding (P. B-164)
		16	0.40	0.4	60.0	0.76	-0.003	150.0	first indication of spalling and flaking along diagonal cracks (P. B-164)
		19	2.00	2.2	150.0	1.90	0.006	75.0	first indication of crushing of outer compression face (P. B-164 - 169)
		22	3.00	3.3	155.0	1.96	0.012	51.7	compression column cracks appeared to remain open (P. B-169), significant spalling and crushing at construction joint (P. B-169)
		25	4.00	4.4	160.0	2.02	0.017	40.0	noticeable reverse curvature developed in lower 3ft 8in of both columns (P. B-169)
		28	5.00	5.6	166.0	2.10	0.023	33.2	maximum measured load (P. B-169)
		29	5.00	5.6	160.0	2.02	0.023	32.0	several compression struts crushed simultaneously (P. B-169 171)
		crushing	4.70	5.2	164.0	2.07	0.021	34.9	web crushing as read from graph (P. B-167)
Oesterle	R1	4	0.20	0.4	15.0	0.14	-0.001	75.0	flexural cracking first observed (P. B-16)
		crack	0.03	0.1	11.0	0.10	-0.002	366.7	first flexural crack as read from graph (P. B-18)
		10	0.45	1.0	22.5	0.21	0.000	50.0	first yielding (P. B-16)
		14	1.00	2.2	23.0	0.22	0.003	23.0	minor spalling and flaking along cracks first observed (P. B-16)
		16	2.00	4.4	27.5	0.26	0.009	13.8	maximum measured load (P. B-16), horizontal bars yielded in the lower 6-ft region (P. B-31)
		19	3.00	6.7	27.0	0.25	0.014	9.0	significant spalling and sliding along the horizontal crack at 3-ft level (P. B-21)
		20	3.00	6.7	24.5	0.23	0.014	8.2	first buckling of main flexural reinforcement, buckled at a location 15-in above base [10 additional bars fractured during test] (P. B-21)
		26	4.00	8.9	24.0	0.23	0.020	6.0	first bar fracture, the two bars that had buckled first [9 additional bars fractured during test] (P. B-21)

Table B.1 Damage Data for Shear Walls Continued

Researcher	Specimen	Ref # per Researcher (cycle)	$\Delta$ max cycle (in)	disp. ductility, $\mu y$	Load (kips)	V/V <sub>n</sub>	$\theta_p$	Secant Stiffness (kip/in)	Response Characteristic
Oesterle	R2	4	0.10	0.1	16.5	0.09	-0.005	165.0	first significant flexural cracking (P. B-41)
		crack	0.10	0.1	13.0	0.07	-0.005	130.0	first flexural crack as read from graph (P. B-43)
		19	1.00	1.0	44.5	0.25	0.000	44.5	first yielding (P. B-41), minor spalling and flaking along horizontal web crack in lower 3-ft (P. B-41)
		22	2.00	2.0	48.5	0.28	0.006	24.3	first indication of crushing of the outer shell at the base of the wall (P. B-46)
		25	3.00	3.0	49.0	0.28	0.011	16.3	cracks in the compression zone remained open (P. B-46), significant increase in spalling and flaking along horizontal cracks (P. B-46)
		26	3.00	3.0	47.5	0.27	0.011	15.8	significant increase in spalling and flaking along horizontal cracks (P. B-46)
		27	3.00	3.0	46.5	0.27	0.011	15.5	significant increase in spalling and flaking along horizontal cracks (P. B-46)
		28	1.00	1.0	27.0	0.15	0.000	27.0	bowing of the compression end observed, compression end was 0.25-in out of plane at a point 3'-6" above base (P. B-46)
		31	4.00	4.0	50.0	0.29	0.017	12.5	considerable grinding and spalling along web cracks (P. B-48)
		32	4.00	4.0	48.8	0.28	0.017	12.2	after cycle 32, compression end of wall was 3-in out of plane at a point 3'-6" above base, test was stopped and lateral bracing was added (P. B-46), considerable grinding and spalling along web cracks (P. B-48)
		33	4.00	4.0	45.0	0.26	0.017	11.3	considerable grinding and spalling along web cracks (P. B-48)
		34	5.00	5.0	50.5	0.29	0.022	10.1	maximum measured load (P. B-48)

Table B.1 Damage Data for Shear Walls Continued

Researcher	Specimen	Ref # per Researcher (cycle)	$\Delta$ max cycle (in)	disp. ductility, $\mu_y$	Load (kips)	V/V <sub>n</sub>	$\theta_p$	Secant Stiffness (kip/in)	Response Characteristic
Oesterle	R2	35	5.00	5.0	48.5	0.28	0.022	9.7	large out of plane displacement of compression zone within lower 3'-6" and load carrying capacity decreased (P. B-48)
		36	5.00	5.0	43.5	0.25	0.022	8.7	maximum load was 79% of the maximum in the first cycle at 5-in (P. B-48)
		fracture	4.20	4.2	34.0	0.19	0.018	8.1	first bar fracture as read from graph (P. B-44)
		37	6.00		36.0			6.0	several bars fractured and out of plane displacement of compression zone progressed further (P. B-48)
		38	6.00		26.5			4.4	considerable crushing and loss of concrete and load carrying capacity continues to decrease (P. B-48)
		39	6.00		13.0			2.2	considerable crushing and loss of concrete and load carrying capacity continues to decrease (P. B-48)
Oesterle	B6	4	0.20	0.2	63.0	0.53	-0.004	315.0	flexural cracking first observed (P. B-14)
		crack	0.10	0.1	48.0	0.41	-0.005	480.0	first flexural crack as read from graph (P. B-16)
		16	1.00	1.0	147.0	1.24	0.000	147.0	first yielding (P. B-14), first indication of splitting in concrete cover (P. B-14)
		22	2.00	2.0	188.0	1.59	0.006	94.0	significant crushing of concrete cover, slight reverse curvature developed in BE (P. B-14)
		23	2.00	2.0	176.0	1.49	0.006	88.0	first indication of spalling and flaking along diagonal cracks (P. B-14)
		24	2.00	2.0	171.0	1.45	0.006	85.5	slight indication of crushing of a compression strut in web (P. B-14)
		25	3.00	3.0	196.0	1.66	0.011	65.3	crushing of compression strut increased, maximum load (P. B-20)
		crush	2.60	2.6	173.0	1.46	0.009	66.5	web crushing as read from graph (P. B-17)
		26	3.00		96.0			32.0	several compression struts crushed simultaneously, failure from struts shearing through a vertical plane (P. B-20)

Table B.1 Damage Data for Shear Walls Continued

Researcher	Specimen	Ref # per Researcher (cycle)	$\Delta$ max cycle (in)	disp. ductility, $\mu y$	Load (kips)	V/V <sub>n</sub>	$\theta_p$	Secant Stiffness (kip/in)	Response Characteristic
Oesterle	B7	10	0.50	0.5	119.0	0.95	-0.003	238.0	first significant cracking (P. B-41), first indication of spalling and flaking along diagonal cracks (P. B-41)
		crack	0.27	0.3	98.0	0.78	-0.004	363.0	first flexural crack as read from graph (P. B-43)
		13	1.00	1.0	170.0	1.35	0.000	170.0	first yielding (P. B-41)
		19	2.00	2.0	209.0	1.66	0.006	104.5	first indication of crushing in the concrete cover (P. B-41)
		22	3.00	3.0	213.0	1.69	0.011	71.0	slight reverse curvature developed in BE (P. B-48)
		25	4.00	4.0	215.0	1.71	0.017	53.8	slight indication of crushing in compression struts in web (P. B-48)
		28	5.00	5.0	218.0	1.73	0.022	43.6	maximum load (P. B-48)
		crush	4.75		200.0			42.1	web crushing as read from graph (P. B-44)
		31	6.00					0.0	several compression struts crushed simultaneously; vertical failure plane developed after web crushing; did not reach 6-in displacement (P. B-48)
Oesterle	B8	10	0.50	0.5	116.0	0.95	-0.003	232.0	first significant cracking (P. B-70)
		crack	0.18	0.2	75.0	0.62	-0.005	416.7	cracking as read from graph (P. B-43)
		13	1.00	1.0	166.0	1.36	0.000	166.0	first yielding (P. B-70)
		14	1.00	1.0	163.0	1.34	0.000	163.0	first indication of crushing in the concrete cover of the outer compression faces (P. B-77)
		20	2.00	2.0	210.0	1.73	0.006	105.0	first indication of spalling and flaking along diagonal cracks (P. B-77)
		26	4.00	4.0	213.0	1.75	0.017	53.3	slight indication of crushing in the web near the horizontal crack (P. B-77)
		28	5.00	5.0	216.0	1.78	0.022	43.2	maximum load (P. B-77), significant increase in spalling and crushing (P. B-77)
		crush	6.00		236.0			39.3	web crushing as read from graph (P. B-73)
		31	6.00		210.0			35.0	slight but noticeable increase in slip along horizontal crack (P. B-77), several compression struts crushed simultaneously; web crushing was immediately followed by development of both horiz and vert failure planes (P. B-77)

Table B.1 Damage Data for Shear Walls Continued

Researcher	Specimen	Ref # per Researcher (cycle)	$\Delta$ max cycle (in)	disp. ductility $\mu_y$	Load (kips)	V/V <sub>n</sub>	$\theta_p$	Secant Stiffness (kip/in)	Response Characteristic
Oesterle	B9	+1	0.50	0.4	119.0	1.00	-0.004	238.0	first load cycle applied to develop cracking, first significant cracking at load of 75 kips (P. B-100)
		-1	0.50	0.4	112.0	0.94	-0.004	224.0	first load cycle applied to develop cracking (P. B-100)
		+2	1.20	1.0	231.0	1.95	0.000	192.5	first yielding occurred at load stage 18 at load of 158 kips, full yielding occurred at load stage 19 at load of 186.4 kips (P. B-100), first indication of crushing in concrete cover at load stage 20 (P. B-105), maximum load (P. B-105)
		-2	2.30	1.9	222.0	1.87	0.006	96.5	indication of crushing in compression strut, first spalling along diagonal cracks, spalling from opening of crosstie end hooks (P. B-105)
		+4	4.75	4.0	219.0	1.85	0.020	46.1	significant increase in spalling along diagonal cracks in web (P. B-105)
		-4	5.20	4.3	112.0	0.94	0.022	21.5	several compression struts in web crushed, crushing immediately followed by development of a failure plane along a diagonal crack (P. B-105 - 107)
		+5	4.25		72.0	0.61		16.9	vertical and horizontal failure planes developed (P. B-107)
Oesterle	B10	+1	0.40	0.4	95.0	0.78	-0.004	237.5	first load cycle applied to develop cracking, first significant cracking at load of 75 kips (P. B-150)
		-1	0.30	0.3	92.0	0.76	-0.004	306.7	first load cycle applied to develop cracking (P. B-150)
		+2	1.10	1.0	173.0	1.42	0.000	157.3	first yielding occurred at load stage 13 at load of 120 kips, full yielding occurred at load stage 14 at load of 139.7 kips (P. B-150), first indication of crushing in concrete cover at load stage 15 (P. B-150), maximum load (P. B-152)
		-2	1.20	1.1	158.0	1.30	0.001	131.7	patched cover on compression column started to spall at load stage 21, patched cover continued to crush and spall as load increased (P. B-150)

Table B.1 Damage Data for Shear Walls Continued

Researcher	Specimen	Ref # per Researcher (cycle)	$\Delta$ max cycle (in)	disp. ductility, $\mu_y$	Load (kips)	V/V <sub>n</sub>	$\theta_p$	Secant Stiffness (kip/in)	Response Characteristic
Oesterle	B10	+6	4.25	3.9	150.0	1.23	0.018	35.3	end hooks on confinement crossties started to open slightly (P. B-155)
		-6	4.00	3.6	148.0	1.22	0.016	37.0	two corner bars started to buckle between confinement hoop, 90° end hooks of horiz shear reinf started to open, crushing of concrete within confined core [apparently honeycombed conc not completely repaired] (P. B-155)
		-8	4.85	4.4	154.0	1.27	0.021	31.8	outer two rows of compression column vertical bars buckled (P. B-155)
		+9	1.25	1.1	?		0.001		one of the previously buckled corner bars fractured (P. B-155)
		+10	4.25		137.0	1.13		32.2	another outer bar fractured (P. B-155)
		-10	4.00		140.0	1.15		35.0	increased buckling and crushing in the compression column (P. B-155)
		+12	4.90		122.0	1.00		24.9	three more previously buckled bars fractured, max load reached was 76% of the max in cycle 2 (P. B-155)
		-14	5.75		145.0	1.19		25.2	compression boundary element crushed completely and all remaining bars in this column buckled, then the web immediately crushed (P. B-158)
Pilakoutas	SW4	2	0.08	0.3	9.0	0.44	-0.003	114.3	initial cracking @ 1mm of displacement (P.101); initial wall stiffness of 31KN/mm (P.101);
		2	0.08	0.3	9.0	0.44	-0.003	114.3	wall stiffness at MDL-2 of 19.3 KN/mm (P.101) cracked to mid-wall P.101 boundary crack every 4" approximately P.102
		4	0.16	0.7	13.5	0.66	-0.002	85.7	cracks propagated through entire wall height(P.101); web crack density was constant while boundary crack density increased P101 boundary crack every 3" approximately P.102
		6	0.24	1.0	18.6	0.91	0.000	78.6	first yield @ 76 KN (of what?) P.102, 193



Table B.1 Damage Data for Shear Walls Continued

Researcher	Specimen	Ref # per Researcher (cycle)	$\Delta$ max cycle (in)	disp. ductility $\mu_y$	Load (kips)	V/V <sub>n</sub>	$\theta_p$	Secant Stiffness (kip/in)	Response Characteristic
Pilakoutas	SW4								full yield (of what?) P.102 crack density increased, boundary and web cracks meet (P. 102); boundary cracks every 2" approximately P.103
		8	0.31	1.3	21.4	1.05	0.002	67.9	
		10	0.39	1.7	23.6	1.16	0.003	60.0	M <sub>p</sub> achieved (disp. Controlled with no load increase) (P.265 Fig. A.(4).1)
		16	0.63	2.7	22.5	1.10	0.008	35.7	lower web cracks opened considerably more than others (P.102); vertical cracking appeared at bottom of wall approx. at position of main reinforcement (P.102); boundary cracks every 1.5" approximately P.103
		22	0.87	3.7	22.3	1.09	0.013	25.7	considerable spalling at both boundary elements at approx. location of two lowest hoops (P.102);
		24	0.94	4.0	22.3	1.09	0.015	23.6	crushing of core concrete at both boundary elements at approx. location of two lowest hoops (P.102); 4% spalled P.103
Pilakoutas	SW5	Crack	0.04		2.4			61.0	initial stiffness of 29.0 KN/mm P.192
		2	0.08		9.5	0.67		120.0	cracking initiated - P.105 Initial stiffness @ 0.5 mm = 34 KN/mm P.105
		2	0.08		9.5	0.67		120.0	Stiffness @ 2mm = 21.7 KN/mm P.105 cracking throughout 3/4 of wall height P.105 boundary cracks every 4" approximately P.106
		4	0.16		14.9	1.05		94.3	cracking throughout entire length of wall P. 105 web cracks - consistent density P.105 boundary crack density increased P. 105 boundary cracks every 3" approximately P.106
		8	0.31		25.9	1.84		82.2	boundary cracks every 2" approximately P.107 First yield @110KN P.193

Table B.1 Damage Data for Shear Walls Continued

Researcher	Specimen	Ref # per Researcher (cycle)	$\Delta$ max cycle (in)	disp. ductility $\mu_y$	Load (kips)	V/V <sub>n</sub>	$\theta_p$	Secant Stiffness (kip/in)	Response Characteristic
Pilakoutas	SW5	10	0.39		26.4	1.87		67.0	M <sub>p</sub> achieved (max load = 117.3 KN) P.106 shear reinforcement first yield P.107 web cracks opening P.107
		-10	-0.39		26.4	1.87		-67.0	"abrupt failure" at load of 110 KN P.107
		14	0.55		16.2	1.15		29.4	less than 80% of load capacity (63%) from graph diagonal cracks (from corner to corner) widening P.107
		-24	-0.94		10.8	0.77		-11.4	6% spalled P.108
Pilakoutas	SW6								initial stiffness of 23.1 KN/mm P.192
		2	0.08	0.3	8.4	0.57	-0.003	107.2	cracking initiated - P.109 Initial stiffness @ 0.5 mm = 33.5 KN/mm P.109
		2	0.08	0.3	8.4	0.57	-0.003	107.2	Stiffness @ 2mm = 20.0 KN/mm P.109 cracking to mid-wall, more prevalent on RHS P.109 boundary cracks every 10" (LHS), 4" (RHS) approximately P.110
		4	0.16	0.7	13.5	0.92	-0.002	85.7	cracked full height P. 109
		6	0.24	1.0	16.9	1.15	0.000	71.4	main reinforcement yielded @ 74 KN P. 109, 193
		8	0.31	1.3	20.3	1.38	0.002	64.3	boundary cracks and web cracks meet P. 111 boundary cracks every 4"(LHS), 3" (RHS) P.111
		16	0.63	2.7	23.9	1.62	0.008	37.9	Max load achieved P. 295
		16	0.63	2.7	23.6	1.61	0.008	37.5	M <sub>p</sub> achieved (max load = 107KN) P.110 bottom edge of wall spalled (no amount recorded) P.110 boundary cracks every 2" (LHS & RHS) P. 111
		-18	-0.71	3.0	23.6	1.61	-0.020	-33.3	crushing of concrete initiated P.111 cracks progressed through compressed area P.111
		22	0.87	3.7	20.3	1.38	0.013	23.4	load capacity reduced to 75% of max. P.111 diagonal cracks opening P.113

Table B.1 Damage Data for Shear Walls Continued

Researcher	Specimen	Ref # per Researcher (cycle)	$\Delta$ max cycle (in)	disp. ductility, $\mu_y$	Load (kips)	V/V <sub>n</sub>	$\theta_p$	Secant Stiffness (kip/in)	Response Characteristic
Pilakoutas	SW7	cracking							initial stiffness of 29.0 KN/mm P.192
		2	0.08	0.3	9.5	0.47	-0.005	120.0	cracking initiated - P.113 Initial stiffness @ 0.5 mm = 33 KN/mm P.113
		2	0.08	0.3	9.5	0.47	-0.005	120.0	Stiffness @ 2mm = 21.3 KN/mm P.113 cracking throughout 3/4 of wall height P.113 boundary cracks every 4" approximately P.113
		4	0.16	0.5	18.3	0.92	-0.003	116.0	cracking throughout entire length of wall P. 113 boundary crack dentsity increased P. 113 boundary cracks every 4"(LHS), 3"(RHS) P.113
		8	0.31	1.0	23.9	1.20	0.000	76.0	boundary cracks and web cracks meet P. 114 boundary cracks every 3" approximately P.111 First yield @ 107 KN P. 193
		14	0.55	1.8	27.7	1.39	0.005	50.3	main web crack pepnetrated the compressive area, at least on surface P. 115 boundary cracks every 2" approximately P.115
		-18	-0.71	2.3	31.4	1.57	-0.022	-44.3	Mp achieved (max load = 127.3KN) P.115 web crack widen P.115
		-22	-0.87	2.8	23.9	1.19	-0.025	-27.5	failure - 6mm reinforcemetn bar fractured on LHS P.115
Pilakoutas	SW8	cracking							initial stiffness of 23.7 KN/mm P.192
		2	0.08		11.6			146.9	initial cracking before 1mm of displacement (P.117) initial wall stiffness @ 0.5mm of 27.8KN/mm P.117
		2	0.08	0.3	11.6	0.76	-0.003	146.9	wall stiffness at MDL-2 of 18.6 KN/mm P.117 cracked to mid-wall P.117 boundary crack every 5" approximately P.117

Table B.1 Damage Data for Shear Walls Continued

Researcher	Specimen	Ref # per Researcher (cycle)	$\Delta$ max cycle (in)	disp. ductility $\mu_y$	Load (kips)	V/V <sub>n</sub>	$\theta_p$	Secant Stiffness (kip/in)	Response Characteristic
Pilakoutas	SW8	18	-0.71	3.0	24.8	1.62	-0.020	-34.9	spalling inside of boundary element P. 118
		22	0.87	3.7	25.1	1.64	0.013	28.9	spalling at intersection of main cracks P. 118
		24	0.94	4.0	21.5	1.41	0.015	22.8	M <sub>p</sub> achieved from graph
		-26	-1.02	4.3	20.3	1.32	-0.027	-19.8	extreme bottom of wall spalled exposing reinforcement P. 118
Pilakoutas	SW9	cracking							load dropped below 75% of ultimate P. 118
									initial stiffness of 23.7 KN/mm P. 192
		2	0.08	0.3	8.8	0.60	-0.003	111.4	initial cracking before 1mm of displacement P.120 initial wall stiffness @ 0.5mm of 38KN/mm P.120
		2	0.08	0.3	8.8	0.60	-0.003	111.4	wall stiffness at MDL-2 of 29.8 KN/mm P.120 cracked to mid-wall P.121 boundary crack every 5" approximately P.121
		4	0.16	0.7	14.3	0.97	-0.002	90.6	cracks propagated through entire wall height P.121 boundary crack every 4" approximately P.121
		6	0.24	1.0	17.8	1.21	0.000	75.4	boundary crack every 2" approximately P.122 First yield @ 70 KN P.193
		18	-0.71	3.0	21.1	1.43	-0.020	-29.8	bottom quarter of wall spalled at web crack intersection P. 122
		24	0.94	4.0	21.9	1.49	0.015	23.2	M <sub>p</sub> achieved from graph
Sittipunt	W1	26	1.02	4.3	8.8		0.017	8.6	bottom of wall spalled 4% approximately P.123
		capacity	0.472		108.5	1.25		229.6	nominal strength
		13	1.30		110.5	1.28		85.0	maximum load
		crush	1.77		79.0	0.91		44.6	web crushing
		13	1.30		136.8	1.21		105.3	maximum load
Thomsen	RW1	crush	1.34		78.8	0.69		58.8	web crushing
		7	1.08	1.0	30.0	0.54	0.000	27.8	yielding of boundary flexural reinf
		9	1.44	1.3	33.0	0.59	0.003	22.9	splitting and minor crushing at wall edge
		max	2.30	2.1	33.0	0.59	0.008	14.3	maximum load
		buckling	3.10	2.9	30.0	0.54	0.014	9.7	buckling of longitudinal reinf

Table B.1 Damage Data for Shear Walls Continued

Researcher	Specimen	Ref # per Researcher (cycle)	$\Delta$ max cycle (in)	disp. ductility $\mu_y$	Load (kips)	V/Vn	$\theta_p$	Secant Stiffness (kip/in)	Response Characteristic
Thomsen	RW2	7	1.08	1.0	30.0	0.53	0.000	27.8	yielding of boundary flexural reinf
		9	1.44	1.3	32.0	0.57	0.003	22.2	splitting and minor crushing at wall edge
		max	3.10	2.9	36.0	0.64	0.014	11.6	maximum load
Vallenas	SW3	21	0.09	0.2	56.3	0.23	-0.003	621.2	initial cracking P. 18
		crack	0.24	0.5	79.9	0.33	-0.002	338.1	first diagonal cracking P.18
		49	0.71	1.5	202.1	0.84	0.002	285.1	first yielding of column bars P.18
		59	5.79	12.3	245.3	1.02	0.044	42.4	max load achieved P.19
		75	6.65	14.1	245.3	1.02	0.052	36.9	bar buckling P.19
Vallenas	SW4	22	0.11	0.2	50.0	0.21	-0.003	446.7	initial flexural cracking P.19
		40	0.33	0.7	79.9	0.33	-0.001	243.6	initial diagonal cracking P.19
		45	0.71	1.5	202.5	0.84	0.002	285.8	first yield P. 19
		60	2.13	4.5	218.3	0.90	0.014	102.7	3mm of sliding shear along the crack on the bottom of the wall P.20
		81	2.80	5.9	218.3	0.90	0.019	78.1	crushing initiated along horizontal flexural crack in panel "indicating shear slippage" P.20
		82	2.80	5.9	218.3	0.90	0.019	78.1	max load achieved P. 138
		96	3.58	7.6	46.1	0.19	0.026	12.9	buckling of column bars P. 20
Vallenas	SW5	cracking	0.04	0.1	24.8	0.12	-0.004	628.7	initial flexural cracking P.101
		102	0.10	0.2	62.5	0.30	-0.003	645.8	First tensile crack occurred at +110 kN and -110 kN P.22
		111	-0.09	0.2	-63.8	0.31	-0.005	686.5	A long diagonal crack was observed in the panel at 250 kN P.22
		134	0.00	0.0	0.0	0.00	-0.004		Horizontal hairline cracks in column at 70mm spacing P.22
		156.6	0.39	0.8	137.9	0.66	-0.001	350.3	Diagonal hairline cracks with 100-140 mm spacing were observed in all panels at 613 kN.
		159	0.47	1.0	159.5	0.77	0.000	337.7	South column reached yield strain (P.22) @ 624 kN P.101 Nominal value of 12.7mm was taken for the initial yielding of force disp. Curve (fig 4.46) P. 22-23
		170	0.75	1.6	177.3	0.85	0.002	237.0	Overall yielding of subassembly wall P.22
		197	1.31	2.8	192.8	0.93	0.007	147.1	Initial concrete crushing at base of column P. 23
		273	1.24	2.6	189.0	0.91	0.006	152.6	Column in compression initially spalled unsymmetrically causing some eccentricity P. 23 Compression region panel showed initial crushing P.23

Table B.1 Damage Data for Shear Walls Continued

Researcher	Specimen	Ref # per Researcher (cycle)	$\Delta$ max cycle (in)	disp. ductility $\mu_y$	Load (kips)	V/V <sub>n</sub>	$\theta_p$	Secant Stiffness (kip/in)	Response Characteristic
Vallenas	SW5	309	2.87	6.1	206.2	0.99	0.020	71.8	M <sub>p</sub> achieved P. 156 Rupturing of steel heard at base of compressive column indicating rupture of lateral confinement hoop P. 23
		314.7	2.93	6.2	167.0	0.80	0.020	57.0	buckling of longitudinal bars at base of north compressive column P.23
		355	2.36		0.0			0.0	reduction in stiffness from virgin cycle of 29.5/5=5.9 P.23
		451	2.90		-85.1			-29.3	small out of plane deformation of panel and compression column along first floor P.23
		526	1.63		-190.7			-116.8	flexural crack initiated at car buckling and crushed concrete region of north column and propagated through whole specimen
Vallenas	SW6	Cracking	0.04	0.1	27.7	0.13	-0.004	702.9	initial flexural cracking
		77	0.10	0.2	63.1	0.30	-0.004	618.6	Cracking initiated, first flexural crack at 27.67 <sup>k</sup> (123 KN) and first diagonal crack propagating from column into panel at 31.5 <sup>k</sup> (140 KN), the crack fully penetrated panel at 63.1 <sup>k</sup> (279KN) P.24
		153	0.53	1.0	164.0	0.79	0.000	312.1	ductility of 1 (note: 12.7mm was used as yield value from SW5) flexural cracks in both column and panels P.24
		255	0.96	1.8	186.4	0.89	0.004	195.1	ductility of 2 spalling initiated in compression region of specimen P.24 0.07 in (1.8mm) cracks in tension region P.24 0.04 in (1mm) crack opened between foundation and wall P.24
		373	1.49	2.8	188.7	0.90	0.008	126.8	ductility of 3 numerous 0.1 in (2.6mm) tensile cracks opened P.24 cracks in column remained open when in compression P.24
		395	-1.52	2.9	-195.9	0.94	-0.017	128.7	M <sub>p</sub> achieved P.162

Table B.1 Damage Data for Shear Walls Continued

Researcher	Specimen	Ref # per Researcher (cycle)	$\Delta_{\max}$ cycle (in)	disp. ductility $\mu_y$	Load (kips)	V/V <sub>n</sub>	$\theta_p$	Secant Stiffness (kip/in)	Response Characteristic
Vallenas	SW6	535	1.94	3.7	192.7	0.92	0.012	99.2	ductility of 4 tensile crack in column of 3.2 mm P.24 5mm crack between wall and transmission P.24
		614	-2.05	3.9	-178.7	0.86	-0.021	87.0	column spalled on one side causing column to buckle, which took part of the wall with it P.24
Wang	SW1	1	0.05		15.0			300.0	initial stiffness
		27	0.09	0.1	50.0	0.21	-0.005	533.3	Initiate flexural cracking in bottom of tension column P.212
		47	0.11	0.2	65.0	0.27	-0.004	590.9	$M_{cr} = 8650$ kip-in P. 174
		48	0.15	0.2	78.0	0.33	-0.004	520.0	Initial diagonal cracking in upper right corner of wall panel P. 212
		78	0.70	1.0	191.0	0.81	0.000	272.9	First yield P.52, 212 flexural cracks in tension column P.52 diagonal cracks (3" spacing) in wall P.52
		157	4.00	5.7	235.0	0.99	0.025	58.8	Crushing of concrete in wall panel in lower left corner P. 51, 212
		158	4.25	6.1	248.0	1.05	0.027	58.4	$M_p$ achieved, ductility of 6.1 P. 54 reinforcement in crushed zone buckled P.53 5/16" flexural crack at base of wall panel P.53
		164	3.00	4.3	105.0	0.44	0.017	35.0	less than 80% of max load (42%) P. 215
		181	-1.73		225.0			-129.8	concrete in lower right side of wall crushed P.53
		186	1.00		70.0			70.0	entire bottom of wall was crushed P.53
Wang	SW2	2	0.05		25.0			500.0	initial stiffness P. 213
		6	0.11	0.2	50.0	0.21	-0.004	454.5	Initial flexural cracking in bottom of tension column P. 67, 213
		18	0.15	0.2	66.0	0.28	-0.004	440.0	Initial diagonal cracking P.212
		19	0.18	0.3	92.0	0.39	-0.004	511.1	$M_{cr} = 8645$ kip-in P.173
		35	0.70	1.0	202.0	0.85	0.000	288.6	Initial yielding P. 174, 213
		124	-2.94	4.2	245.0	1.03	-0.028	-83.3	$M_p$ achieved P. 59, 213 largest flexural crack or 5/16" in bottom of tension column P. 57 largest diagonal crack in 1st story wall panel of 3/32" P. 57

Table B.1 Damage Data for Shear Walls Continued

Researcher	Specimen	Ref # per Researcher (cycle)	$\Delta$ max cycle (in)	disp. ductility $\mu_y$	Load (kips)	V/V <sub>n</sub>	$\theta_p$	Secant Stiffness (kip/in)	Response Characteristic
Wang	SW2	129	2.90	4.1	237.0	1.00	0.017	81.7	lower left corner of wall crushed P.58
		133	-2.64	-3.8	219.0	0.92	-0.025	-83.0	lower right corner of wall crushed P.59
		135	2.90	4.1	131.0	0.55	0.017	45.2	entire length of wall crushed approx. 10" up from footing P.58 less than 80% of max load (53%) P. 217
Zhang	SW7	yield	0.233	1.0	38.8	0.87	0.000	166.6	yielding load
		14	0.866	3.7	45.3	1.01	0.009	52.3	load capacity (max load)
		85%	1.231	5.3	38.5			31.3	85% of max load
Zhang	SW8	1st crack	0.087	0.4	26.7	0.59	-0.002	308.6	1st cracking load
		yield	0.219	1.0	42.8	0.95	0.000	195.4	yielding load
		max	0.453	2.1	50.4	1.12	0.003	111.3	load capacity (max load)
		85%	0.943		42.8			45.4	85% of max load
Zhang	SW9	1st crack	0.112	0.3	33.4	0.73	-0.003	298.0	1st cracking load
		yield	0.330	1.0	57.5	1.26	0.000	174.2	yielding load
		max	0.945	2.9	68.3	1.49	0.009	72.3	load capacity (max load)
		85%	1.24		58.0			46.8	85% of max load



[illegible]

Table C.2 – Reduced Interior Joint Data Set  $\chi^2$  and K-S tests for lognormal, Weibull and Beta Distributions of the Preferred EDPs

[illegible]

Table C.3 – Exterior Joint Data Set  $\chi^2$  and K-S tests for lognormal, Weibull and Beta Distributions of the Preferred EDPs

[illegible]

## D. Appendix – Shear Wall Distribution and Goodness-of-Fit Parameters

Table D.1 – Full Shear Wall (Rectangular and Barbell) Data Set  $\chi^2$  and K-S tests for lognormal, Weibull and Beta Distributions of the Preferred EDPs

MOR	<b>Lognormal Distribution</b>				
	Drift				
	$\chi^2$ Test			K-S Test	
	Eq. 6	correct CDF	P	correct CDF	
0	2.96	TRUE	0.23	TRUE	
1	3.27	TRUE	0.52	TRUE	
2	2.01	TRUE	0.76	TRUE	
3	7.24	FALSE	0.45	TRUE	
4	2.54	TRUE	0.81	TRUE	
MOR	<b>Weibull Distribution</b>				
	Drift				
	$\chi^2$ Test			K-S Test	
	Eq. 6	correct CDF	P	correct CDF	
0	3.07	TRUE	0.23	TRUE	
1	4.96	TRUE	0.27	TRUE	
2	2.14	TRUE	0.65	TRUE	
3	4.83	TRUE	0.68	TRUE	
4	3.38	TRUE	0.60	TRUE	
MOR	<b>Beta Distribution</b>				
	Drift				
	$\chi^2$ Test			K-S Test	
	Eq. 6	correct CDF	P	correct CDF	
0	18.73	FALSE	0.09	TRUE	
1	7.27	FALSE	0.12	TRUE	
2	3.37	TRUE	0.74	TRUE	
3	4.31	TRUE	0.69	TRUE	
4	45.36	FALSE	0.72	TRUE	